INSIGHTS INTO MECHANISMS AND CLINICAL IMPLICATIONS OF MYOCARDIAL FIBROSIS AND ITS PROGRESSION IN HYPERTROPHIC CARDIOMYOPATHY

BETTY RAMAN

MBBS FRACP

CHRIST CHURCH

DIVISION OF CARDIOVASCULAR MEDICINE

RADCLIFFE DEPARTMENT OF MEDICINE

UNIVERSITY OF OXFORD



THESIS SUBMITTED FOR THE DEGREE OF

DOCTOR OF PHILOSOPHY

MICHAELMAS TERM 2019

I dedicate this Thesis to my incredibly supportive fiancé - Morten Larsen and my extremely loving family: Dr K.P Raman and Ms Deepa Raman, Merrill Raman and Amanda Raman, Dr Indu Raman and Dr Sameer Kaul, without whom, none of this would have been possible.

ACKNOWLEDGEMENTS

“Enjoy the little things, for one day you may look back and realize they were the big things.” —Robert Brault

To my supervisor Professor Stefan Neubauer: I would like to thank you for believing in me and giving me the opportunity to grow as an independent researcher. You have been an incredible mentor and a constant source of encouragement and support. I will never forget your kindness, particularly at the start of my DPhil, when my father was ill. Thank you for being such an inspiration to us all and always teaching us something new every day.

To my supervisor Dr Masliza Mahmod: From you, I have learned the value of humility, patience, hard work and perseverance which are, without doubt, the reasons I admire and respect you so much. Thank you for being a great supervisor, dear friend and trusting confidant, constantly providing both emotional and intellectual support, for which, I am eternally grateful.

To my supervisor Professor Hugh Watkins: Thank you for always making time to discuss things, despite your busy schedule. Your measured and critical feedback has been invaluable at every step of my DPhil. I would also like to thank you for welcoming me into the world of Inherited Cardiomyopathies and giving me an opportunity to care for patients with HCM.

I want to thank Professor Joseph Selvanayagam for encouraging me to come to Oxford for a DPhil. I am honored and grateful for this opportunity to learn so much about CMR and share my skills and knowledge to others.

To Dr Adam Lewandowski: Thank you for not only being an amazing friend but an incredibly inspirational scientist. I am yet to master the art of being super productive while travelling the world, a skill I am told, only exceptionally talented people possess.

I would like to especially thank Dr Rina Ariga for showing me the ropes at the start of my DPhil, sharing her scans and data and setting a fine example of how to do research well. I thank all my fellow colleagues at OCMR for the support I have received particularly during those ‘stress’-full adenosine scans in OCMR. I would like to sincerely thank Dr Elizabeth Tunniclife, Dr Aaron Hess, Dr Sanjay Sivalokanathan, Dr Kenneth Chan, Dr Marco Spartera and Dr Moritz Hundertmark for their invaluable help with the work outlined in this thesis.

Thank you to all the radiographers at OCMR, in particular, Ms Jane Francis whose meticulous training and guidance helped make much of this work possible. A special thanks to Dr Hanan Lanlum, Ms Karen Whatley, Ms Roser Farras and Ms Judith Delos Santos for providing me immense support throughout the DPhil. Finally, I am extremely grateful to the National Institute for Health Research, Oxford Biomedical Research Centre, and the British Heart Foundation, Centre of Research Excellence for funding the work outlined in this Thesis.

DECLARATION

I declare that the work presented in this thesis is my own. Dr Sairia Dass and Dr Rina Ariga provided some of the participant CMR data (hypertrophic cardiomyopathy patients) for this study. Dr Sairia Dass and Dr Rina Ariga also provided ethics for the use of their participant data for Chapters 3 and 4. For the blinded analysis of data, Dr Marco Spartera and Dr Sanjay Sivalokanathan helped with processing of late gadolinium enhancement quantification. Dr Kenneth Chan helped with blinded analysis of myocardial perfusion reserve index and blood oxygen level-dependent imaging (BOLD) assessment. Dr Moritz Hundertmark was the blinded second operator for processing of BOLD data in Chapter 5. Dr Masliza Mahmod reviewed all clinical events in Chapter 3. Dr Liz Tunnicliffe and Dr Aaron Hess provided help with statistical analysis, physics support and critical feedback on the content in Chapter 5. I recruited and imaged the majority of patients in this work with the invaluable assistance of the Inherited Cardiac Conditions clinic staff, Oxford Centre for Clinical Magnetic Resonance Research (OCMR) research nurses, OCMR radiographer and fellows. I interpreted the data and carried out statistical analysis with the help of Dr Eric Ohuma, senior statistician from University of Oxford. This work was funded by the National Institute for Health and Research, Oxford Biomedical Research Centre and British Heart Foundation Research Centre of Excellence.

ABBREVIATION

AMARES	Advanced method for accurate, robust, and efficient spectral fitting
AHA	American Heart Aassociation
ATP	Adenosine Triphosphate
BOLD	Blood Oxygen Level-dependent Imaging
BP	Blood pressure
CMR	Cardiac magnetic resonance
ECG	Electrocardiogram
EDV	End diastolic volume
EF	Ejection Fraction
ESC	European Society of Cardiology
ESV	End systolic volume
FLASH	Fast low angle shot
GBCA	Gadolinium-based contrast agent
HCM	Hypertrophic cardiomyopathy
HLA	Horizontal long axis
HR	Heart rate
ICD	Implantable cardioverter-defibrillators
LGE	Late gadolinium enhancement
LV	Left ventricular
LVH	Left ventricular hypertrophy
LVOT	Left ventricular outflow
LVWT	Left ventricular wall thickness
MPRI	Myocardial perfusion reserve index
MRI	Magnetic resonance imaging
MRS	Magnetic resonance spectroscopy
nBOLD	Normalised BOLD
NOE	Nuclear Overhauser Effect
NSVT	Non-sustained ventricular tachycardia
NYHA	New York Heart Association Class
PET	Positron emission tomography
RPP	Rate Pressure Product
sBOLD	Standardised BOLD
SCD	Sudden cardiac death
SD	Standard deviation
SI	Signal Intensity
SSFP	Steady-state Free Precession
SV	Stroke volume

TE	Echo time
TR	Repetition time
UTE	Ultrashort echo time
VLA	Vertical long axis
WIP	Work In Progress
1.5T	1.5 Tesla
3D UTE-CSI	3-dimensional acquisition-weighted chemical shift imaging
3T	3 Tesla

TABLE OF CONTENTS

ACKNOWLEDGEMENTS ***4***

DECLARATION ***5***

ABBREVIATION ***6***

TABLE OF CONTENTS ***8***

THESIS ABSTRACT ***11***

CHAPTER 1: GENERAL INTRODUCTION ***13***

1.1 OVERVIEW **13**

1.2 MYOCARDIAL FIBROSIS **14**

1.3 MICROVASCULAR DYSFUNCTION AND IMPAIRED OXYGENATION **18**

1.4 GENETIC BASIS OF HCM **19**

1.5 MYOCARDIAL ENERGETICS **20**

1.6 HYPOTHESES **24**

1.7 AIMS OF THIS RESEARCH: **24**

CHAPTER 2: GENERAL METHODS ***26***

2.1 OVERVIEW **27**

2.2 ELIGIBILITY CRITERIA **27**

2.3 CLINICAL ASSESSMENT **28**

2.4 CMR SCAN PROTOCOL **28**

2.4.1 PHOSPHORUS MAGNETIC RESONANCE SPECTROSCOPY 29

2.4.2. LEFT VENTRICULAR INDICES (VOLUMES, FUNCTION, STRAIN, MASS) 30

2.4.3 FIRST-PASS PERFUSION IMAGING 31

2.4.4 BLOOD OXYGEN LEVEL-DEPENDENT IMAGING 32

2.4.5 LATE GADOLINIUM IMAGING 34

CHAPTER 3: PREDICTORS AND CLINICAL IMPLICATIONS OF FIBROSIS PROGRESSION ***36***

3.1 ABSTRACT **37**

3.2 INTRODUCTION **38**

3.3 METHODS **39**

3.4 STATISTICAL ANALYSES **44**

3.5 RESULTS **45**

3.6 DISCUSSION **60**

3.7 CLINICAL IMPLICATIONS **64**

3.8 STUDY LIMITATIONS **64**

3.9 CONCLUSIONS **65**

CHAPTER 4: ROLE OF MICROVASCULAR DYSFUNCTION AND MYOCARDIAL ENERGETICS IN FIBROSIS PROGRESSION ***66***

4.1 ABSTRACT **67**

4.2 INTRODUCTION **68**

4.3 METHODS **69**

4.4 STATISTICAL ANALYSIS **73**

4.5 RESULTS **74**

4.6 DISCUSSION **83**

4.7 CLINICAL IMPLICATIONS **86**

4.8 STUDY LIMITATIONS **87**

4.9 CONCLUSION **87**

CHAPTER 5: IMPROVING THE PRECISION OF STRESS MYOCARDIAL OXYGENATION ASSESSMENT ***88***

5.1 ABSTRACT **89**

5.2 INTRODUCTION **90**

5.3 METHODS **92**

5.4 STATISTICAL ANALYSIS **95**

5.5 RESULTS **97**

5.7 CLINICAL IMPLICATIONS **114**

5.8 STUDY LIMITATION **115**

5.9 CONCLUSIONS **116**

CHAPTER 6: STRESS MYOCARDIAL OXYGENATION: DETERMINANTS AND ASSOCIATION WITH FIBROSIS ***117***

6.1 ABSTRACT **118**

6.2 INTRODUCTION **119**

6.3 METHODS **120**

6.4 STATISTICAL ANALYSIS **123**

6.5 RESULTS **124**

6.6 DISCUSSION **138**

6.7 CLINICAL IMPLICATIONS **142**

6.8 STUDY LIMITATIONS **143**

6.9 CONCLUSIONS **143**

CHAPTER 7: GENERAL CONCLUSIONS AND FUTURE DIRECTIONS ***144***

REFERENCES ***148***

APPENDIX 1: EXTENT OF INVOLVEMENT IN THE WORK ***160***

APPENDIX 2: FIGURE ***162***

APPENDIX 3: PAPERS AND ABSTRACTS 163

THESIS ABSTRACT

Hypertrophic cardiomyopathy (HCM) is the most common inherited cardiomyopathy and has a diverse phenotypic expression and clinical course. Sudden cardiac death is a devastating and feared complication of this disease, but is preventable. The appropriate identification of individuals at risk of fatal arrhythmic events has led to the quest for more powerful and sensitive markers of risk. Relevant to this aim, myocardial fibrosis as assessed non-invasivley by late gadolinium enhancement (LGE) has emerged as a robust prognostic marker. The extent of myocardial fibrosis is linked to both the risk of sudden cardiac death and heart failure. Recent studies suggest that myocardial fibrosis can be progressive; however, its clinical significance and underlying causal mechanisms remain unclear.

In this thesis, the phenotypic predictors and prognostic significance of fibrosis progression in HCM patients were examined. The role of microvascular dysfunction and myocardial metabolism, as potential causal mechanisms, in fibrosis progression were also explored. In HCM, LGE mass increased in patients with HCM from a median mass of 4.98g (IQR 0.97–13.48g) on the first cardiac magnetic resonance scan (CMR1) to 6.30g (IQR 1.38-17.51g) on CMR2 at an interval of 5.3±2.7 years. Substantial LGE progression (increase in LGE mass, ΔLGE, ≥4.75g) was seen in 26% of HCM patients and predicted the occurrence of clinical events with reasonable diagnostic accuracy (AUC 0.74, $p<0.001$). ΔLGE ≥4.75g increased the odds of a combined clinical endpoint of heart failure progression, new onset ventricular tachycardia and cardiac hospitalisation in HCM, by five-folds (Hazard ratio: 5.04, 95% CI 1.85–13.79, $p=0.002$),

performing better than baseline LGE mass on CMR1 in predicting outcomes. Impaired myocardial perfusion (n=18/38) and energetics (n=7/38) at baseline (CMR1) were associated with greater progression in LGE mass from CMR1 to CMR2 ($p \leq 0.01$ for both). Substantial LGE progression was accompanied by left ventricular thinning, dilatation and reduction in systolic function, a potential explanation for the preponderance of clinical events in this subgroup.

To further understand the relationship between microvascular dysfunction, myocardial metabolism and fibrosis, the association between myocardial ischaemia and fibrosis was examined. To achieve this, a novel method with significantly improved precision and reduced variability for stress oxygenation assessment was developed and validated against the standard method. This permitted the precise assessment of stress-induced myocardial oxygenation in a large, cross-sectional, cohort (n=103) of HCM patients. In this work, HCM patients in the lowest quartile of oxygenation had the highest burden of LGE. Severe blunting of stress oxygenation (BOLD SI <6.5%) independently associated with myocardial fibrosis ($\beta=5.2$, $p=0.02$). The sarcomeric mutation status was a strong independent determinant of the extent of stress oxygenation.

Taken together, the non-invasive assessment of myocardial perfusion, metabolism, oxygenation along with fibrosis, using a multi-parametric CMR approach, has provided a number of novel insights into potential causal mechanisms and clinical implications of fibrosis and its progression in HCM.

CHAPTER 1: GENERAL INTRODUCTION

1.1 OVERVIEW

Hypertrophic cardiomyopathy (HCM) is a common genetic cardiomyopathy with a prevalence of 1 in 500 (1-3). HCM is characterised by unexplained thickening of the myocardium (**Figure 1**) and follows an autosomal dominant pattern of inheritance. Up to 60% of patients with HCM have a pathogenic variant in genes that code for sarcomeric proteins (4, 5). Other genetic disorders characterised by metabolic and neuromuscular manifestations account for 5-10% of presentations (6).

HCM is an important cause of sudden and unexpected death in young people and continues to cause disability in patients of all ages (6, 7). Earlier studies suggest that in an unselected series of HCM patients, the annual mortality of this disease is 1%, with atleast half of these deaths attributable to sudden cardiac arrests (8). Additionally, 20-30% of patients are found to develop atrial fibrillation with the incidence of stroke estimated to be 0.8%/year (9-12). Up to 10% of HCM patients may develop end-stage heart failure (13, 14). Predicting the risk of cardiac death, progression to heart failure and arrhythmias in HCM present significant challenges to physicians globally. The variability in risk stratification tools across countries reflects the inability of current tools to resolve the marked heterogeneity seen in disease expression (3, 6).

1.2 MYOCARDIAL FIBROSIS

Since its initial description by Teare in 1958, HCM has been the focus of intense clinical and pathophysiological investigation (15). Myocyte hypertrophy, disarray, fibrosis and microvascular abnormalities have become pathological hallmarks of this disease and frequently described in postmortem or myomectomy studies (16-19). Left ventricular hypertrophy may result from an increase in myocyte cell size or layers of fibrous tissue and is typically accompanied by architectural disorganisation or disarray of cells (16). Myocardial fibrosis is also seen to occur independent of hypertrophy and can be diffuse, patchy or extensive (as in the case of replacement fibrosis) and occasionally found in a perivascular distribution (16, 20). The relative abundance of different types of fibrosis is thought to influence the clinical phenotype - with diffuse fibrosis contributing to myocardial stiffness and replacement fibrosis manifesting as impaired contractility (20-23).

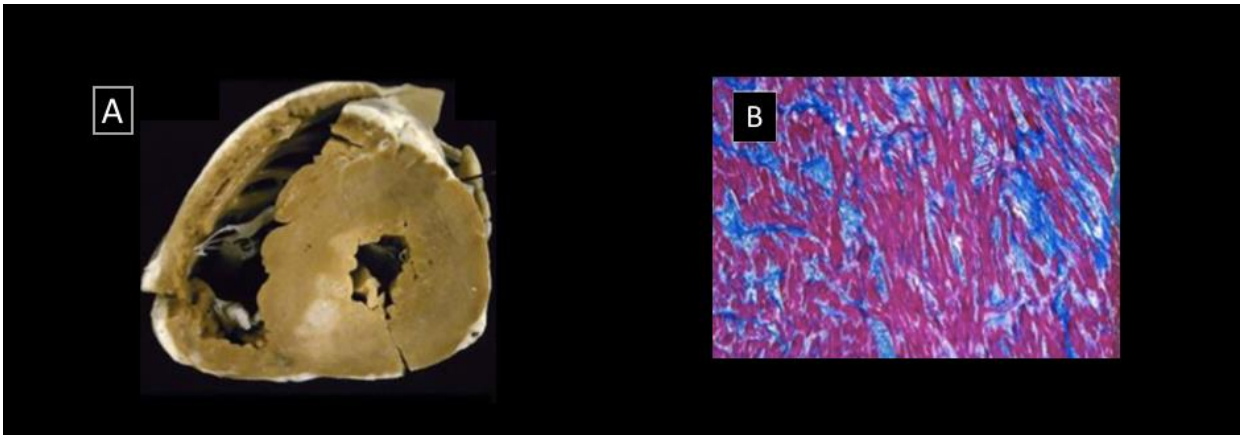

Figure 1. A) Transverse section of the heart demonstrating both left ventricular hypertrophy and regions of dense fibrosis in the septum (white discolouration) B) Myocyte disarray with interstitial fibrosis with collagen strands (blue stain) interlaced between myocytes in hypertrophic cardiomyopathy (HCM). (Adapted from "Defining phenotypes and disease progression in sarcomeric cardiomyopathies: contemporary

role of clinical investigations" by *Olivotto et al.*, Cardiovascular Research, 105, p.413. Copyright 2005 by The Author)

A dominant component of the myocardial interstitium in HCM is fibrillar collagen. Both quantitative and qualitative differences in the type of collagen have been shown to contribute to the phenotypic heterogeneity seen in this disease (24, 25). In one study of 35 HCM patients, a comprehensive assessment of myocardial biopsy specimens from the septum revealed an abundance of type III, IV and VI collagen, all of which correlated with indices of left ventricular performance including diastolic and systolic function (24). The type of fibrosis may also reflect the nature of inducing factor (26). For example, myocardial fibrosis seen in hypertensive hearts tend to be reactive or additive to the cellular architecture (27). While the fibrosis secondary to ischaemic injury tends to be reparative in nature, replacing necrotic myocytes in order to preserve the integrity of collagen network (28, 29). Of interest, the myocardium in HCM displays an increased content of both replacement scar and interstitial fibrosis indicating that both reactive and reparative processes are at play (16, 20, 30).

The pattern and distribution of fibrosis also apear to be distinct in HCM, with a predominance of mid wall fibrosis followed by midwall and subepicardial fibrosis, followed by transmural, and then midwall and subendocardial fibrosis (30, 31). Importantly, subendocardial and subepicardial fibrosis rarely occurs exclusively in HCM. On the other hand, subendocardial replacement fibrosis is usually seen in ischaemic cardiomyopathy (32), while subepicardial fibrosis is pathognomic of myocarditis (33, 34). These findings suggest that a number of mechanisms (fibroblast proliferation, ischaemic necrosis, inflammation) are potentially involved in promoting

myocardial fibrosis in HCM. A detailed histological study of end stage HCM hearts by Galati et al (30), has also revealed an increasing gradient in fibrosis burden from base to apex which is distinct from cardiac amyloidosis, an alternative model of hypertrophy, where the apex is generally spared (35, 36). This is believed to occur due to a reduced density of capillaries seen to commonly affect the hypertrophied apical myocardium in HCM patients (37).

Although the primary trigger for myocardial fibrosis in hypertrophic cardiomyopathy is unknown (38-40), stress induced premature myocyte death resulting from sarcomere mutations and subsequent development of pathological abnormalities such as small-vessel disease, intracavitary obstruction, and ischemia are believed to contribute to the process (16, 41, 42). Cellular and molecular processes arising from a direct expression of sarcomeric mutations have also been implicated with evidence arising from a number of invivo and invitro studies (43-45). Activation of profibrotic pathways mediated by an increased expression of transforming growth factor beta 1(TGF–β1), connective tissue growth factor and periostin, is also seen to occur even before the onset of hypertrophy suggesting that fibrosis is not exclusively linked to pathological abnormaities such as hypertrophy or microvascular dysfunction (46). This is further supported by another study where elevated serum levels of C-terminal pro-peptide of type I procollagen, a marker of increased myocardial collagen synthesis, was detected in sarcomere-mutation carriers without overt hypertrophy (45).

A remarkable development in cardiac magnetic resonance imaging was the discovery of late gadolinium enhancement (LGE) imaging (21, 47-49). LGE permits the in vivo assessment of myocardial fibrosis and relies on the concept that gadolinium bound

chelates diffuse into the interstitial space between cells and not through cell membranes (49). In HCM, gadolinium chelates accumulate in regions of fibrosis which have greater extracellular space. Due to the slower distribution kinetics, there is a persistently high concentration of gadolinium in extracellular tissue which is enhanced on a T1 weighted image (49-51). Validated against histology, late gadolinium imaging has now become the gold standard for non-invasive assessment of myocardial fibrosis in HCM, with the advantage of providing more complete coverage of the heart for serial monitoring of disease progression (30, 49, 52). A number of studies have also emerged indicating that both the presence and extent of LGE on CMR are powerful predictors of cardiovascular mortality in HCM (21, 48, 53). These fundamental insights have enhanced our understanding of the risks associated with myocardial fibrosis in HCM.

Despite the advances made in risk stratification, several important gaps in our knowledge remain. The rate of fibrosis progression in HCM is unclear as are factors that promote fibrosis progression. Furthermore, the prognostic value of fibrosis progression is unknown, with several implications for clinical practice including the early detection of patients at risk of end-stage disease and prevention of sudden death and heart failure in HCM.

1.3 MICROVASCULAR DYSFUNCTION AND IMPAIRED OXYGENATION

Abnormalities in vascular remodelling were first described by Maron *et al.* in 1986 (54). Several groups have since reported findings of capillary rarefaction, small vessel luminal narrowing and perivascular fibrosis on histological studies (16, 20, 54, 55). Interestingly, such changes in the microvascular architecture are found to associate closely with replacement myocardial fibrosis, which has led to the belief that microvascular dysfunction may be responsible for ischemia-mediated myocyte death, and ultimately replacement fibrosis. Indeed, this association between microvascular dysfunction and fibrosis has also been seen in in vivo imaging studies of HCM patients undergoing positron emission tomography (PET) and CMR (56-58).

Despite this cross-sectional evidence, much controversy remains with regards to the contribution of microvascular dysfunction to fibrosis. For instance, in a study by Varnava *et al.*, microvascular abnormalities were detected in myocardium without fibrosis and vice versa, leading the authors to conclude that fibrosis may be promoted by factors other than ischemia (16). Nevertheless, the evidence for ischemic injury in HCM is compelling and originates from an early post-mortem study of HCM patients who suffered sudden cardiac deaths, in whom a range of ischaemic changes from acute coagulative necrosis and neutrophilic infiltrate to a chronic post-necrotic replacement-fibrosis were described, despite the absence of atherosclerotic coronary disease (59). Furthermore, a number of contemporary imaging studies using CMR and PET have shown that severely impaired perfusion portends ischaemia and strongly associates with regions of fibrosis, predicting the risk of adverse left ventricular remodelling (57, 58).

Therefore, efforts focused on clarifying the role of microvascular dysfunction and ischemia on fibrosis progression and ultimately adverse remodelling can be insightful for the early initiation of treatment strategies to potentially alter the natural history of HCM (60).

1.4 GENETIC BASIS OF HCM

Inherited in an autosomal dominant Mendelian pattern, HCM exhibits variable expressivity and age-related penetrance (61-63). Over the years, more than a thousand mutations have been reported in 11 or more genes that code for proteins found primarily in heart, such as the thick and thin myofilament proteins in the sarcomere (5, 64). The majority of mutations are seen to involve three protein-encoding genes: β-myosin heavy chain (*MYH7*) (35% to 40%), myosin- binding protein C (*MYBPC3*) (25% to 40%), cardiac troponin T (*TNNT2*) (5-10%) (5, 65-68). Other than in *MYBPC3*, nearly all mutations are missense mutations where one amino acid is exchanged for another, altering the physical and functional properties of proteins. In *MYBPC3*, frameshift mutations also occur, causing a more drastic change in protein structure such as shortened truncated proteins or abnormal slicing of messenger ribonucleic acid (5).

The mechanisms by which genetic mutations give rise to phenotypic manifestations such as asymmetrical hypertrophy, myocardial fibrosis and disarray are unknown, but many experts believe that abnormalities in energy handling form the basis of such pathological findings. Indeed, evidence for metabolic abnormalities and oxygenation

impairment have been reported in patients before the onset of hypertrophy, indicating that the longitudinal assessment of these parameters may yield valuable mechanistic insights into hypertrophy and adverse remodelling (38, 69). Interestingly, the extent of pathology detected non-invasively may differ between sarcomeric and non-sarcomeric mutation HCM patients (70, 71). For instance, in a PET study by Olivotto *et al*., sarcomeric HCM had more severe microvascular dysfunction and increased focal fibrosis, than genotype-negative individuals (70). In another study by Ellims *et al.* , the prevalence of focal fibrosis was greater in sarcomeric HCM, while that of diffuse fibrosis was more in genotype negative HCM (72). Indeed, such differences, attributable to genotype status, were also recently seen in clinical outcomes. In a registry study of 4591 HCM patients, sarcomeric HCM was associated with higher mortality and morbidity than genotype negative HCM (73). Of interest, HCM patients with a variant of uncertain significance (VUS) involving sarcomeric genes also experienced a high rate of clinical events, underscoring the need to review the status of VUS in the context of prospective clinical data (73). Nevertheless, a systematic assessment of genotype-phenotype correlation in more adequately powered prospective studies could shed further light into factors that contribute to differential clinical outcomes seen in this large registry study (73).

1.5 MYOCARDIAL ENERGETICS

The myocardial hypertrophy seen in HCM is widely accepted as a response to perturbed sarcomeric function due to mutations in sarcomeric gene proteins, particularly in the absence of a significant afterload increase (74, 75). Hypertrophy was initially thought to be a compensatory response to depressed cardiac function induced

by mutant proteins (76); however, subsequent studies have shown that mutant myofilaments give rise to increased contractility through altered myosin kinetics, increased thin filament calcium sensitivity and changes in myosin binding regulation (76, 77). While thin filament mutations are commonly characterised by increased calcium sensitivity resulting in increased contraction velocity despite submaximal force output (76, 78-80), mutations in myosin alter cycling rates of myosin heads, leading to more cross-bridge detachment and increased energy consumption, before the completion of power stroke (76).

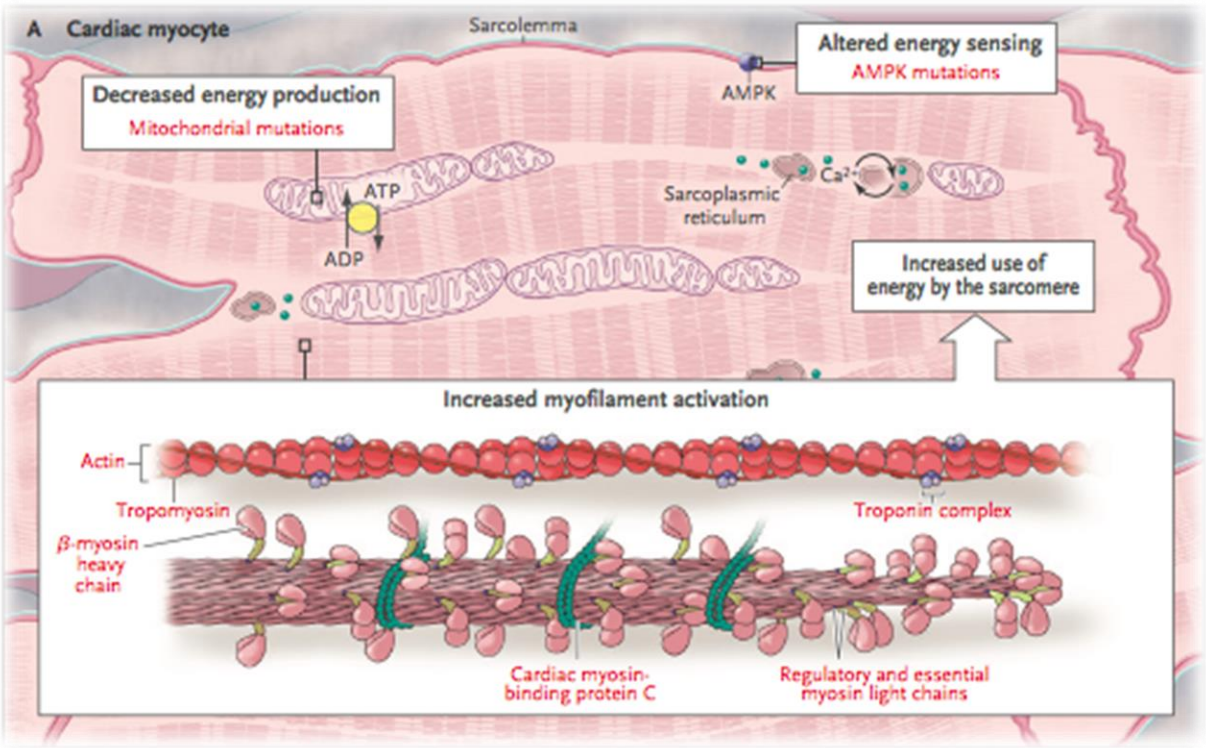

Figure 2. Mutations in sarcomeric proteins, mitochondrial defects and cardiac energy-sensing apparatus are associated with altered energetic status and give rise to HCM or HCM phenotypes. Adapted from "Inherited Cardiomyopathies" by Watkins H *et al.* , New Eng J Med, 364, p.416,417. Copyright 2011 by Massachusetts Medical Society.

These observations form the basis of the energy depletion hypothesis, first put forward by Ashrafian *et al.* (74). The energy depletion hypothesis states that the increased energy demands imposed by pathogenic mutations affect the cardiomyocyte's ability to maintain energy levels necessary for contraction, pump function and ion homeostasis such as calcium reuptake which, in turn, results in myocyte dysfunction including elevated diastolic calcium, a potent stimulus for pathological hypertrophy (74). Further evidence for this hypothesis stems from the observations that diseases which directly affect cellular metabolism (mitochondrial function, glucose transport, free fatty acid transport) and energy production also present with hypertrophy and can be indistinguishable from sarcomeric HCM (81-83). Additionally, sarcomeric mutation carriers exhibit evidence of energetic depletion even before the onset of hypertrophy (38).

A link between myocardial energetics and fibrosis has also been suggested. For the myocyte to function, adenosine triphosphate or ATP is instrumental in maintaining many vital energy consuming reactions including the activity of sodium potassium adenosine triphosphatase - Na/K+ ATPase pump - and calcium uptake via sarco/endoplasmic reticulum Ca^{2+} ATPase (84). Delayed calcium reuptake by the sarcoplasmic reticulum may activate a number of calcium-dependent signals (myocyte enhancer factor-2/ MEF2, nuclear factor of activated T cells/ NFAT) via calcium/calmodulin-dependent (CaMKII) protein kinase II phosphorylation, which in turn regulate inflammation and cell death (85, 86). As much of the mitochondrial activity (tri-carboxylic cycle) also relies on calcium signalling and active efflux pumps, it is conceivable that significant energetic depletion may disrupt mitochondrial

homeostasis, forming a potent source of oxidative stress (74). The release of oxygen free radicals may, in turn, activate fibroblasts to myofibroblasts (87), a critical step in the formation of fibrosis. These factors, compounded by hypoperfusion from microvascular dysfunction, could result in further hypoxic injury and inflammation (88-90). As the cell is continuously primed to repair damage, a number of energy-consuming signal pathways are activated leading to further energetic depletion, feeding into a vicious cycle of energy depletion, damage and repair, eventually leading to mitochondrial failure and apoptosis (91-93). Therefore, the long term consequence of energetic depletion warrants further investigation. In particular, its role in promoting myocardial fibrosis can be important, as metabolic therapies, shown to improve myocardial energetics, may be beneficial in preventing adverse cardiovascular remodelling.

1.6 HYPOTHESES

1. Myocardial fibrosis is progressive in HCM patients and substantial fibrosis progression is associated with poor clinical outcomes.

2. The underlying genetic subtrate contributes to the growing fibrotic burden through a process of ischaemic injury mediated by increased metabolic demands and microvascular dysfunction.

1.7 AIMS OF THIS RESEARCH:

This is a study of hypertrophic cardiomyopathy (HCM) using a multiparametric magnetic resonance

(CMR) approach. The work outlined in this thesis aims to understand the natural history of fibrosis progression in HCM, its prognostic significance and potential causal mechanisms.

In order to address this, the following were explored:

1.In this thesis, I examined the rate of progression of fibrosis as detected by CMR on late gadolinium (LGE) imaging and investigated factors that are associated with fibrosis progression including the role of genotype in Chapter 3. The predictive utility of LGE progression for clinical events was further examined and incremental value of LGE progression over baseline LGE was explored.

2. As mechanisms underlying fibrosis progression are unclear, I examined the association of microvascular dysfunction and increased energetic cost with fibrosis progression in Chapter 4.

3. Myocardial ischaemia may be an important trigger for fibrosis progression. Existing methods for ischaemia detection suffer from poor precision. The work in Chapter 5 aimed to improve the precision of oxygenation assessment and to visualise stress-induced de-oxygenation in HCM.

4. In Chapter 6, I examined the relationship between myocardial ischemia and fibrosis and investigated the factors that promote blunted stress-induced oxygenation in HCM.

The work outlined in Chapters 3 and 4 of this thesis have been published in a manuscript in the European Heart Journal Cardiovascular Imaging, of which I am first author (https://doi.org/10.1093/ehjci/jey135) (94).

CHAPTER 2: GENERAL METHODS

2.1 OVERVIEW

This study was approved by the Oxford research ethics committee (ref: 07/Q1607/66, 12/LO/1979). Each participant gave informed consent to be involved in the study. Subjects were recruited from the Inherited Cardiac Conditions Clinic, John Radcliffe Hospital.

2.2 ELIGIBILITY CRITERIA

Subjects were eligible for inclusion in the study if:

1. Aged between 18 and 65
2. Willing to participate in the research study as a volunteer
3. Genotyped HCM with hypertrophy (maximum left ventricular wall thickness >15mm unexplained by hypertension alone or valvular dysfunction or infiltrative disease)
4. Genotyped HCM without hypertrophy: Carrier of pathogenic or likely pathogenic sarcomeric gene mutation.

Subjects were excluded if any of the following was present

1. History of coronary disease or significant valvular disease
2. Suspected amyloidosis
3. In healthy volunteers, family history of sudden cardiac death or cardiomyopathy.
4. Contraindications to magnetic resonance (MR) scanning (MR implants, pacemakers, claustrophobia, previous head or eye surgery) and adenosine (advanced heart block, severe asthma)
5. Suspected pregnancy or positive pregnancy test or breastfeeding
6. Impaired renal function (estimated glomerular filtration rate <30ml/s ml/min/1.73m^2)

GENETIC SCREENING

All patients enrolled underwent sequencing of 13 genes associated with HCM as part of routine clinical care (*MYBPC3*: myosin binding protein C; *MYH7*: myosin heavy chain; *TNNI3*: cardiac troponin I; *TNNT2*: cardiac troponin T; MYL2: regulatory myosin light chain; *MYL3*: essential myosin light chain; TPM1: alpha-tropomyosin; *ACTC1*: cardiac actin; *CSRP3*: muscle *LIM* protein; *PRKAG2*: *AMPK γ2*; *PLN*: phospholamban; *GLA*: alpha-galactosidase; *FHL1*: four and a half *LIM* domains 1) including a screen (in DNA from blood) for selected mitochondrial mutations if no pathogenic or likely pathogenic sarcomeric mutations were identified.

2.3 CLINICAL ASSESSMENT

All subjects underwent clinical assessment including a history of:

1. Drug history allergies
2. Weekly alcohol intake

Cardiovascular examination was performed to exclude any other valvular disease such as severe aortic stenosis. The following measurements were also undertaken:

1. Blood pressure using a manual sphygmomanometer
2. 12 lead electrocardiogram, height and weight using calibrated scales
3. Blood tests for full blood count, haematocrit, creatine check and sugar levels.

2.4 CMR SCAN PROTOCOL

The following cardiac magnetic resonance (CMR) sequences were used to measure the endpoints in each chapter:

(1) 31-phosphorus (^{31}P MRS) at rest- to assess myocardial energetics for Chapter 4

(2) Cine imaging to assess cardiac mass, volumes and function for Chapters 3-6.

(3) Rest and adenosine stress first-pass perfusion imaging - to assess myocardial perfusion reserve index for Chapters 4-6.

(4) Rest and adenosine stress blood oxygen level-dependent (BOLD) imaging - to assess myocardial oxygenation for Chapters 5 and 6.

(5) Late gadolinium enhancement (LGE) - to assess myocardial fibrosis for Chapters 3-6.

All scans for assessment of perfusion, energetics and oxygenation were undertaken at 3 Tesla (3T) (Trio MR scanner, Siemens, Erlangen, Germany) except for LGE progression assessment (details in Chapter 3), whereby some of the serial scans were undertaken at 1.5 Tesla (1.5T).

2.4.1 PHOSPHORUS MAGNETIC RESONANCE SPECTROSCOPY

Acquisition

^{31}P MRS was performed to measure myocardial energetics. Subjects were placed prone with their hearts over the centre of the coil as previously described (95). The phosphocreatine to adenosine triphosphate (PCr/ATP) ratio from a mid-ventricular septal voxel in a position matching a mid ventricular perfusion slice and a BOLD slice was obtained. Further details of sequence parameters are described in Chapter 4.

Analysis

The spectrum from a mid-ventricular septal voxel was fitted using a custom implementation of AMARES (the advanced method for accurate, robust, and efficient spectral fitting) in the Oxford Spectral Analysis or “OXSA” semi-automated spectroscopy post-processing pipeline as using prior knowledge (**Figure 1**) (96). Details of post procession analysis are described in Chapter 4.

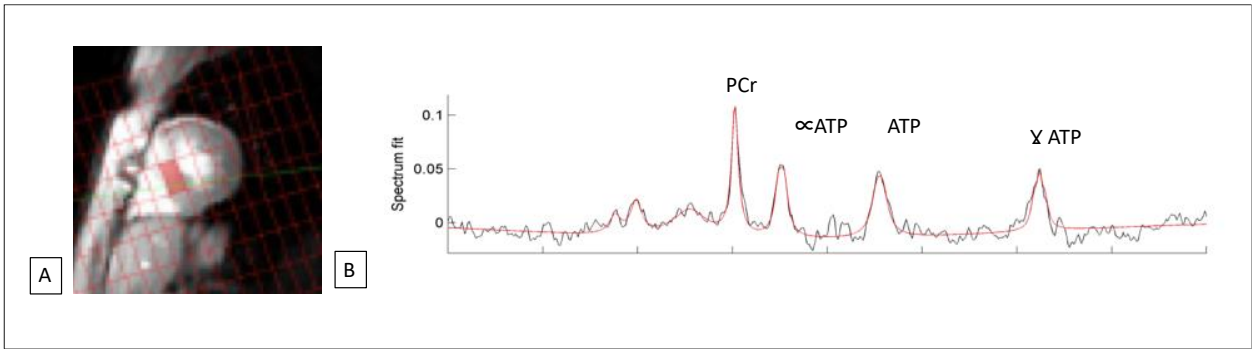

Figure 1. Phosphorus spectrum from a mid-ventricular septal voxel was fitted using a custom implementation of AMARES showing spectral peaks of PCr, α, β and γ ATP. Fitting was accomplished using prior knowledge.

2.4.2. LEFT VENTRICULAR INDICES (VOLUMES, FUNCTION, STRAIN, MASS)

Acquisition

Cardiac volumes were acquired using steady-state free precession (SSFP) imaging. Slices were acquired at the end of expiration to minimise the effects of respiratory motion. Scan parameters were typically: voxel size 2.0 x 2.0 x 8.0mm, field of view (FOV)=380 x 380mm, TR/TE 3ms/1.5ms, flip angle 50°, matrix 192 x 192, GRAPPA=3, 24 reference lines, segments=15, concatenations=1. Pilot images were initially acquired and used to plan and acquire horizontal long axis (HLA), vertical long axis (VLA), left ventricular outflow tract (LVOT) long axis and short axis stack images (69).

Analysis

Left ventricular (LV) short axis epicardial and endocardial borders were manually contoured at end diastole and end systole (95). LV end systolic (ESV) and end diastolic (EDV) volumes were used to calculate stroke volume (SV) as SV = EDV-ESV (97). Ejection fraction (EF) and cardiac output (CO) were calculated as EF = SV/EDV and

CO = SV x HR, respectively. LV mass was calculated by subtracting the endocardial volume from the epicardial volume, based on prior knowledge of myocardial specific gravity (1.05 g/cm^3) (95).

2.4.3 FIRST-PASS PERFUSION IMAGING

Acquisition

Myocardial perfusion was assessed on three short axis cine images (base, mid and apical slices) from the short axis stack (48). Adenosine 140 microgram/kg/min was infused through a large bore cannula in the antecubital fossa. At peak vasodilator stress after the commencement of adenosine, images were acquired. Haemodynamics (heart rate and blood pressure) were measured at 1-minute intervals during and after adenosine stress. A bolus of contrast agent (details in Chapters 4-6) was administered intravenously to assess regional perfusion. For every heartbeat, stress perfusion images were acquired during first-pass using T1 weighted fast (spoiled) gradient echo sequence in the three short axis image planes. Rest perfusion was acquired 10-15 minutes after stress for which another dose of bolus contrast was administered (69).

Analysis

For the analysis of myocardial perfusion, signal intensity (SI) over time curves was generated by tracing endocardial and epicardial contours (Circle Cardiovascular Imaging Inc., Calgary, Canada) after correction for displacement during breathing (69, 95). A region of interest was drawn in the LV blood pool to obtain an arterial input function. Post-adenosine rest and stress myocardial perfusion up slopes were calculated using a five-point linear fit model of SI versus time and normalised to the LV blood pool upslope. Myocardial perfusion reserve index (MPRI), defined as the ratio of

stress to rest normalised myocardial perfusion upslope (**Figure 2**), was derived for 18 segments and averaged per patient (98).

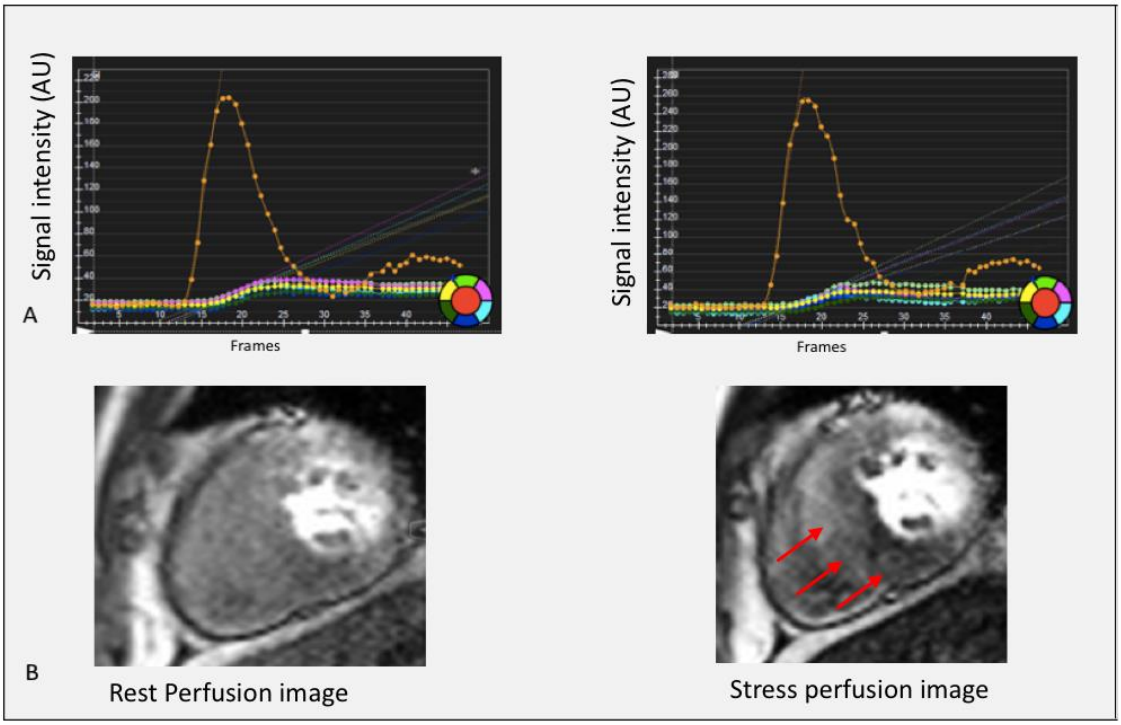

Figure 2. (A) Signal intensity (SI) curves from rest and stress first-pass perfusion images demonstrating the SI slopes for each of the six myocardial segments and corresponding blood pool from a HCM patient. (B) Rest and stress first-pass perfusion imaged demonstrating evidence of inducible perfusion defect (red arrows) in the inferoseptal myocardial segments.

2.4.4 BLOOD OXYGEN LEVEL-DEPENDENT IMAGING

Acquisition

Before the acquisition of BOLD images, cardiac-gated B0 shimming (Siemens WIP 452) and frequency adjustments were undertaken to generate images free from off-resonance artefacts. For BOLD-CMR, a single mid-ventricular slice was acquired at systole using the electrocardiogram (ECG)-gated T2-prepared segmented SSFP sequence with interleaved low flip angle FLASH (fast low angle shot) reference

readouts on alternate heartbeats (99) (Siemens WIP 567, VB17). The sequence parameters were: TE prep=40ms, SSFP TR/TE = 2.86ms/1.43ms, 72 readout lines per heartbeat, and an SSFP flip angle of 44°. The SSFP and FLASH data were acquired in an interleaved fashion over three heartbeats each (six in total) with dummy SSFP and FLASH acquisitions beforehand (eight heartbeats total). Adenosine was then infused at a dose of 140 mcg/kg/min and at peak vasodilator stress (at least 3-4 minutes), a slice-matched stress BOLD image was acquired. Blood pressure was recorded by a vital-signs monitor machine at baseline and 1-minute intervals during stress.

Analysis

For BOLD, myocardial signal intensity was measured after manually tracing the endo and endocardial and epicardial borders (69). Commercially available software (Circle Cardiovascular Imaging Inc., Calgary, Canada) was used to trace contours. The mid-ventricle was divided into six segments as per the AHA segmentation (**Figure 3**). For Chapter 5, the traditional method using required HR correction was also used. The equation for HR correction of standard images was

$$S = \frac{S_0}{1 - 0.98e^{-RR/980}} \quad (1)$$

Where S0 is the measured signal intensity, S is the HR-corrected signal intensity, and RR denotes the RR interval during the BOLD acquisition in ms.

The relative SI change or BOLD ΔSI was calculated as:

$$\text{BOLD } \Delta SI\% = \frac{Stress\ SI - RestSI}{RestSI} \text{ x } 100$$

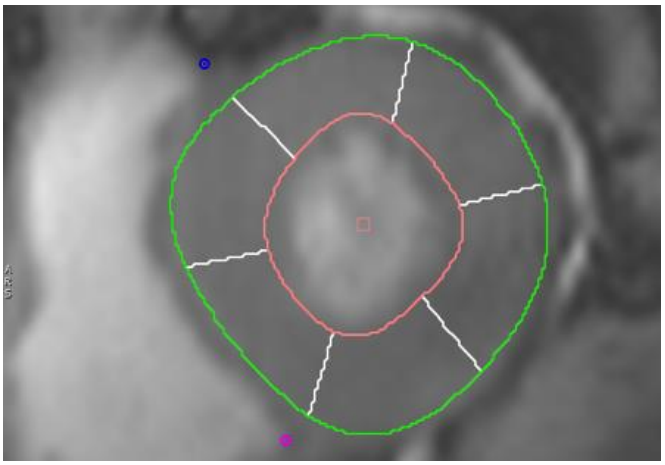

Figure 3: Example of blood oxygen level-dependent image (greyscale) with endo (red) and epicardial (green) contours drawn to divide slice into six AHA segments.

2.4.5 LATE GADOLINIUM IMAGING

Acquisition

LGE imaging was acquired using a T1-weighted phase-sensitive inversion recovery sequence. Scan parameters were typically: voxel size 2.0 x 1.5 x 8.0 mm, matrix 144 x 256, field-of view=380 x 285mm, TR/TE=800.20/3.36ms, flip angle 25°, GRAPPA=2, 24 reference lines, segments=25, phases=1, concatenations=1, measurements=1, bandwidth=130Hz/Px using a bolus of 0.06 mmol/kg of body weight of gadolinium-based contrast agent followed by a 10 mL saline flush through an intravenous cannula in the antecubital fossa. Details on the type of gadolinium-based contrast agent and field strengths are described in the respective chapters.

Analysis

LGE was also quantified using (Circle Cardiovascular Imaging Inc., Calgary, Canada). Endocardial and epicardial borders were drawn as well as a reference region with normal myocardial intensity as 'remote' region. Hyper enhanced pixels were defined as those at five standard deviations (5-SD) above the mean intensity of a reference region of interest placed in a remote area of myocardium with no visual evidence of enhancement (6, 19). The values reported in this Thesis refer to the absolute mass of myocardium highlighted by pixels in that segment with signal intensity greater than the five standard deviations from the reference mean (**Figure 4**). The 5-SD method was used, given its excellent level of agreement with histological evidence of fibrosis in the largest histological validation study of LGE in HCM (52).

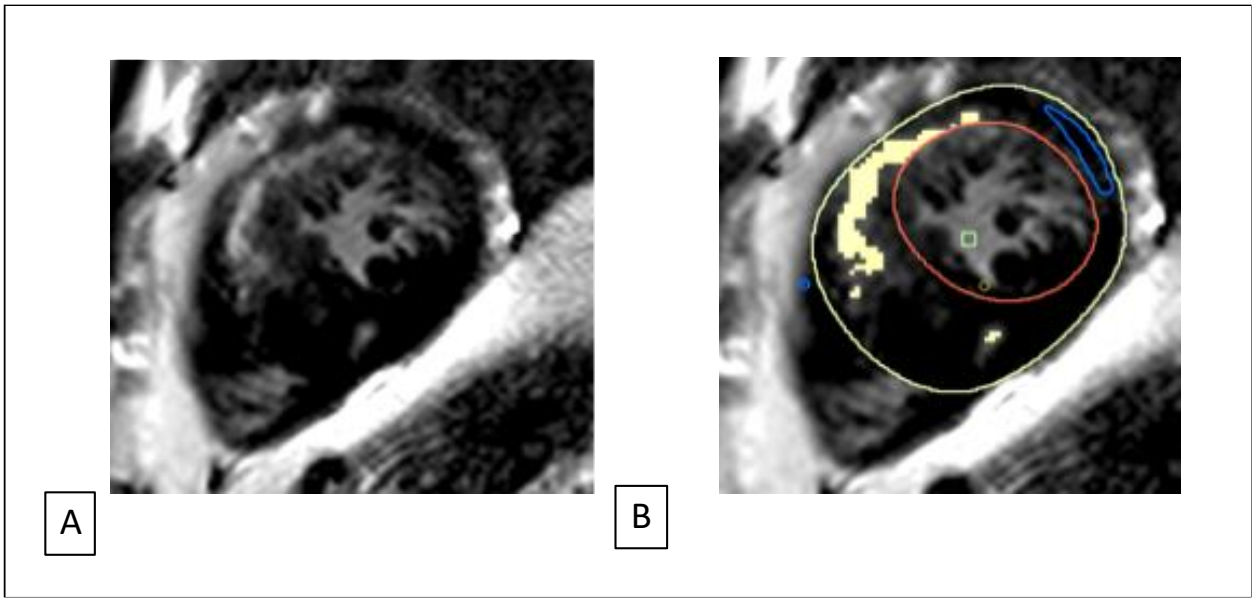

Figure 4: (A) Late gadolinium enhanced (LGE) images from a patient with HCM, (B) Endocardial (red) and epicardial (green borders) were traced. Blue region of interest drawn in the normal myocardium (blue) as reference and pixels ≥ 5-standard deviations from reference mean (blue) were detected as LGE mass.

CHAPTER 3: PREDICTORS AND CLINICAL IMPLICATIONS OF FIBROSIS PROGRESSION

3.1 ABSTRACT

Background: Myocardial fibrosis or late gadolinium enhancement (LGE) on cardiac magnetic resonance is a powerful prognostic marker in hypertrophic cardiomyopathy (HCM) and shown to progress.

Objectives: To examine the clinical utility of LGE progression in HCM and investigate the determinants of LGE progression.

Methods and results: Seventy-two HCM patients had two CMR (CMR1-CMR2) at an interval of 5.7±2.8 years. All patients were followed up clinically for 6.3±3.6 years from CMR1. A combined endpoint of heart failure progression, cardiac hospitalisation, new onset ventricular tachycardia was assessed. Left ventricular (LV) volumes and ejection fraction did not differ from CMR1 to CMR2, but LV mass was mildly elevated. LGE was present in 75% of HCM patients at CMR1 and increased to 82% by CMR2. LGE mass increased from median 4.98g (IQR 0.97–13.48g) to 6.30g (IQR 1.38–17.51g), as did relative LGE mass. LGE increment was more significant in sarcomeric and mitochondrial HCM, compared to genotype negative HCM. An LGE increment (ΔLGE) of 4.75g had a reasonable diagnostic accuracy (AUC 0.74, $p<0.01$) for predicting clinical events. ΔLGE≥4.75g conferred a five-fold increased risk of subsequent clinical events (Hazard ratio: 5.04, 95% CI 1.85–13.79, $p=0.002$). The extent of LGE mass at CMR1 was the only independent predictor of substantial LGE progression on multivariable analysis.

Conclusion: LGE is progressive in HCM patients, and substantial progression predicts an increased risk of clinical events. The baseline extent of LGE is an important determinant of future progression.

3.2 INTRODUCTION

Sudden cardiac death and advanced heart failure are well-known complications of hypertrophic cardiomyopathy (HCM) (6, 100, 101). Myocardial fibrosis is an essential substrate for both life-threatening arrhythmia and adverse cardiac remodelling in HCM (102). Histopathological studies confirm a high burden of myocardial fibrosis in both young adults (41) who suffered a sudden cardiac death (SCD) and older patients with end-stage heart failure and HCM (30, 49).

Late gadolinium imaging (LGE) on cardiac magnetic resonance imaging (CMR) is a well established and highly reproducible method for the assessment of focal myocardial fibrosis in HCM (30, 52). Over the years, both the presence and extent of LGE have shown to be prognostically useful for HCM patients (21, 53, 103). Interestingly, a recent study by Raja *et al.* suggests that LGE is not limited to adults alone but also detectable in children and adolescents with HCM on CMR (104).

To date, three studies have shown that serial CMR can detect progression of LGE in both adults and children with HCM (37, 104, 105). However, the clinical relevance of LGE progression on serial CMR remains unclear. Furthermore, progression appears to be heterogeneous, with some patients exhibiting a more stable phenotype than others. To understand the source of this heterogeneity further clarification of clinical and phenotypic predictors of LGE progression is required.

We, therefore, set out to examine the prognostic value of LGE progression on serial CMR and investigate the determinants of clinically relevant LGE progression in HCM.

3.3 METHODS

Study population

This study was a retrospective analysis of data from an observational study approved by local ethics committee (reference: 07/Q1607/66, 12/LO/1979). All patients with HCM enrolled in this study were recruited from the University of Oxford Inherited Cardiac Conditions Clinic and were invited to have a repeat CMR. Genetic screening was undertaken for 13 HCM genes and mitochondrial mutations (Details in Chapter 2 General Methods). Diagnosis of HCM was based on the presence of unexplained left ventricular hypertrophy (LVH) (maximum left ventricular wall thickness of ≥15mm) or the presence of a pathogenic HCM-causing sarcomeric mutation and no hypertrophy (phenotype negative sarcomeric mutation carrier or Sarc+P-).

Patients with known coronary artery disease, aortic stenosis, amyloidosis or contraindications to CMR were excluded. A total of 88 patients were included in the study. Of them, 16 were excluded after CMR1. Ten had implantable cardioverter defibrillator's (ICD) implanted, two had pacemakers, two had reveal devices implanted. One had LGE indicating previous myocardial infarction and one had coronary disease on coronary angiography leaving 72 patients with two CMR scans (CMR1-CMR2) (**Figure 1**).

CMR Protocol

Serial CMR was undertaken in all 72 patients and included cine and LGE assessment at 1.5 Tesla (1.5T) or 3T at an interval of 5.7±2.8 years. Sixteen patients had follow-up CMR at different field strengths.

Cine was undertaken using a series of single breath-hold balanced steady-state free precession images for the estimation of cardiac volumes and function as previously described (95). LGE imaging was acquired in multiple short axis slices to match cine views and long axis planes ~8-10 minutes after intravenous administration of the gadolinium-based contrast agent (GBCA) (total dose 0.15mmol/kg) for all scans. The inversion time was adjusted for optimal nulling of remote normal myocardium (69). For all CMR scans before 2012, Gadodiamide (Omniscan, Nycomed Amersham, UK) was used as contrast agent. Due to the emerging safety concerns of Gadodiamide (Omniscan), in particular the associated risk of nephrogenic systemic fibrosis, Gadobuterol (Gadovist®, Bayer Inc., Toronto, Ontario, Canada) was used as contrast agent at 1.5T and Gadoterate meglumine (Dotarem, Guerbet LLC, France) at 3T for all scans from 2012 (106-108).

Image analysis

Commercially available software (Circle Cardiovascular Imaging Inc., Calgary, Canada) was used to remodelling left ventricular (LV) volumes, mass, ejection fraction, peak systolic 2-D global longitudinal, circumferential and radial strain as previously reported (109). The assessment of LV indices and LGE mass were undertaken by two

observers blinded to the clinical information (MS and SS). Quantitative analysis of LGE was undertaken by setting a signal intensity threshold at five standard deviations (5-SD) above the mean intensity of a reference region of interest placed in a remote area of myocardium with no visual evidence of enhancement (52, 110). A binary visual score (1=progression; 0=no progression) was also provided by an experienced (>5 years) CMR clinician (MM) to assess the level of agreement between semiquantitative assessment and observed changes seen by an expert clinician. ΔLGE was defined as an absolute increase in LGE mass from CMR1 to CMR2.

The level of agreement between visual assessment of LGE progression versus semiquantitative assessment was high with Cohens kappa 0.90 (95% CI 0.79-1.00), p<0.01. Inter-observer intra-class correlation coefficient (two-way mixed effect) for (n=15) was excellent at 0.89 (95% CI 0.80-0.95, p<0.01), as was intra-observer ICC (one-way random effect) 0.97 (95% CI 0.95-0.99, p<0.01).

Clinical follow-up

Clinical follow-up was performed annually for 6.3±3.6 years from CMR1. In cases of a suspected event, all medical records were obtained and reviewed by two observers (BR and MM) blinded to the CMR data.

Major risk factors for sudden cardiac death (SCD) included traditional risk factors (see supplementary material). Additionally, the European Society of Cardiology (ESC) risk calculator was used to estimate 5-year SCD risk for all patients (111).

Given the low event rate (attributable to a low baseline SCD risk) in this selected population undergoing serial CMR, we used a composite clinical endpoint of: heart failure progression defined as a progressive increase in New York Heart Association (NYHA) class necessitating optimisation (increase) of medical therapy, new onset non-sustained ventricular tachycardia (≥3 heartbeats, ≥120bpm) and hospitalization from cardiac cause (arrhythmia or heart failure). A change in NYHA class or medical therapy due to intolerance to medications did not constitute a clinical event in this study.

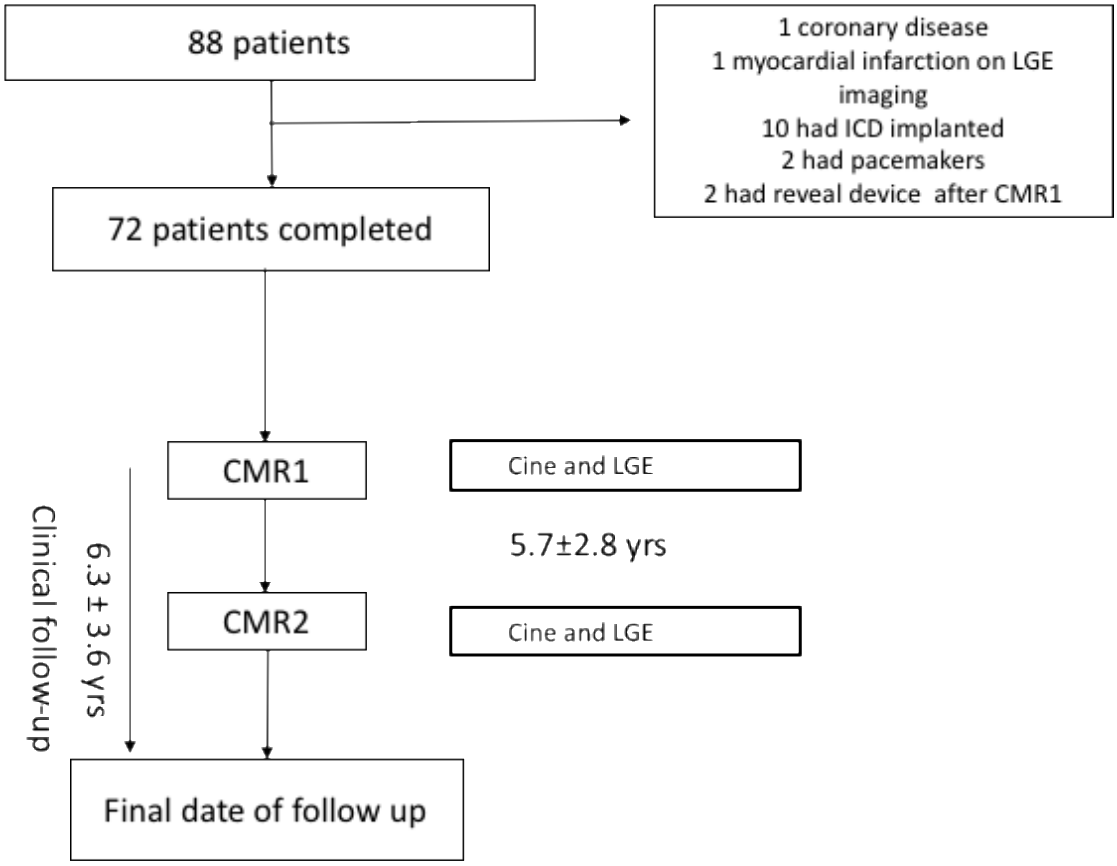

Figure 1. Flow chart of hypertrophic cardiomyopathy (HCM) patients through the study. (CMR; cardiovascular magnetic resonance imaging; ICD implantable cardioverter defibrillator; LGE late gadolinium imaging,)

3.4 STATISTICAL ANALYSES

All statistical analyses were undertaken using IBM SPSS Statistics 23.0 (IBM Corp., Armonk, NY, USA), STATA/SE 15.0 (Stata Corp, College Station, Texas USA) and GraphPad Prism 7.0 (GraphPad Software, San Diego, California, USA). Normality of data was assessed by visually inspecting the plots. Mean (with standard deviation, SD), and median (with interquartile range, IQR or confidence intervals, CI for median differences) were computed as appropriate. Paired t-test and Mann Witney tests were used for normally distributed and non-Gaussian data respectively. The $\chi 2$ and Fisher's exact tests were used to compare proportions. Spearman correlation was used to assess the correlation between LGE progression and wall thickness. Given the current lack of a generally accepted cut off for 'significant' LGE progression, a receiver operator curve was used to estimate an optimal LGE increment or ΔLGE (ΔLGE = absolute increment in LGE mass from CMR1-CMR2) threshold (Youden index) predictive of clinical events. Univariate and multivariable binary logistic regression models were then utilised to assess predictors of this ΔLGE (112). LGE mass at CMR1 was treated as a continuous variable. The covariates included were variables known to be potential confounders and were adjusted for in the model. All tests were two-tailed, and p-values <0.05 (after Bonferroni correction) were considered significant.

3.5 RESULTS

Study population

The final population consisted of 72 patients with paired CMR data. **Table 1** lists their background clinical characteristics at baseline CMR (CMR1) and second CMR (CMR2).

Mean age of patients at CMR1 was 45±12 years and 68% were male. At CMR1, the majority (94%) had 1 or no sudden cardiac death (SCD) risk factors, and four (6%) had two or more SCD risk factors. The mean 5-year estimated risk of SCD on European Society of Cardiology (ESC) risk calculator (6) was low at 2.01±0.86% (**Table 1**).

By CMR2, the 5-year estimated risk of SCD (6) was also marginally higher (2.31±1.44%, p=0.01) at CMR2 (**Table 1**). Other baseline characteristics did not vary significantly.

Table 1. Clinical characteristics of patients at CMR1 and CMR2

	CMR 1 (n=72)	CMR 2 (n=72)	p-value
Age (years)	45 ±12	51 ±12	<0.001
Male, % (n)	68 (49)	68 (49)	1 .00
Body mass index (kg/m$^{2)}$	27±5	27±5	0.08
Hypertension % (n)	10 (7)	11 (8)	1.00
Diabetes % (n)	3 (2)	6 (4)	0.68
Smoker, % (n)	7 (5)	6 (4)	1.00
Atrial fibrillation, % (n)	7 (5)	10 (7)	0.76
SCD risk			
Family history of SCD, % (n)	26 (19)	26 (19)	1.00
Unexplained syncope, % (n)	4 (3)	4 (3)	1.00
NSVT on Holter monitor, % (n)	10 (7)	24 (17)	0.04
Abnormal exercise BP response, % (n)	1 (1)	3 (2)	1.00
Maximum LV wall thickness ≥30 mm, % (n)	4 (3)	4 (3)	1.00
LV outflow tract gradient, % (n)	15 (11)	15 (11)	1.00
NYHA Class I,II,III,IV, % (n)	82,14,4,0 (59,10,3,0)	67,25,8,0 (48,18,6,0)	0.11
ESC risk score (%)	2.01±0.86	2.31±1.44	0.01
SCD risk factors (0/1/2/3 risk factors), %(n)	61,33,6,0 (44,24,4,0)	47,46,6,1 (34,33,4,1)	0.29
Medications			
β-Blockers, % (n)	50 (36)	65 (47)	0.06
Calcium channel blockers, % (n)	8 (6)	17 (12)	0.27
Disopyramide, % (n)	6 (4)	15 (11)	0.09
ACEI/ ARB, % (n)	14 (10)	14 (10)	1.00
Diuretics, % (n)	6 (4)	7 (5)	1.00
Aspirin, % (n)	25 (18)	47 (34)	0.006
Warfarin, % (n)	6 (4)	11 (8)	0.36

Data are mean±standard deviation. ACEI angiotensin converting enzyme inhibitor; ARB angiotensin receptor blocker; BP blood pressure; ESC European Society of Cardiology; HCM hypertrophic cardiomyopathy; LVOT left ventricular outflow tract; NSVT Non sustained ventricular tachycardia; NYHA new York Heart Association; SCD sudden cardiac death.

Forty-five (63%) patients had sarcomeric mutations; three (4%) had mitochondrial mutation; three (4%) had a variant of uncertain significance in a sarcomeric gene; no pathogenic mutation was found in 21 (29%) of patients (**Table 2**). Nine patients were pre-hypertrophic (max left ventricular wall thickness or LVWT≤13mm) sarcomeric mutation carriers (Sarc+P-).

Table 2. Genotype and patterns of hypertrophy in HCM patients

Genotype	
MYH7, %(n)	26(19)
MYBPC3, %(n)	32(23)
ACTC1, %(n)	1(1)
TNNI3, %(n)	1(1)
MYL, %(n)	1(1)
Mitochondrial, %(n)	4(3)
VUS (MYBPC3, MYH7)	4(3)
Gene negative, %(n)	29(21)
Pattern of hypertrophy (113)	
Normal, %(n)	13(9)
Septal, %(n)	64(46)
Reverse septal, %(n)	3(2)
Mid-ventricular, %(n)	0(0)
Apical, %(n)	9(6)
Concentric, %(n)	12(9)

ACTC1 Alpha cardiac actin; HCM; beta-myosin heavy chain; Hypertrophic cardiomyopathy; MYH7, Myosin heavy chain, MYBPC3, myosin-binding protein C, TNNI3, Troponin I, MYL myosin regulatory light chain.

Influence of field strengths and contrast agents on LGE progression

In this observational study, 16/72 patients had follow-up CMR at different field strengths. Despite this, there was no association between changing field strength and fibrosis progression (β=-0.08, p=0.64). We further assessed if the use of a specific combination of GBCA was associated with LGE progression. On univariate analysis, there was no association between the varying GBCA combinations and LGE progression (β -0.73, p =0.10).

Left ventricular volumes, function, mass, and LGE from CMR1-CMR2

The mean LV end-diastolic volume (LVEDV), ejection fraction (LVEF) and mass at CMR1 were 152±30ml, 67±6% and 146±52g respectively. LVEDV and LVEF did not differ between CMR1-CMR2 (**Table 3**). In contrast, a significant increase in LV mass between scans was detected (146±52g vs 151±52g, p=0.02). Modest reductions in both peak LV global circumferential (GCS) and longitudinal (GLS) strain were also seen from CMR1 to CMR2 (GCS -18±3% vs -17±4%, GLS -17±3% vs -16±3%, p<0.05 for both) with no significant difference seen in global radial strain (GRS).

LGE was present in 75% of HCM patients at CMR1, increasing to 82% at CMR2 (**Table 3**). LGE mass progressed from a median 4.98g (IQR 0.97–13.48g) on CMR1 to 6.30g (IQR 1.38-17.51g) on CMR2 (**Figure 2**). The median increment was 1.15g (95% CI 0.42 g to 2.07g, p<0.0001). As a relative proportion of LV mass, the median increment was 0.74% (95% CI 0.25–1.27%, p<0.0001) from CMR1–CMR2 (**Figure 2**).

Table 3. Comparison of CMR indices for all patients from CMR2 to CMR2.

CMR findings	CMR1	CMR2	P value
LVEF, %	67±6	67 ±7	0.44
LVEDV (ml)	152±30	155±32	0.12
LVEDV index (ml/m^2)	79±14	79±14	0.43
LVESV (ml)	51±15	51±18	0.67
LA diameter (in LVOT view)	37±6	37±7	0.37
Stroke volume (ml)	101±19	104±20	0.11
LV Mass (g)	146±52	151±52	0.02
LV Mass index (g/m^2)	75±25	76±27	0.15
Max LVWT(mm)	19±6	19±5	0.79
Presence of LGE, % (n)	75%(54)	82%(59)	0.31
LGE mass (g)	4.98g (IQR 0.97–13.48g)	6.30g (IQR 1.38-17.51g)	<0.0001

Data are mean±standard deviation except for LGE (median and IQR)

EDV end-diastolic volume; EF ejection fraction; ESV end-systolic volume; LA left atrial; LGE late gadolinium enhancement (5-SD); LV Left ventricular; OT Outflow tract obstruction; LVWT Left ventricular wall thickness.

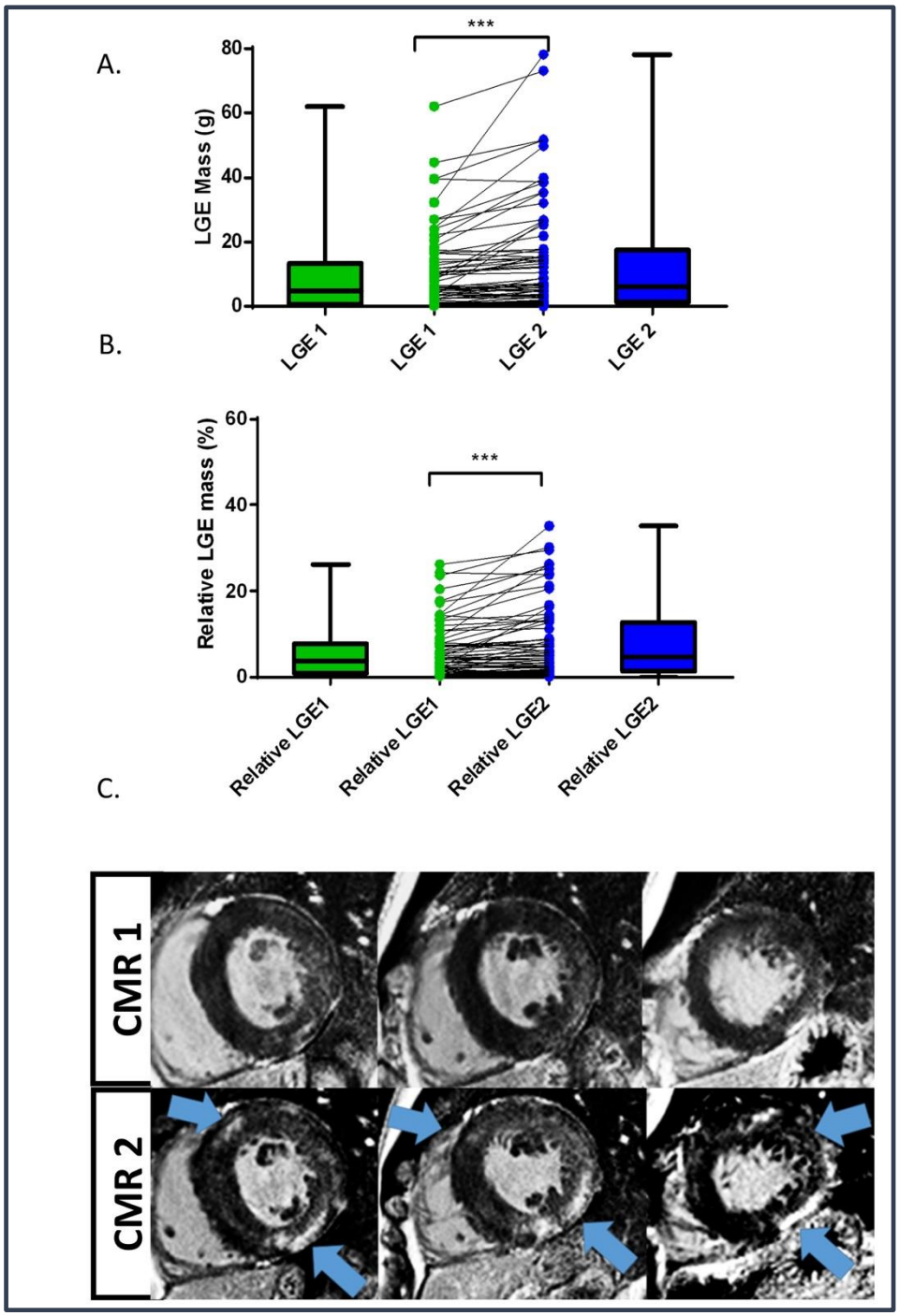

Figure 2. Comparison of late gadolinium enhanced (LGE) mass (A) and relative LGE mass (B) from CMR1 to CMR2 (error bars represent median with minimum and maximum; ***p<0.0001) (C) A representative case of fibrosis progression in HCM (Blue arrows indicate new regions of fibrosis which are enhanced on LGE imaging)

Relationship between left ventricular wall thickness and LGE progression

Maximum end-diastolic left ventricular wall thickness (LVWT) did not differ significantly between the two CMR scans (19±6mm vs 19±5mm, p=0.79) (**Table 3**). Thirty-two (45%) had stable LVWT on follow up, 24 (33%) had a modest increase (3.0±1.6mm) in LVWT, and 16 (22%) patients had a reduction of LVWT. Seven (10%) had a reduction of >3mm. Interestingly, patients with regression of wall thickness (WT-) had a significantly greater extent of LGE increment (**Figure 3 A, B**) versus those with stable or increasing LVWT (WT0/+) with a median LGE difference of 6.92g (95% CI 2.72–10.40g, p<0.0001) between groups. Two individuals with LVWT regression may have been reclassified to a lower SCD risk group based on the assessment of traditional SCD risk factors at CMR2 alone. Maximum LVWT at CMR1 correlated moderately with LGE progression (r=0.36, p<0.002). At CMR2, a weaker association was seen between LVWT and LGE progression (r=0.28, p=0.03). With regards to morphological variants, there was no significant difference in LGE increment between apical (n=6) and non-apical HCM.

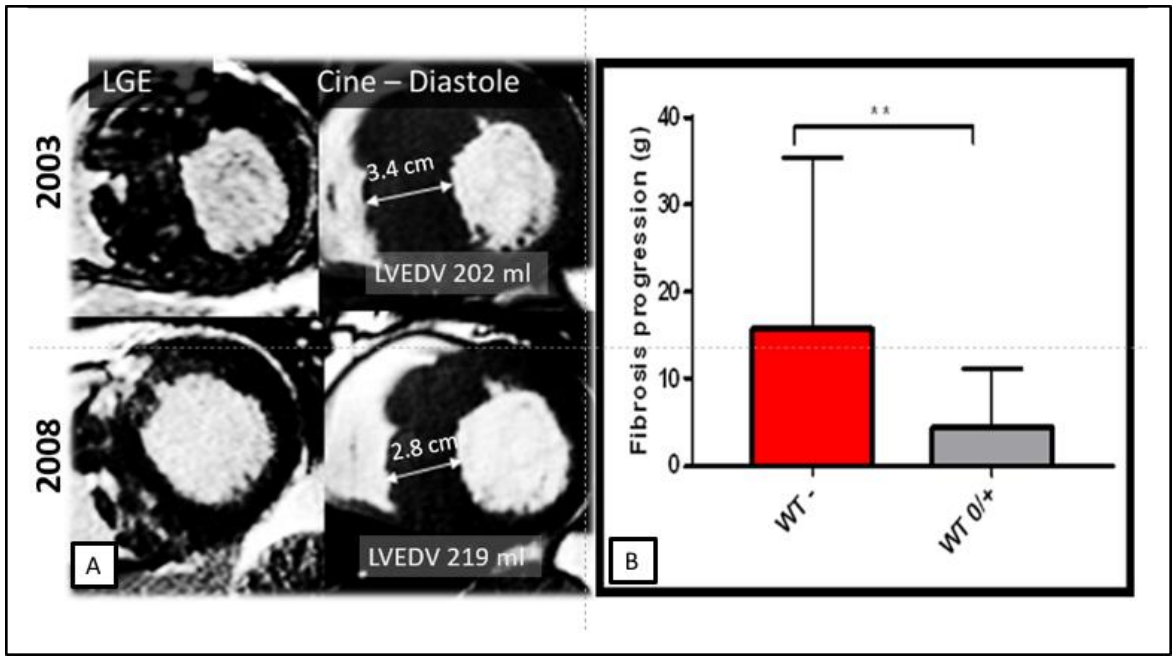

Figure 3. (A) Illustrative case of fibrosis progression (increase in regions of white hyperenhancement) on a transverse slice of the heart in a HCM patient over a five year (2003 to 2008) CMR interval demonstrating thinning (3.4 cm→2.8cm) of myocardium (B) Regression of wall thickness wall thickness (WT-) was associated with more extensive fibrosis progression (Error bars represent standard deviation, ** $p<0.001$; Cine non-contrast cine or movie images of the heart; LGE late gadolinium images; WT- HCM cases where wall thickness decreased, WT+/0 HCM cases where there was an increase or stable wall thickness).

Clinical outcomes and diagnostic ability of substantial LGE progression to predict clinical events

Out of the final cohort of 72 patients, eight underwent primary prevention ICD implantation subsequent to CMR2. There were no deaths, aborted cardiac deaths or appropriate ICD shocks. Twenty-four had clinical events as previously defined. Nine had a progression of heart failure. Three had hospital admission for heart failure or arrhythmia. New onset ventricular tachycardia was detected in 13 patients. All cases of new onset NSVT were detected on 24 hour ECG monitor prior to the implantation of a device. LGE progression ≥4.75g had a good specificity 93% (95%CI 85-97%) and reasonable sensitivity 63% (95%CI 53-72%), AUC 0.74, (95%CI 0.60-0.88), p<0.001) for predicting clinical events and is referred to as substantial progression (Appendix **Figure 1**). LGE increment ≥4.75g was seen in 26% (n=19) of patients. Amongst those with any LGE at baseline, 41% developed a clinical event during the follow-up period (CMR1 to end of study). In contrast, 79% of those with ΔLGE≥4.75g developed a clinical event on follow up. In a univariate Cox regression analysis, maximum LVWT on CMR1, initial LGE mass, ΔLGE≥4.75g were significant predictors of clinical outcomes (**Table 4**). On multivariable analysis, ΔLGE≥4.75g remained an independent predictor of the outcome after adjusting for age at outcome, maximum LVWT and LGE mass at CMR1 (HR 5.04, 95% CI 1.85–13.79, p=0.002) (**Table 4**). HCM patients with ΔLGE≥4.75g had significantly lower freedom from clinical events compared to others. Similarly, patients with baseline LGE of ≥15% of LV mass had low freedom from clinical events but to a lesser extent than LGE progression (**Figure 4 A, B**)

Table 4. Association of baseline LGE mass and LGE progression with composite clinical endpoint

Univariate Cox	HR	95% CI	p-value
Age at outcome	0.98	0.95-1.01	0.36
Gender	0.83	0.36-1.91	0.66
Maximum LVWT at CMR1	1.10	1.03-1.17	0.007
LV mass at CMR1	1.01	0.99-1.01	0.12
LGE mass at CMR1	1.04	1.01-1.07	0.002
LGE Progression ≥4.75g	5.53	2.39-12.78	<0.001
Interval between CMR1-CMR2 (days)	1.00	0.99-1.00	0.39
LVEF CMR1	1.01	0.94-1.08	0.85
Apical vs non apical hypertrophy	2.21	0.63-7.33	0.22
Genotype*	1.94	0.66-5.69	0.23
Baseline SCD risk factors	0.51	0.21 -1.25	0.14
Multivariable Cox	**HR**	**95% CI**	**p-value**
Age at outcome	0.98	0.94-1.01	0.19
Maximum LVWT at CMR1	1.07	0.96-1.19	0.25
LGE mass at CMR1	0.98	0.94-1.03	0.52
LGE Progression ≥4.75g	5.04	1.85-13.79	**0.002**

CI confidence interval; CMR Cardiac magnetic resonance imaging; HR hazard ratio; LVEF left ventricular ejection fraction; LVWT left ventricular wall thickness, SCD sudden cardiac death;* Sarcomeric and mitochondrial mutations versus genotype negative

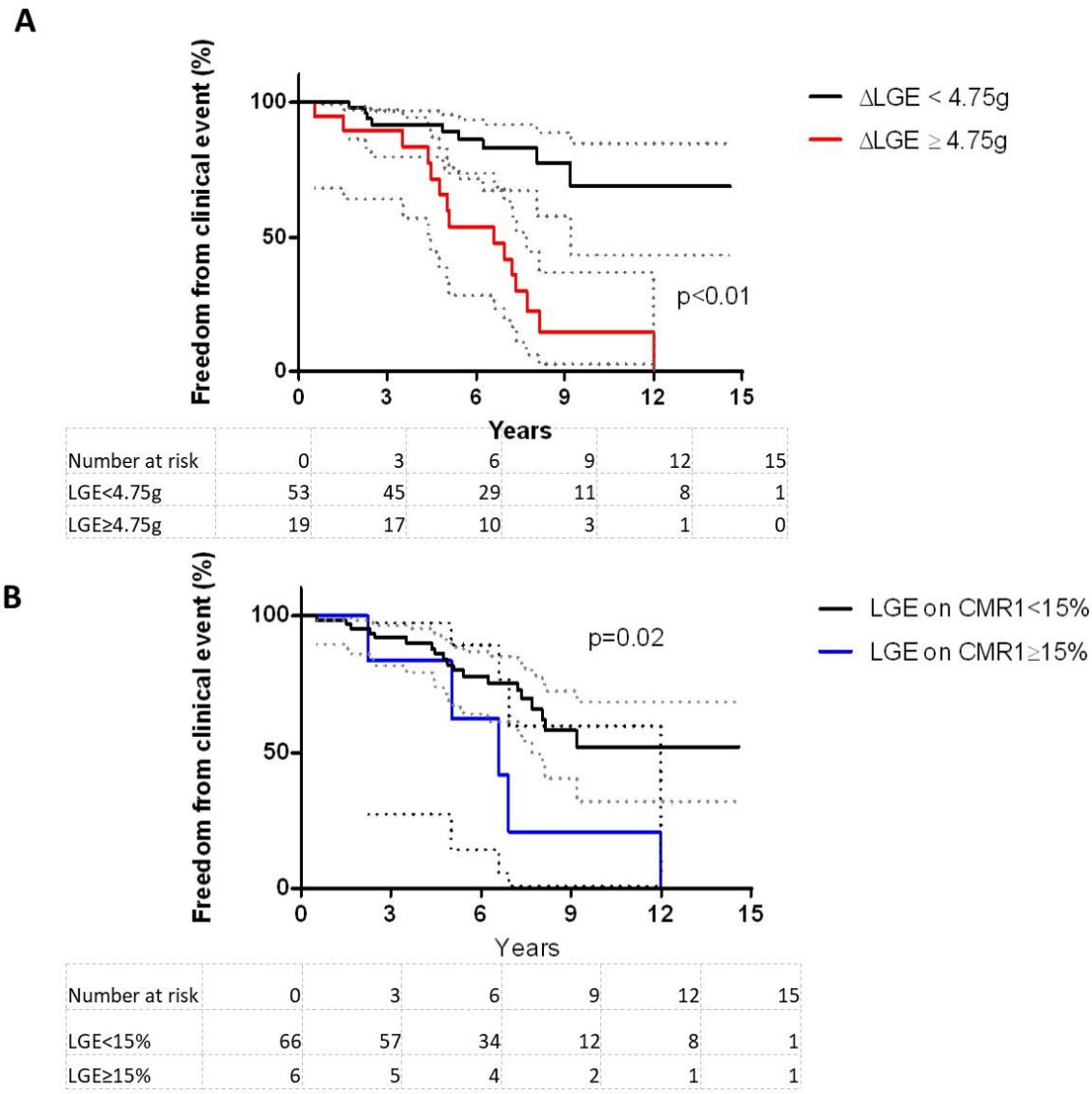

Figure 4. (A) Kaplan Meier curves depict freedom from clinical events in HCM patients with LGE increment ≥ 4.75g or less and (B) in those with LGE on CMR1 ≥15% of LV mass or less (Error bars represent 95 % confidence intervals).

Predictors of substantial LGE progression

On univariate analysis, maximum LVWT, LV mass and LGE mass at CMR1 were significant predictors of ΔLGE≥4.75g (**Table 5**). The scan interval between CMR1 and CMR2 and apical phenotype were not predictors of LGE progression. On multivariable analysis, only LGE mass at CMR1 remained a predictor of ΔLGE≥4.75g (**Table 5**).

Table 5. Univariate and multivariable predictors of ΔLGE≥4.75g

Univariate analysis	OR	95% CI	p-value	Multivariable analysis	OR	95% CI	p-value
Age at CMR1	1.01	0.97-1.06	0.70	Age at CMR1	1.01	0.95-1.07	0.70
Max LVWT at CMR1	1.25	1.10-1.42	0.001	Max LVWT CMR1	1.14	1.10-1.34	0.14
LV mass at CMR1	1.01	1.01-1.03	0.005	LV mass at CMR1	0.99	0.99-1.01	0.94
LGE mass at CMR1	1.13	1.06-1.21	<0.001	LGE mass at CMR1	1.10	1.02-1.19	0.02
LVEF at CMR1	0.94	0.86-1.02	0.13				
Interval between CMR1-CMR2 (days)	1	1.00-1.01	0.50				
Genotype*	1.93	0.55-6.73	0.30				
Apical vs non apical hypertrophy	1.44	0.24-8.59	0.68				
Baseline SCD risk (0 or ≥1)	0.47	0.15-1.48	0.19				

CI confidence interval; CMR cardiac magnetic resonance imaging; LGE late gadolinium enhancement; LV left ventricular; LVEF left ventricular ejection fraction; LVWT left ventricular wall thickness, OR odds ratio; SCD sudden cardiac death; *Genotype refers to sarcomeric and mitochondrial mutations (0) versus genotype negative (1)

Role of genotype

None of the nine Sarc+P- patients had substantial LGE progression over a CMR interval of 6±3 years. LGE progression was greater in sarcomeric HCM (Sarc+HCM) (2.79g IQR 1.12–7.39g, p<0.01) versus Sarc+P- patients (0.17g IQR-0.18-1.03g) (**Figure 5**). In patients with hypertrophy, differences in LGE increments could also be seen between those with and without sarcomeric mutations (**Figure 5**). Mitochondrial mutation carriers had the highest median LGE increment of 23.16g (IQR 16.84–45.78g) (p<0.01 for all comparisons) followed by sarcomeric HCM 2.79g (IQR 1.12–7.39g) and then genotype negative patients 0.52g (IQR -0.38–2.43, p=0.01 for comparison between G-HCM and Sarc+HCM) (**Figure 5**).

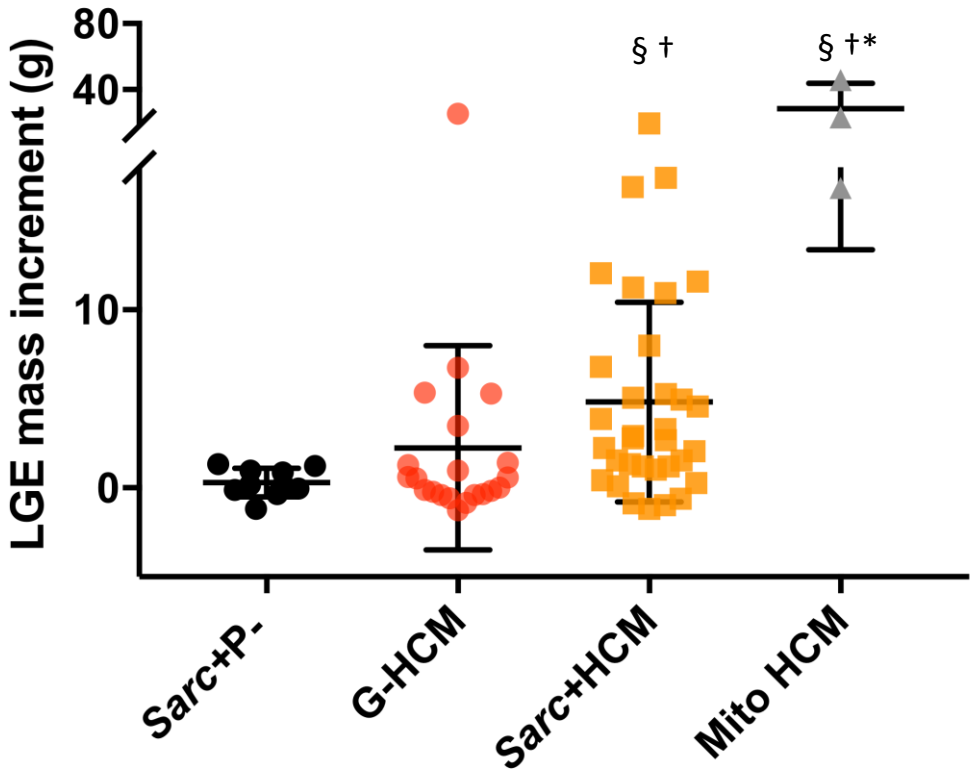

Figure 5. Comparison of LGE increment between genotype groups. Sarcomeric HCM (Sarc+HCM) and mitochondrial HCM (Mito HCM) had significantly greater LGE progression compared to genotype negative (G-HCM) and pre-hypertrophic sarcomeric mutation carriers (Sarc+P-). (Error bars represent mean±SD; $p<0.05$: † comparison with Sarc+P-; § comparison with genotype negative, *comparison with Sarcomeric HCM)

3.6 DISCUSSION

The present study demonstrates that after a median period of six years, both the prevalence and extent of LGE in HCM increases. Maximum wall thickness may regress due to a progression of LGE. Substantial LGE progression is associated with a significantly higher risk of clinical events. The extent of fibrosis on a baseline scan (CMR1) can help identify those at risk of substantial LGE progression. Energy costly mutations are associated with a greater extent of fibrosis progression after the development of left ventricular hypertrophy.

LGE progression predicts the occurrence of clinical events in HCM

In hypertrophic cardiomyopathy, late gadolinium imaging measures myocardial fibrosis or scarring with a high degree of sensitivity (49). Areas of delayed enhancement correlate well with histologically proven myocardial scar (49, 52). Recent studies suggest that LGE or replacement fibrosis is not static and that an increase in LGE may be detectable in HCM patients as early as 1.5 to 2 years from the first scan (37, 105). In line with others, we found that there was a progression of LGE in HCM patients.

The cross-sectional assessment of LGE has been shown to be a valuable marker of poor prognosis in HCM with a recent metanalysis of pooled data from 2993 patients confirming the strong association between myocardial fibrosis and cardiovascular mortality (114). Here, we show for the first time that monitoring LGE progression has the potential to further refine risk stratification in HCM. Substantial LGE progression ($\Delta LGE \geq 4.75g$) was associated with a five-fold increased risk of the composite clinical endpoint in a model adjusted for the extent of baseline LGE and left ventricular

hypertrophy. These findings emphasise the importance of longitudinal assessments of LGE as a dynamic pathological process. Although LGE was seen in the majority of individuals at baseline, only 41% of them experienced a clinical event. In contrast, 79% of those with LGE progression had a clinical event highlighting the common discordance between LGE prevalence and clinical outcomes. Therefore, assessing the temporal profile of disease activity (LGE progression) rather than just the presence of LGE, a 'fossil' of disease activity, may help identify those at risk of clinical deterioration. This is further illustrated by the freedom from clinical event curves which show that LGE progression was better than baseline LGE extent ≥15% at CMR1 at predicting clinical events.

Determinants of clinically relevant fibrosis progression

With the rising burden of health care costs worldwide (115), the use of diagnostic tests without clinical benefit is increasingly being scrutinised. Hence, defining patients groups most likely to benefit from closer monitoring can be a cost-effective strategy. The early identification of factors that associate with progression also provides the added benefit of helping one select well characterised patient groups suitable for specific pharmacotherapy to slow and prevent fibrosis progression in HCM.

Previous studies examining LGE progression on interval CMR have found the pattern of hypertrophy (apical versus non-apical) (37) and initial LGE burden (37, 105) to be important in predicting fibrosis progression. In the present study, we found only baseline LGE or the initial LGE burden to be a significant predictor in a multivariable model, while apical phenotype did not predict LGE progression. One possible

explanation is that the number of apical HCM were small in this study. Hence, more adequately powered studies are required to test the association between specific phenotypes and fibrosis progression. Consistent with others (37), we also found that the interval between CMR1 and CMR2 did not a predict LGE progression, indicating that LGE is highly varied and not necessarily time dependent.

Regression of left ventricular hypertrophy may be associated with LGE progression

In the management of HCM patients, the general perception of clinicians is that the more severe the hypertrophy, the greater is the risk. However, a few studies have shown that patients with a maximum wall thickness of ≥35 mm are not necessarily at a higher risk of SCD compared with patients with less hypertrophy (116, 117). The assessment of wall thickness, in isolation, may therefore not comprehensively reveal hidden risks seen in HCM. Indeed, the present study provides an explanation for these observations.

Here, we found that while some patients developed an increase in maximum wall thickness on interval CMR, others had thinning or regression of maximum wall thickness. In those with significant thinning, LGE mass was significantly higher on interval CMR. As the extent of LGE mass strongly associates with arrhythmic risk (118), the finding that maximum wall thickness alone may be insufficient in predicting SCD risk in HCM is not surprising. These observations highlight the complex relationship between progression of LGE and degree of left ventricular hypertrophy which may inform clinical protocols for follow-up surveillance.

Role of genotype and fibrosis progression

Here we examined the significance of underlying genotype and LGE progression in HCM for the first time. Genotype did not associate with LGE progression, possibly due to the inclusion of Sarc+P- patients in our cohort who did not develop hypertrophy or significant LGE progression. Indeed, in a previous study by Ho *et al.* , the lack of LGE in Sarc+P- patients despite evidence of increased collagen synthesis, was posited to be due to a compensatory increase in collagen degradation (45). In the same study, patients with sarcomeric mutation and overt hypertrophy lost this equilibrium between collagen synthesis and degradation resulting in a significantly higher LGE burden (45). In line with this, we found that sarcomeric mutation carriers with overt hypertrophy (Sarc+HCM), had more severe progression in LGE than Sarc+P-. Interestingly, Sarc+HCM also demonstrated more progression than G-HCM patients (70). These findings suggest that factors arising either directly from the expression of sarcomeric mutations or due to modifier gene effects (119, 120) possibly promote both hypertrophy and fibrosis in sarcomeric HCM (46). Another observation from the present study was the high rates of progression in the three mitochondrial patients, never previously described. Previous studies in transgenic mouse models indicate that increased ATP utilisation, and altered calcium-dependent signalling and mitochondrial dysfunction may play a central role in disease progression in HCM (121). Our data provide further evidence that HCM characterised by ‘energy costly’ mutations are at greatest risk for fibrosis progression following the onset of left ventricular hypertrophy (122). The validation of these findings in larger genotyped HCM cohort will hence be necessary.

3.7 CLINICAL IMPLICATIONS

Current management of HCM patients involves a combination of clinical assessment, electrocardiogram (ECG), and echocardiography at intervals of 1-2 years from adolescent to adulthood and at frequencies of 2-5 years after adult hood for monitoring of disease activity (6, 123). Contemporary guidelines recommend the use of CMR only to clarify the extent of hypertrophy in patients with suboptimal imaging (124). However, echocardiography remains limited in its ability to provide more in-depth information on myocardial tissue characteristics such as fibrosis burden. By contrast, CMR can provide precise measurements of left ventricular wall thickness, volumetric indices and myocardial pathology such as myocardial fibrosis. Additionally, here we show that the assessment of maximum wall thickness, without knowledge of LGE burden, can potentially miss hidden risks in HCM patients. More adequately powered multicentre studies are therefore required to examine the clinical utility of LGE progression in predicting hard endpoints.

3.8 STUDY LIMITATIONS

This study is limited by the small sample size with low SCD risk due to the exclusion of those with ICD after CMR1. LGE technique used in this study detects mostly focal fibrosis. More novel methods for diffuse fibrosis assessment such as native and post contrast T1 mapping were not used in this study due to the lack of availability of such methods in previous scans (before 2011). The accuracy of prevalence estimates of LGE progression may also be limited due to the small sample size. In this study, histological validation of LGE progression by endomyocardial biopsy was not feasible.

However, previous studies of septal myomectomy and endomyocardial biopsies from HCM patients confirm a strong correlation between the extent of myocardial fibrosis detected on biopsy and LGE on CMR (52, 125). We acknowledge that the use of different contrast agents at CMR1 and CMR2 and different field strengths for some patients on serial CMR assessments are potential limitations of this study, but there was no evidence that these factors affected the rate of LGE progression. Despite our encouraging data, given the lack of hard clinical endpoints in our cohort, the prognostic value of LGE progression for major cardiovascular events requires further investigation – in this context, the recent large international multicenter Hypertrophic Cardiomyopathy Registry study (HCMR; n=2764) could provide an ideal platform for repeat imaging of phenotype progression over time (126).

3.9 CONCLUSIONS

Myocardial fibrosis is progressive in HCM patients, and substantial LGE progression (≥4.75g) is associated with an increased risk of future clinical events. Baseline LGE can help identify those at risk of LGE progression. Energy costly mutations may confer an increased risk of fibrosis progression after left ventricular hypertrophy develops.

.

CHAPTER 4: ROLE OF MICROVASCULAR DYSFUNCTION AND MYOCARDIAL ENERGETICS IN FIBROSIS PROGRESSION

4.1 ABSTRACT

Background: In hypertrophic cardiomyopathy (HCM), mechanisms underlying fibrosis or late gadolinium (LGE) progression are unclear. Microvascular dysfunction and impaired energetics are believed to play a pathophysiological role.

Objective: To examine if impaired myocardial perfusion and energetics in HCM relate to progression of myocardial fibrosis and describe the effects of substantial LGE progression on left ventricular remodelling.

Methods and results: Seventy-two HCM patients had two CMR (CMR1-CMR2) at an interval of 5.7±2.8 years. In a subset of 38/72 patients, stress perfusion imaging and cardiac energetics were undertaken at baseline CMR (CMR1). HCM patients with impaired myocardial perfusion reserve (MPRI<1.40) and energetics (phosphocreatine/adenosine triphosphate<1.44) on baseline CMR had higher LGE progression than those with preserved perfusion (median 9.00g IQR 1.47–17.91g vs 0.74g IQR -0.08–2.37g, p<0.01) and energetics (median increment 7.99g IQR 5.01–17.41g vs 1.20g IQR -0.05–25.39, p=0.01). In those with clinically relevant LGE progression (ΔLGE≥4.75g), myocardial perfusion and energetics were impaired at baseline. ΔLGE≥4.75g was associated with left ventricular dilatation and reduced systolic function.

Conclusion: Impaired myocardial energetics and perfusion abnormalities are possible mechanistic drivers of the fibrotic process, which in turn, is associated with adverse left ventricular remodelling and dysfunction in HCM.

4.2 INTRODUCTION

In the last 60 years, it has become increasingly apparent that hypertrophic cardiomyopathy (HCM) is common cardiomyopathy with the risk of rare but devastating complications of sudden cardiac death, stroke and heart failure (127). In an attempt to improve risk stratification, considerable efforts have been undertaken to identify novel molecular, genetic and phenotypic markers of risk (128, 129). Late gadolinium enhancement (LGE) on cardiac magnetic resonance imaging (CMR) is one such promising biomarker and measures the burden of myocardial fibrosis (49, 52), a potent substrate for fatal arrhythmias and heart failure (21, 53). Recent studies suggest that LGE in HCM may be evolutive, with evidence of LGE progression seen in adults (37, 105) and children (104) with HCM. However, the causal mechanisms underlying fibrosis progression are poorly understood.

For years, it has been observed that the myocardium in HCM exhibit abnormalities in substrate metabolism and vascular remodelling (38, 60). For example, an impaired phosphocreatine to adenosine triphosphate concentration ratio (PCr/ATP) on phosphorus magnetic resonance spectroscopy (^{31}P-MRS) has been reported in pre-hypertrophic sarcomeric mutation carriers and may play a critical role in the pathophysiology of HCM (38, 130). Similarly, microvascular abnormalities have been extensively described on histological studies (20, 55) and believed to trigger fibrosis progression in HCM, promoting contractile dysfunction (30, 131). Dissecting the pathophysiological factors that cause fibrosis, rather than merely associate, remains a challenge.

In this chapter, the relationships between both microvascular dysfunction and impaired energetics at a single time point and the subsequent increase or change in LGE were examined, and the functional consequence of substantial LGE progression on cardiac remodelling are described.

4.3 METHODS

Population

This work was approved by the local ethics committee (reference: 07/Q1607/66, 12/LO/1979). The inclusion and exclusion criteria for this study are outlined in Chapter 2. Briefly, a total of 88 patients were enrolled as discussed in Chapter 3. Of them, 16 were excluded after CMR1 leaving 72 patients with two CMR scans (CMR1-CMR2). Of the 72 with serial CMR, 38 had an assessment of myocardial perfusion and energetics at baseline or CMR1 only (**Figure 1**).

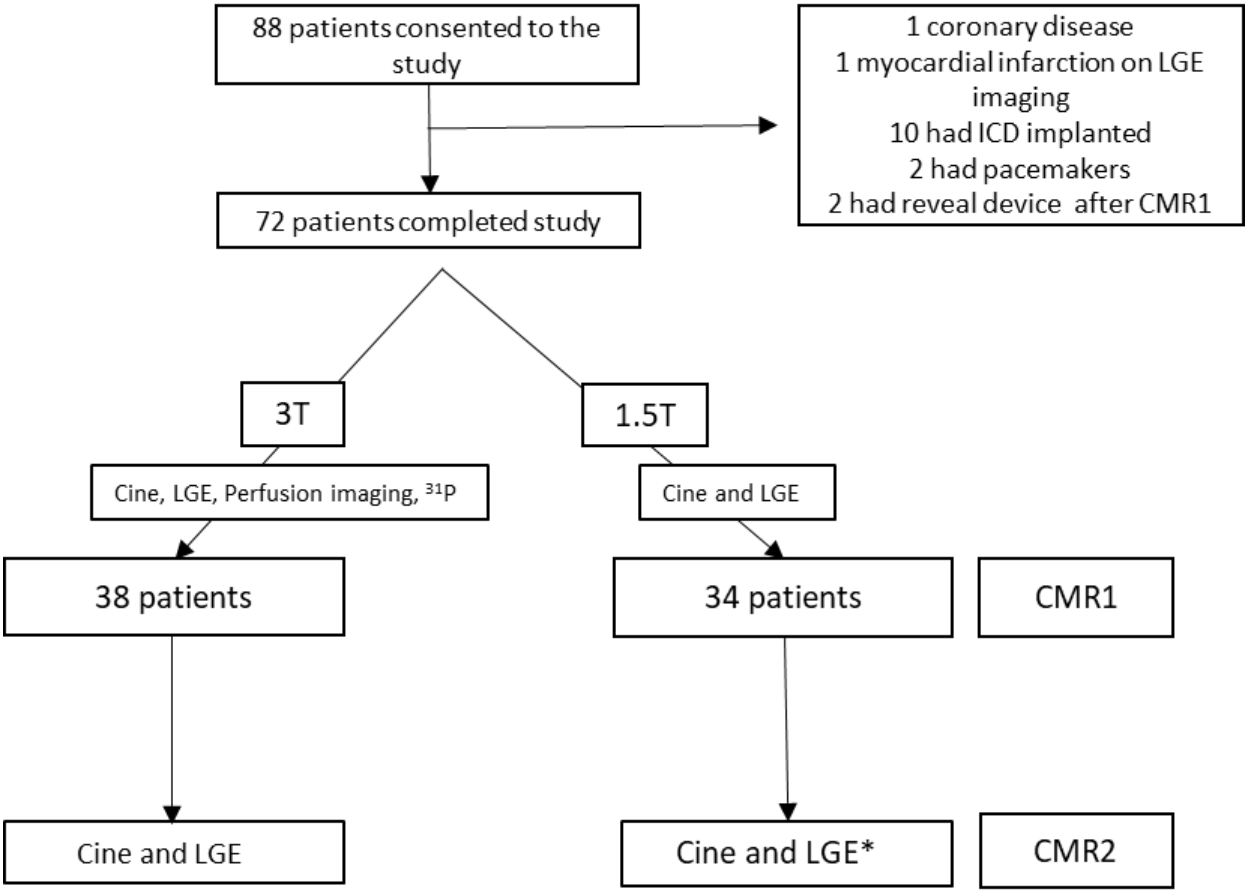

Figure 1. Flowchart of HCM patients through the study. (CMR cardiovascular magnetic resonance imaging, LGE Late gadolinium imaging, ^{31}P Phosphorus - 31 Spectroscopy, ICD Implantable cardioverter defibrillator, T Tesla). *CMR2 was at 1.5T or 3T (see supplemental section)

CMR Protocol

Cine and LGE imaging were undertaken in all 72 patients as described in Chapter 3.

In 38 (out of 72) patients, perfusion imaging was undertaken (before LGE imaging) only at CMR1 (3 Tesla; 3T) using a T1-weighted gradient echo sequence with saturation recovery magnetisation preparation (echo time 0.99 ms, repetition time 2 ms, saturation recovery time 95 ms, voxel size 2.1 × 2.6 × 8 mm^3, flip angle 17°, slice thickness 8 mm). Adenosine was used as pharmacological stress at a rate of 140µg/kg/min and up-titrated by the haemodynamic response. Three short axis slices (base, mid and apex) were acquired. A dose of 0.03 mmol/kg of Gadolinium-based contrast agent (GBCA) (refer to Chapter 3 for details) was injected at 6ml/sec during stress followed by a saline flush 12ml at 6ml/sec and the same dose for rest acquisition. Three patients were excluded (failure of contrast injection (n=2) or intolerance to adenosine (n=1)). The remaining patients were adequately stressed as evidenced by the presence of appropriate hemodynamic response and splenic switch off (69, 95).

^{31}P MRS was performed at CMR1 (3T) before cine LGE and perfusion imaging, to measure myocardial energetics in the same 38 HCM patients. Subjects were placed prone with their hearts over the center of the coil as previously described (95). The phosphocreatine (PCr) to adenosine triphosphate (ATP) ratio (PCr/ATP) from a mid-ventricular septal voxel in a position matching mid ventricular perfusion slice was obtained (95). A 3-dimensional acquisition-weighted chemical shift imaging technique (3D UTE-CSI) was used with an acquisition matrix of 16 x 8 x 8 over the field of view of 240 x 240 x 200 mm^3 with 10 averages at the centre of k-space (132). The sequence

used the ultrashort echo time (UTE) approach to minimise T_2 effects and first-order phase artefacts. The total acquisition time was ~9 min. An optimised radiofrequency pulse centred between the γ- and α-ATP resonance frequencies was used to ensure uniform excitation of all spectral peaks. Five Nuclear Overhauser Effect (NOE) pulses (2.5 ms, 222.2 V separated by 80.5 ms) were used to increase signal to noise. Three 25-mm-thick saturation bands were used to minimise signal contamination in the heart, 2 placed over chest wall muscle and 1 placed over liver. The chemical shift imaging grid was placed with a central voxel in the mid-ventricular septum and rotated to maximise coverage of the septal myocardium (95).

CMR Image analysis

As described in Chapter 2, a commercially available software (Circle Cardiovascular Imaging Inc., Calgary, Canada) was used to analyse left ventricular (LV) volumes, mass, ejection fraction, peak systolic 2-D global longitudinal, circumferential and radial strain. Assessment of left ventricular indices and LGE mass were undertaken by two observers blinded observers. Quantitative analysis of LGE was undertaken by setting a signal intensity threshold at five standard deviations (5-SD) above the mean intensity of a reference region of interest placed in a remote area of myocardium with no visual evidence of enhancement (52, 110).

For perfusion analysis, signal intensity curves were generated to measure myocardial perfusion reserve index (MPRI) (69). A region of interest was drawn in the LV blood pool to obtain an arterial input function. Rest and post-adenosine stress myocardial perfusion up slopes were calculated using a five-point linear fit model of SI versus time

and normalised to the LV blood pool upslope. Myocardial perfusion reserve index (MPRI), defined as the ratio of stress to rest normalised myocardial perfusion upslope, was derived for 18 segments and averaged per patient (98)

Post-processing of ^{31}P-MRS data was performed using the OXSA toolbox. The spectrum from a mid-ventricular septal voxel was fitted using a custom implementation of AMARES (the advanced method for accurate, robust, and efficient spectral fitting) in the "OXSA" semi-automated spectroscopy post-processing pipeline (**Figure 1**) (96). Fitting using prior knowledge specifying 11 Lorentzian peaks (α,β,γ-ATP multiplet components, PCr, PDE, and 2x2,3-DPG) and fixed amplitude ratios and scalar couplings for the multiplets. The fitted amplitudes were then corrected for blood contamination by subtracting 30% of the average of the two 2,3-DPG signals from each of the ATP amplitudes. The remaining PCr and ATP signals were corrected for the effects of partial saturation using the flip angle at the centre of the voxel, assuming no motion effects and with literature T_1 values (96).

4.4 STATISTICAL ANALYSIS

Statistical analyses were undertaken using IBM SPSS Statistics 23.0 (IBM Corp., Armonk, NY, USA), STATA/SE 15.0 (Stata Corp, College Station, Texas USA) and GraphPad Prism 7.0 (GraphPad Software, San Diego, California, USA). Normality of data was assessed by visually inspecting the plots. Mean (with standard deviation, SD), and median (with interquartile range, IQR or confidence intervals, CI for median differences) were computed as appropriate. Paired t-test and Mann Witney tests were

used for normally distributed and non-Gaussian data respectively. Independent student t-test and Wilcoxon R was used for group differences between unpaired normally distributed and non-Gaussian data.

4.5 RESULTS

Study population

A total of 38 patients had myocardial perfusion and energetics assessment at CMR 1 out of 72 patients with paired CMR scans. Baseline characteristics of all patients (72) are listed in Chapter 3 (Table 1). Baseline characteristics of those with perfusion and energetics assessment are listed in **Table 1**.

The mean age of those with myocardial perfusion and energetics assessment at CMR1 was 46±12 years, of whom, 74% were men. The majority had a low 5-year risk of sudden cardiac death (2.3±0.4%) and 39% were treated with β-blockers.

Table 1. Baseline characteristics and CMR indices

	(n=38)
Age (years)	46 ±12
Male, % (n)	74 (28)
Body mass index (kg/m$^{2)}$	27±5
Hypertension % (n)	11 (4)
Atrial fibrillation, % (n)	3 (1)
SCD risk	
Family history of SCD, % (n)	32 (12)
Unexplained syncope, % (n)	0 (0)
NSVT on Holter monitor, % (n)	11 (4)
Abnormal exercise BP response, % (n)	0 (0)
Maximum LV wall thickness ≥30 mm, % (n)	3 (2)
LV outflow tract gradient, % (n)	18 (7)
NYHA Class I,II,III,IV, % (n)	82,14,4,0 (59,10,3,0)
ESC risk score (%)	2.27±0.42
SCD risk factors (0/1/2/3 risk factors), %(n)	89,11,3,0 (34,4,1,0)
Medications	
β-Blockers, % (n)	39 (15)
Calcium channel blockers, % (n)	11 (4)
Disopyramide, % (n)	8 (3)
ACEI/ ARB, % (n)	8 (3)
Diuretics, % (n)	3 (2)
Aspirin, % (n)	21 (8)
Warfarin, % (n)	3 (1)
CMR findings	CMR1
LVEF, %	66±6
LVEDV (ml)	149±30
LVEDV index (ml/m2)	76±16
LVESV (ml)	51±17
LA diameter (in LVOT/3 chamber view)	37±6
Stroke volume (ml)	98±19
LV Mass (g)	148±53
LGE present (%)	71(27)
LGE Mass	1.26 IQR (0.26-7.99)

Data are mean±SD except for LGE (median); ACEI angiotensin converting enzyme inhibitor; ARB angiotensin receptor blocker; BP blood pressure; EDV end-diastolic volume; EF ejection fraction; European Society of Cardiology; ESV end-systolic volume; HCM hypertrophic cardiomyopathy; LV Left ventricular; LVOT left ventricular outflow tract; LA left atrial; HCM hypertrophic cardiomyopathy; NSVT Non sustained ventricular tachycardia; NYHA new York Heart Association; SCD sudden cardiac death, LGE late gadolinium enhancement (5-SD)

Myocardial perfusion reserve and LGE progression

Adenosine first-pass perfusion imaging was successfully performed in 35 patients out of 38 at CMR1. Inducible perfusion abnormalities were seen in 25 (out 35) patients, and ΔLGE≥4.75g was seen in 13 patients. LGE progression was seen frequently in myocardial segments with inducible perfusion defects at baseline. Seven subjects developed *de novo* LGE in regions without inducible perfusion defects. Based on previous studies (133, 134), an MPRI<1.40 was considered suggestive of microvascular dysfunction. Patients with impaired MPRI on baseline CMR (CMR1) had a higher LGE increment on interval scans compared with normal MPRI (median 9g IQR 1.47–17.91g vs 0.74g IQR -0.08–2.37g, p<0.01) (**Figure 2 A**). In patients with ΔLGE≥4.75g, MPRI was severely impaired on CMR1 compared to those with ΔLGE<4.75g (1.18±0.23 vs 1.74±0.53, p=0.001) (**Figure 2 B**).

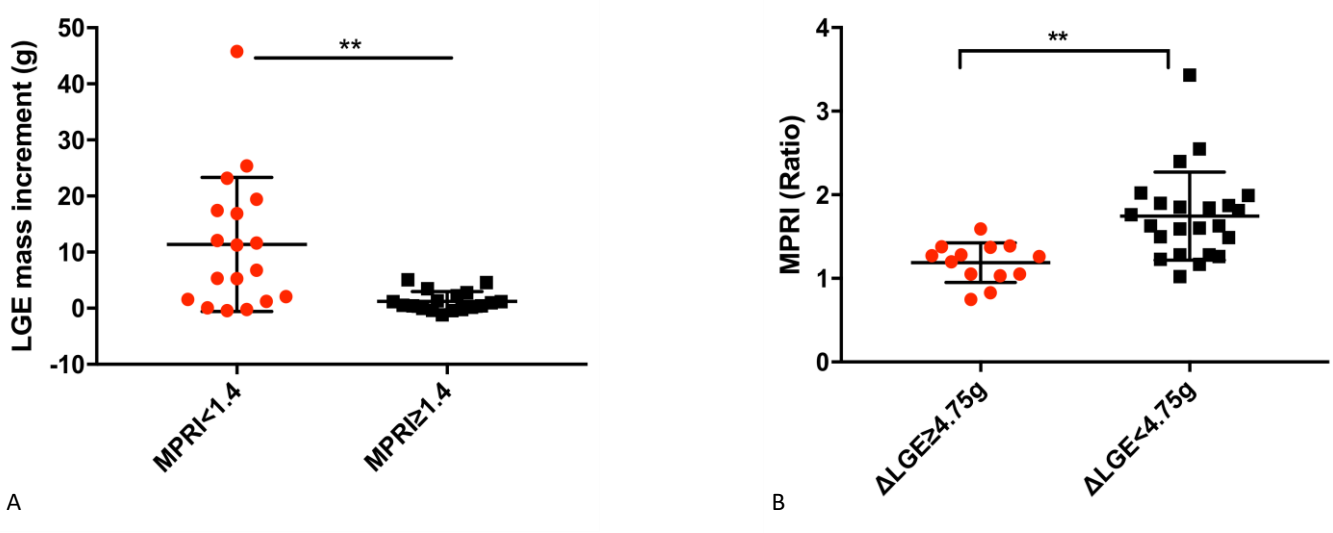

Figure 2. (A) In HCM patients with impaired perfusion (MPR<1.4) at baseline, LGE mass increased significantly from CMR1-CMR2 in HCM patients. (B) Myocardial perfusion reserve index was impaired on baseline CMR in those with substantial (ΔLGE≥4.75g) LGE progression. (Error bars represent mean±standard deviation; **p<0.01; MPRI myocardial perfusion reserve index, ΔLGE≥4.75g Late gadolinium enhancement progression of ≥4.75g,).

Myocardial energetics and LGE progression

Myocardial energetics were assessed in 38 patients at CMR1. ΔLGE≥4.75g was seen in 14 patients. An impairment in energetics was defined as less than two standard deviations of previously reported healthy range (1.71±0.35) (95). In those with impaired energetics (PCr/ATP<1.44), there was a significantly higher LGE increment on follow up compared to those with normal energetics (median increment 7.99g IQR 5.01–17.41g vs 1.20g IQR -0.05–25.39, p=0.01) (**Figure 3 A**). Additionally, patients with ΔLGE≥4.75g had reduced myocardial energetics on baseline CMR compared to those with less progression (PCr/ATP 1.58±0.34 vs 1.96±0.41, p=0.006) (**Figure 3 B**).

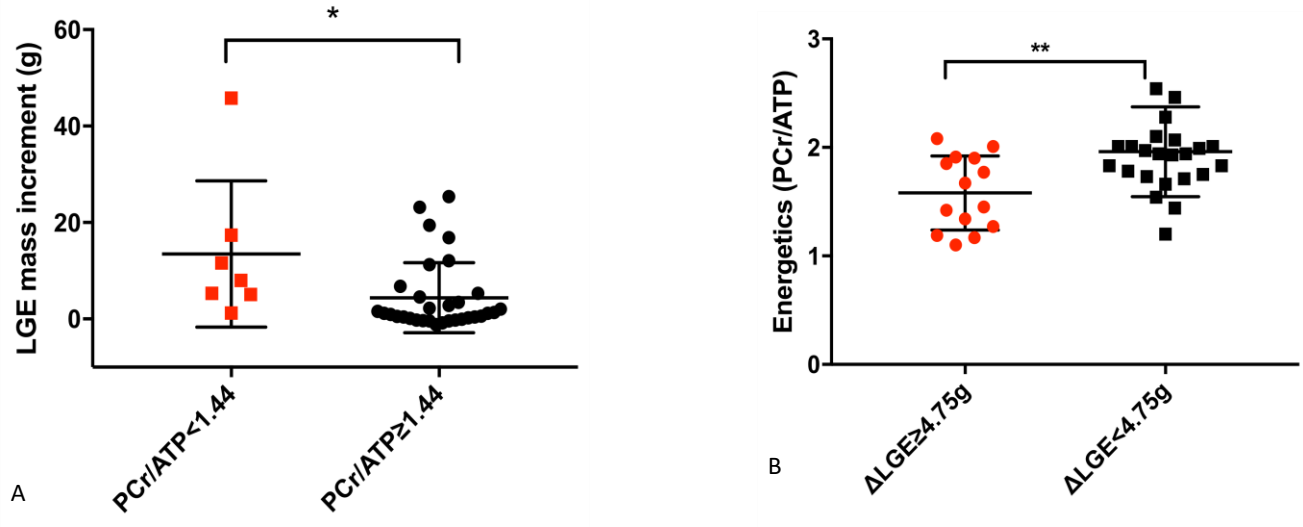

Figure 3. (A) In HCM patients with impaired myocardial energetics (PCr/ATP<1.44), fibrosis progression was greater than those with preserved energetics (PCr/ATP>1.44) (B) Myocardial energetics was more impaired in those with substantial (ΔLGE≥4.75g) LGE progression (Error bars represent mean±standard deviation; *p<0.05; **p<0.01; PCr/ATP Phosphocreatine to adenosine triphosphate ratio; ΔLGE≥4.75g LGE progression of ≥4.75g or substantial LGE increment;).

Effects of substantial LGE progression on LV volumes and function

Baseline characteristics and CMR findings of those with and without substantial progression are listed in **Table 2**. Substantial progression, ΔLGE≥4.75g (n=19/72), in HCM was associated with a significant increase in LVEDV from CMR1-CMR2 (CMR1 161±30ml vs CMR2 169±37ml, p=0.04) with a reduction in LVEF (CMR1 65±7% vs CMR2 62±7%, p=0.03) and reduction in GLS (-16±3% vs -15±3%, p=0.04). There was no difference seen in LV mass, despite these changes**.** In those with less LGE progression (ΔLGE <4.75g), LVEDV, LVEF or GLS from CMR1 to CMR2 were relatively stable.

Table 2. Baseline characteristic of HCM patients with substantial LGE progression (ΔLGE≥4.75g) versus those with less substantial progression.

	Progression of fibrosis (n=19)	Less progression (n=53)		Progression of fibrosis (n=19)	Less progression (n=53)
Age (years)	46±12	45±12	**CMR findings**		
Male%, (n)	12(63)	37(70)	LVEF, %	65±7	68±6
Body mass index (kg/m$^{2)}$	29±5	27±5	LVEDV, ml	161±30	149±29
Hypertension, (n)	1	6	LVESV, ml	56±17	49±14*
Diabetes, (n)	2	0	Stroke volume, ml	103±20	101±20
Smoker, (n)	1	4	LA diameter (LVOT view)	39±7	36±5
Family history of SCD, (n)	2	17	LV Mass, g	178±60	135±46*
Unexplained syncope, (n)	1	2	LV Mass/m^2	89±30	70±21*
NSVT on Holter monitor(n)	2	5	Max wall thickness, mm	23±5	17±5*
Abnormal exercise BP response, (n)	0	1			
Maximum LV wall thickness ≥30 mm, (n)	22±5	17±5			
LVOT obstruction (n)	3	8			
(0/1/2/3 risk factors), (n)	14,4,1,0	30,20,3,0			
ESC 5-yr SCD risk, %	3.0±2.2	2.1±0.9			
Medications					
β-Blockers, (n)	8	28			
Calcium channel blockers, (n)	3	3			
Disopyramide, (n)	3	1			
ARB/ACEI , (n)	3	7			
Diuretics, (n)	2	2			
Warfarin ,(n)	2	2			
Aspirin, (n)	4	14			

Data are mean±standard deviation. ACEI angiotensin converting enzyme inhibitor; BP blood pressure; EF ejection fraction; ESV end-systolic volume; EDV end-diastolic volume; HCM hypertrophic cardiomyopathy; LV Left ventricular; LA left atrial; LGE, late gadolinium enhancement (5 SD); LVOT left ventricular outflow tract; NSVT Non sustained ventricular tachycardia; SCD Sudden cardiac death; *p<0.05

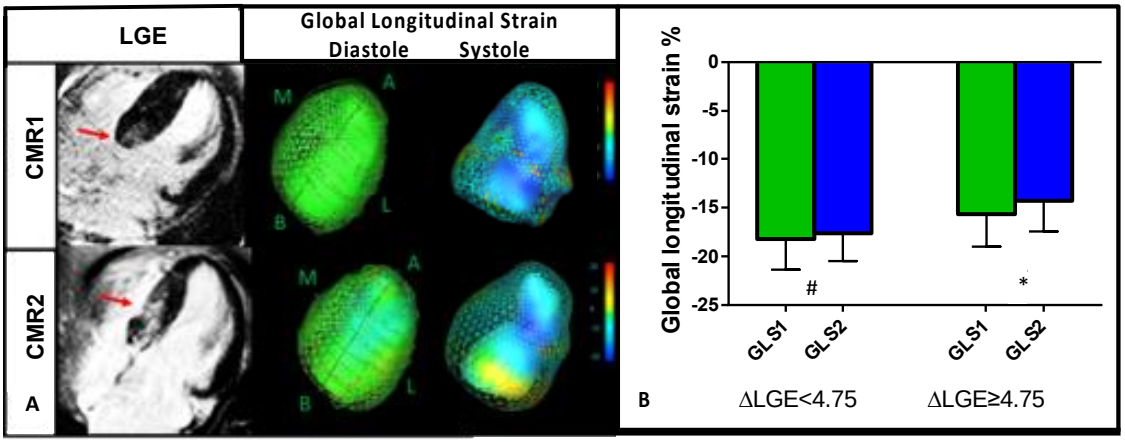

Figure 5. (A) Illustrative image of fibrosis progression in a case of HCM with impairment seen in global longitudinal strain on interval CMR scans (B) Effects of substantial LGE progression on peak global longitudinal strain (# p=ns, * p<0.05; GLS Global longitudinal strain, ΔLGE ≥4.75g LGE increment of greater than 4.75g)

4.6 DISCUSSION

In this chapter, we have shown for the first time that impaired myocardial perfusion reserve and reduced myocardial energetics are associated with an increased risk of LGE progression. Substantial/ clinically relevant LGE progression is also characterised by impaired myocardial perfusion and energetics at baseline and is associated with adverse left ventricular remodelling on follow up CMR imaging.

Microvascular dysfunction and fibrosis progression

Hypertrophic cardiomyopathy is characterised by microvascular dysfunction which may manifest as reduced myocardial blood flow in response to vasodilator stress (56, 57). Both structural and functional changes, including decreased capillary density, reduced luminal area due to medial thickening and increased vascular resistance due to compressive forces, are believed to contribute to the blunted vascular reserve (16, 20, 135). Many have suggested that myocardial ischemia may promote replacement fibrosis in HCM (20, 136). In an early study, Basso *et al.* provided histological evidence of ischaemic necrosis along with fibrosis in young adults with HCM who died suddenly (55). More recently, Petersen *et al.* found a strong association between the presence of LGE and hyperaemic MBF in 35 HCM patients on non-invasive CMR (57). Histological evidence of micro-vasculopathy has consistently been shown to occur alongside regions of dense fibrosis (20, 30). Therefore, we tested the hypothesis that patients with impaired perfusion reserve are more likely to develop fibrosis progression on serial imaging.

In the present study, we found that patients with impaired perfusion at baseline had a higher burden of fibrosis progression compared to those with preserved perfusion. Similarly, in those with substantial LGE progression (LGE ≥4.75g), MPRI was impaired at baseline. Interestingly, in a positron emission tomography (PET) study of 51 HCM patients, microvascular dysfunction was shown to be associated with an increased risk of adverse remodelling and left ventricular dysfunction (131). It is therefore likely that microvascular dysfunction promotes fibrosis progression, which in turn causes adverse cardiac remodelling. The development of *de novo* regions of fibrosis in regions not affected by hypoperfusion on the baseline CMR, suggests that factors other than microvascular dysfunction also potentially contribute to fibrosis progression in HCM such as increased metabolic demands, pro-fibrotic signalling and inflammation (38, 45, 137)

Impaired myocardial energetics in hypertrophic cardiomyopathy

Abnormal myocardial energetics is thought to play a vital role in the pathophysiology of HCM (74, 121, 122, 138). Data from in vitro animal models and HCM patients strongly support the energy depletion hypothesis which states that mutations in hypertrophic cardiomyopathy may increase the energy cost of force production by the sarcomere, leading to less energy available for other critical functions of the cardiac myocyte, such as Ca^{2+} reuptake into the sarcoplasmic reticulum (74, 121). This chronic energy depletion is believed to lead to myocyte dysfunction, elevation of cytosolic Ca2+, and 5′-AMP-activated protein kinase (AMPK) activation, which may be a stimulus for downstream hypertrophy and potentially pathological progression (74). Indeed, it has

been suggested that the increase in mechanical forces of HCM myocytes, and calcium-dependent signalling, also influence the behaviour of surrounding non-myocyte cells and activate specific transcriptional responses (139). For instance, increased expression of RNA encoding for TGF-β 1 and 2, periostin, collagen, and connective tissue growth factor has been observed in non-myocyte cells isolated from pre hypertrophic mice carrying the HCM causing mutation ($MHC^{Arg403Gln}$) (139). Such responses promote the proliferation and secretion of profibrotic molecules, which expand the extracellular matrix. The altered biophysical properties of mutant sarcomeres and the extrinsic strain imposed by energetic depletion is also thought to augment myocyte stress and promote early myocyte death through mitochondrial failure and subsequent focal scarring (87-90).

In this work, we found that HCM patients with impaired myocardial energetics at baseline were more likely to develop progression of LGE on follow up. Of interest, in patients with substantial LGE progression, myocardial energetics was also significantly impaired at baseline. This suggests myocardial energetic depletion may potentially contribute to the risk of fibrosis progression in HCM. Indeed, in HCM phenocopies where metabolism is compromised due to defects in ATP generation such as Friedrichs ataxia, very long chain acyl CoA dehydrogenase deficiency and mitochondrial disease, a high burden of myocardial fibrosis is reported in cross-sectional studies (81-83). Future studies evaluating the effects of metabolic therapies on LGE progression may provide valuable insights into the role of impaired energetics in disease progression.

Effects of substantial progression in cardiac structure and function

Another important finding from this work is the impact of substantial LGE progression on cardiac structure and function. Chan *et al.* have previously shown that the extent of LGE at a single time point predicts the risk of developing left ventricular dysfunction in HCM (53). Here, we found that patients with substantial progression had an increase in left ventricular end diastolic volume and reduction in systolic function from baseline. Myocardial deformation analysis also revealed a significant reduction in myocardial contractility (global longitudinal strain) in patients with significant LGE progression. These findings are unique to this study and likely reflect the longer interval between CMR scans of these patients (mean of 5.7 years versus 1.5-1.9 years). Additionally, this would also explain why patients with substantial LGE progression are at a higher risk of clinical events. Given that impaired perfusion is associated with fibrosis progression, these findings support the notion that adverse left ventricular remodelling seen in patients with microvascular dysfunction is potentially mediated by myocardial fibrosis (131).

4.7 CLINICAL IMPLICATIONS

Our data suggest that augmenting myocardial perfusion and metabolism in HCM may have favourable effects on the natural history of HCM. Both vasoactive drugs (eg. calcium channel blockers, beta-blockers) and drugs that modulate myocardial metabolism by facilitating glucose utilisation such as perhexiline and trimetazidine offer considerable promise (130). Indeed, in a small study of symptomatic HCM perhexilene improved both cardiac energetics and exercise capacity. Studies examining the long term effects of such therapies on pathological progression may therefore be insightful.

4.8 STUDY LIMITATIONS

This is a single centre study limited by relatively small sample size with low SCD risk due to the exclusion of those with ICD after CMR1. First-pass perfusion and myocardial energetics were attempted in a subset of patients. Although both impaired perfusion and energetics precede the development of significant LGE progression, the present study lacks the power to systematically assess the contribution of each of these parameters in the multivariable model and therefore only limited conclusions may be made on the causal role of such parameters. The LGE technique used here detects mostly focal fibrosis. Native and post contrast T1 mapping were not used in this study due to the lack of availability of such methods in earlier scans. We did not undertake a coronary angiogram in all patients to exclude coronary disease, however, all patients underwent exercise testing and those with a subjectively or objectively positive stress test were investigated with a coronary angiogram.

4.9 CONCLUSION

In this chapter, impaired perfusion reserve and impaired energetics were shown to associate with fibrosis progression on serial CMR. Substantial fibrosis progression, is characterised by impaired perfusion and energetics at baseline and potentially contributes to adverse left ventricular remodelling and dysfunction seen occur in HCM.

CHAPTER 5: IMPROVING THE PRECISION OF STRESS MYOCARDIAL OXYGENATION ASSESSMENT

5.1 ABSTRACT

Background: During vasodilator stress, myocardial oxygenation can be detected on oxygen-sensitive T2-prepared steady-state free precession (SSFP) blood oxygen level-dependent (BOLD) imaging. However, this can be highly variable due to its dependence on heart rates (HR). Fast low angle shot (FLASH) normalised T2-prepared SSFP BOLD is less sensitive to HR changes and may improve the precision of BOLD.

Objectives: To examine the normal range variability and reproducibility of FLASH-normalised T2-prepared SSFP BOLD compared to standard method.

Methods and results: Twenty healthy controls underwent cine imaging and adenosine stress BOLD and perfusion imaging on a 3 Tesla CMR. T2-prepared SSFP images were produced with (nBOLD) and without (sBOLD) interleaved FLASH normalisation.

Results: Mean sBOLD and nBOLD ΔSI were similar at 17±10% and 18±3% (p=0.79) respectively. Stress BOLD response was more variable for sBOLD compared to nBOLD ΔSI (F=13.77, p<0.001). sBOLD ΔSI showed a statistically significant dependence on stress heart rate, but nBOLD ΔSI did not. Segmentally, nBOLD ΔSI had higher inter- and intraobserver intraclass correlation coefficients compared with sBOLD. Applying a colour map to nBOLD ΔSI allowed the visual assessment of oxygen sensitive signal during vasodilator stress.

Conclusion: FLASH-normalised T2-prepared SSFP BOLD detects stress-induced changes in myocardial oxygenation with tight ranges and improved inter-and intra-operator segmental variability.

5.2 INTRODUCTION

The non-invasive assessment of tissue oxygenation is possible using blood oxygen level-dependent (BOLD) imaging which harnesses the paramagnetic property of deoxyhaemoglobin (140). BOLD has been successfully applied to other cardiovascular diseases to understand the relationship between myocardial blood flow and tissue oxygenation (141, 142). Stress BOLD was recently shown to detect myocardial ischaemia due to a critical flow limiting coronary stenosis without the need for extrinsic contrast agents, addressing a key limitation of existing non-invasive diagnostic techniques for ischaemia detection (143). In a study by Vöhringer *et al.* , the change in contrast on steady-state free precession (SSFP) cine-BOLD induced by vasoactive substances strongly associated with myocardial oxygenation rather than blood flow (144). As BOLD is also capable of detecting impaired oxygenation under pharmacological stress, it has been applied to other models of hypertrophy such as hypertrophic cardiomyopathy (HCM) and aortic stenosis to understand the effect of increasing metabolic demands on oxygenation (17).

Traditionally, T2*-weighted images (145) or T2* mapping (146) methods were used to assess BOLD effects but suffered from relatively low signal-to-noise ratio and artefacts caused by magnetic field inhomogeneity and motion. As a result, more recently the field has moved towards SSFP-based methods. These include long-TR SSFP cine (144), using the native T2 sensitivity of steady-state balanced SSFP, or using a T2 preparation module with an SSFP readout (147). However, all techniques have shown wide normal ranges, with population standard deviations comparable in size to the

mean BOLD change on adenosine stress, for example BOLD T2* changes of 17±9% (146), cine signal changes of 3.9±6.5% (148), and T2-prepared SSFP signal changes of 12±11% (149) to 20±7% (150). The sensitivity and specificity of the technique in detecting disease are therefore limited which has, in turn, prevented the regional or segmental assessment of tissue oxygenation using the technique. For instance, in the study by Arnold *et al.*, a segmental analysis could not identify regions affected by critical flow-limiting stenosis (149). While the cine SSFP method relies on a true steady-state of the magnetisation and thus has no heart-rate (HR) dependence, T2*-weighted or T2-weighted methods usually rely on some form of HR correction to account for the change in steady-state longitudinal magnetisation during stress imaging (145, 151).

In 2007, Kellman *et al.* reported a T2-prepared SSFP sequence for imaging myocardial oedema which manages surface coil sensitivity variations by interleaving low-flip angle Fast low angle shot (FLASH) reference images between the SSFP readouts (99). The SSFP images are normalised by the FLASH images, and the correction of signal intensity variation across the image enhanced the visibility of subtle changes in signal intensity due to myocardial oedema. However, the normalisation of the SSFP images by the FLASH images should also account for changes in steady-state longitudinal magnetisation due to changing heart rate and differing saturation by the T2 preparation and SSFP readout train. We aimed to test whether this method gives a tighter normal BOLD range with improved reproducibility, and, in addition, whether segmental variation in T2-prepared SSFP BOLD is reduced using this method.

5.3 METHODS

Bloch simulations

Bloch simulations were carried out in order to modify the heart rate (HR) correction previously reported (151) to account for the additional FLASH readout and heartbeat between SSFP readouts. The sequence was simulated at RR intervals from 400ms to 1500ms in 50ms increments. An exponential of the form

$$M_z = 1 - \beta e^{-RR/T_{1,mod}}$$

was fit to the resulting steady-state Mz to produce an expression for HR correction in the same form as used in previous work (145, 151).

Population

Cardiac magnetic resonance imaging (CMR) data from twenty healthy subjects were analysed to study the normal range of both standard and FLASH-normalised T2-prepared SSFP BOLD and its repeatability. These subjects were scanned as a part of a study that was approved by the institutional ethics committee (reference12/LO/1979) and were selected as the first 20 healthy subjects in the study with SSFP BOLD imaging free of susceptibility artefacts. All subjects were regarded as healthy with no previous medical history, cardiac disease or risk factors for cardiac disease.

CMR Protocol

All 20 participants underwent cardiac magnetic resonance (CMR) in a 3T Trio MR scanner (Siemens, Erlangen, Germany) for cine, adenosine stress BOLD and perfusion imaging. Participants were instructed to refrain from caffeine-containing drinks and food for at least 24 hours preceding the study. Cine CMR was planned and acquired from standard pilot images. Short-axis cine images covering the entire left ventricle were acquired using a retrospectively ECG-gated SSFP sequence (TR/TE 3/1.5 ms; flip angle, 50°). Cardiac-gated B_0 shimming (Siemens WIP 452) and centre frequency adjustments were performed before BOLD imaging to generate images free from off-resonance artefacts. For BOLD-CMR, a single mid-ventricular slice was acquired at systole using the ECG-gated T2-prepared segmented SSFP sequence with interleaved low flip angle FLASH reference readouts on alternate heartbeats (99) (Siemens WIP 567, VB17). The sequence parameters were: $TE_{prep=}$40ms, SSFP TR/TE = 2.86ms/1.43ms, 72 readout lines per heartbeat, and an SSFP flip angle of 44°. The SSFP and FLASH data were acquired in an interleaved fashion over three heartbeats each (six in total) with dummy SSFP and FLASH acquisitions beforehand (eight heartbeats total). This sequence outputs two images, the SSFP image alone, labelled “mag”, and the SSFP normalised by the interleaved FLASH image, labelled “norm”. We use “standard” and “normalised” throughout this paper to refer to these images and signal intensities derived from them. Adenosine was then infused at a dose of 140 mcg/kg/min and at peak vasodilator stress (at least 3-4 minutes) a slice-matched stress BOLD image was acquired. Blood pressure was recorded by a vital signs monitor machine at baseline and 1-minute intervals during stress. First-pass perfusion

imaging was undertaken right after the acquisition of BOLD image using a T1-weighted gradient echo sequence with saturation recovery magnetisation preparation. A dose of contrast (Gadoterate Meglumine) 0.03 mmol/kg of was injected at 6ml/sec during stress followed by a saline flush 12 ml at 6 ml/sec and the same dose for rest acquisition (95).

CMR Image analysis

We used a commercially available software (Circle Cardiovascular Imaging Inc., Calgary, Canada) to analyse left ventricular (LV) volumes, mass, ejection fraction (109, 152), myocardial perfusion reserve index (MPRI) and BOLD SI. For the normal volunteers, quantitative analysis of rest and stress BOLD images without (standard image) and with FLASH normalisation (normalised image) were undertaken by two observers (MH and KC). The signal intensity in the standard images was HR corrected using the equation derived from Bloch simulations. BOLD ∆SI was estimated as the relative increase in signal intensity between rest and stress BOLD images as previously described (151), to give sBOLD ∆SI from standard SSFP images and nBOLD ∆SI from FLASH-normalised images.

The relative SI change or BOLD ΔSI:

$$\text{BOLD } \Delta\text{SI}\% = \frac{Stress\ SI\ - RestSI}{RestSI} \text{ x } 100$$

For perfusion analysis, signal intensity curves were generated to measure MPRI as previously described (69).

To assess intra-observer variability on the normal volunteer measurements, the analysis was repeated on both standard and normalised images for the same subjects by one of the observers (KC) after two weeks.

A colour map to visually represent normalised SI variations in the myocardium, based on the ranges at rest and stress in normal volunteers, was developed and implemented in commercially available software (Circle Cardiovascular Imaging Inc., Calgary, Canada). Bright green was used to represent pixels with SI two standard deviations (2 SD) lower than the mean rest SI (~200 AU) and orange for SI 2 SD above the mean rest SI ~ 238 AU. Coincidentally, this SI was also 2 SD below the mean segmental stress SI. Finally red was used for the highest signal intensity ~ 280 AU (2SD above the mean stress SI). For SI below the physiological range (~175 AU), blue was used.

5.4 STATISTICAL ANALYSIS

Statistical analyses were undertaken using IBM SPSS Statistics version 23.0 (IBM Corp., Armonk, NY), except for the tests for normality and linear mixed modelling which were carried out in Matlab (Mathworks, Natick, MA). Analysis was carried out for slice-averaged data for the signal intensities in the FLASH-normalised and HR-corrected standard SSFP images, and for both slice-averaged and segmental nBOLD and sBOLD ΔSI. All variables were tested for normality with the Kolmogorov–Smirnov test

with $p > 0.1$ (for normality tests only) taken to indicate data consistent with a normal distribution.

Data (slice/segmentally averaged, signal intensities and BOLD ΔSI) were characterised by mean, standard deviation and coefficient of variation. A one-sided F-test was used to test whether the population variance was reduced in slice-averaged SI from normalised images relative to that from standard images.

Paired, two-sided t-tests were used to test whether nBOLD and sBOLD ΔSI were statistically significantly different from each other, both for the whole slice and for each segment, and f-tests used to test whether both whole slice and segmental nBOLD variance was lower than sBOLD variance. Linear mixed models were used to assess the dependence of segmental sBOLD, nBOLD and BOLD difference (sBOLD-nBOLD) on the fixed effects segment, rest HR, stress HR, and segmental MPRI. The subject intercept was included as a random parameter and models were compared using likelihood ratio tests to determine whether the inclusion of the fixed effects one by one improved the model and should, therefore, be included. Visual inspection of residual plots did not reveal any obvious deviations from homoscedasticity or normality. Statistical significance was indicated by $p < 0.05$.

Two-way random Intra Class Correlation (ICC) was used to assess the level of agreement between observers and two-way mixed ICC was used to assess the level of agreement within the same observer at a per-segment level and per-subject level. Reproducibility was deemed to have improved statistically significantly if the confidence intervals did not overlap.

5.5 RESULTS

Bloch simulations

The equation for HR correction of standard images was

$$S = \frac{S_0}{1 - 0.98e^{-RR/980}} \quad (1)$$

Where S_0 is the measured signal intensity, S is the HR-corrected signal intensity, and RR denotes the RR interval during the BOLD acquisition in ms.

Baseline characteristics

Data from all 20 normal volunteers and all 240 (rest and stress) segments were included for the statistical analysis. Baseline characteristics are listed in **Table 1**. Left ventricular indices and MPRI were within normal limits (MPRI 1.99±0.31). All subjects had low (<10%) 10 year Framingham risk of coronary disease.

Signal intensities and BOLD ΔSI, both whole slice and segmental, as well as HR changes, were all normally distributed.

Table 1. Baseline characteristics and cardiac magnetic resonance indices of healthy controls.

	CMR (n=20)
Age (years)	47±15
Male, % (n)	55(11)
Body mass index (kg/m^2)	25±3
Rest heart rate (bpm)	62±13
Stress heart rate (bpm)	93±20
Absolute increase in heart rate	31±11
Relative increase in heart rate	50±16%
CMR findings	
LVEF, %	63±7
LVEDV (ml)	158±41
LVESV (ml)	55±25
Stroke volume (ml)	103±19
LV Mass (g)	101±25
LV Mass index (g/m^2)	55±12
MPRI	1.96±0.35
Data are mean±standard deviation; EDV end-diastolic volume; ESV end-systolic volume; EF ejection fraction; LV Left ventricular; MPRI Myocardial perfusion reserve index, bpm beats per minute.	

FLASH-normalised and HR-corrected standard SSFP image signal intensities

Slice level comparisons

The mean HR-corrected standard SSFP SI and (HR uncorrected) normalised SI at rest and stress for normal volunteers are shown in **Table 2**, and in **Figure 1**. An F-test showed that the variance in SI were significantly reduced in the normalised images compared with HR corrected standard SSFP images at both rest (SI 219±9 vs 116±31 AU) and stress (SI 258±10 vs 136±39 AU) ($p<0.0001$ for both).

Table 2. Signal intensities for standard and normalised images for normal volunteers

	Mean±SD	CoV
HR-corrected standard rest SI	116±31	27%
HR-corrected standard stress SI	136±39	29%
Normalised rest SI	219±9	4%
Normalised stress SI	258±10	4%

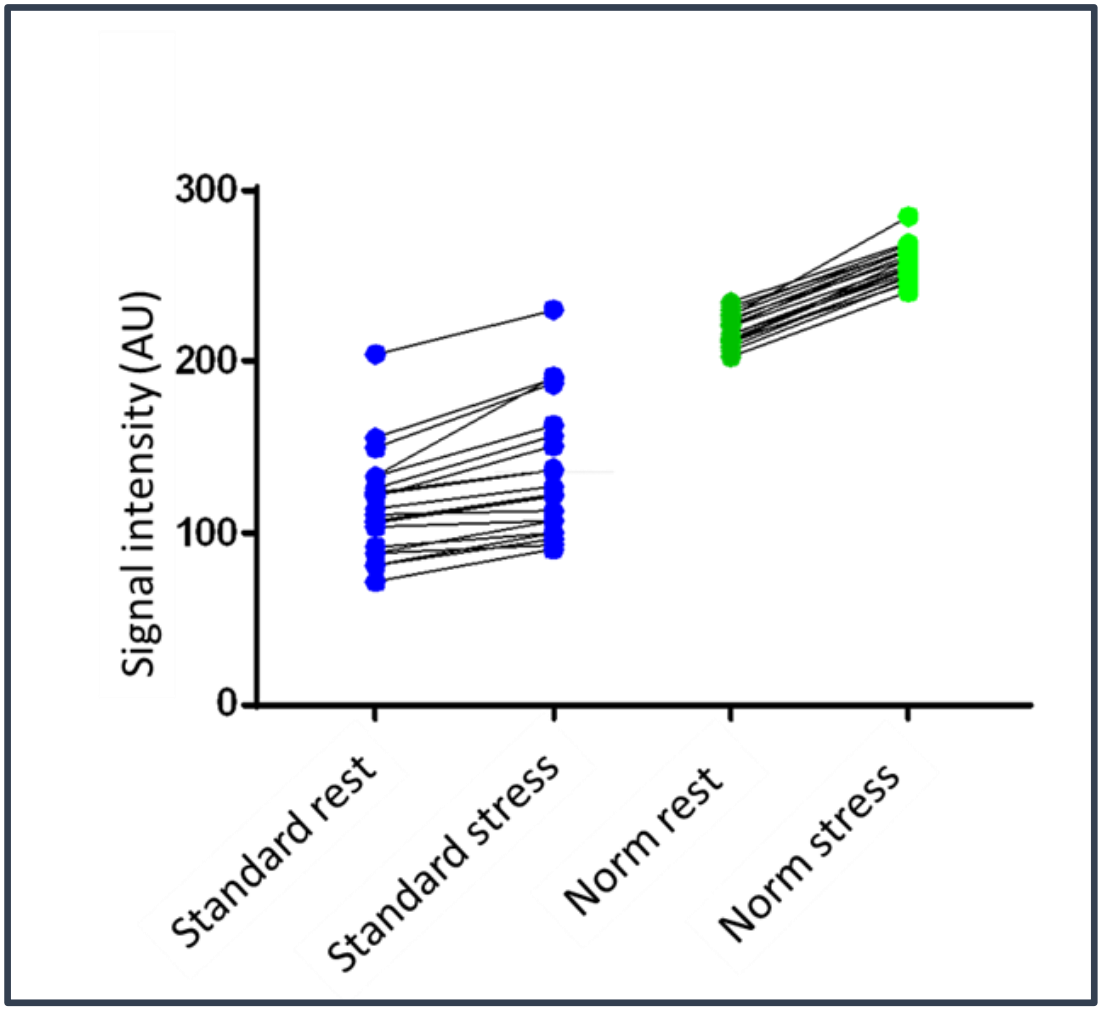

Figure 1. Rest and stress BOLD signal intensities in normal volunteers for HR-corrected standard images and FLASH normalised images demonstrating tight range of signal intensities for the normalised images. (Norm normalised BOLD; AU arbitrary units)

sBOLD and nBOLD ∆SI

Slice comparisons

In normal volunteers, the relative increase in SI for sBOLD and nBOLD during stress were similar at 17±10% and 18±3% respectively, with no statistically significant difference between the two (p=0.79, **Figure 2**), corresponding to coefficients of variance of 59% and 17%. sBOLD ∆SI had a significantly higher variance compared to nBOLD ∆SI on a per-slice/subject basis (F=13.77, p<0.0001) (**Figure 2**).

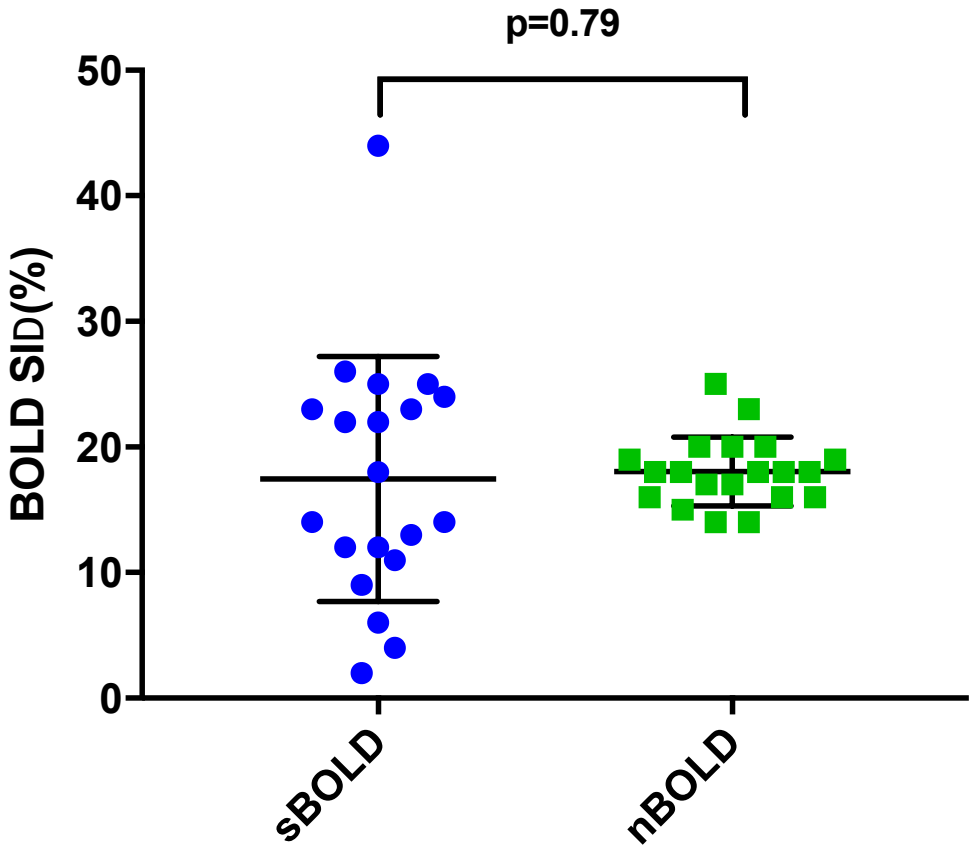

Figure 2. Comparison of signal intensity change of sBOLD and nBOLD for normal volunteers showing the wide variance of sBOLD compared to nBOLD. (Error bars represent mean±standard deviation; sBOLD standard BOLD, nBOLD normalised BOLD).

Segmental comparisons

Segmental sBOLD and nBOLD ΔSI in normal volunteers are shown in **Table 3**, along with the results of the statistical comparisons of values and variances. There was no significant difference in BOLD values between sBOLD and nBOLD, and all but the anteroseptal segment showed a statistically significant improvement in variance with nBOLD over sBOLD. The data are also presented in **Figure 3**.

Table 3. Comparison of segmental ΔSI for standard (sBOLD) and FLASH-normalised (nBOLD) images in normal volunteers.

	sBOLD ΔSI		nBOLD ΔSI		Comparison p-values	
	Mean±SD(%)	CoV	Mean±SD(%)	CoV	T-test (difference in means)	F-test (difference in variances)
Slice average	17.4±9.8	56%	18.1±2.8	16%	0.792	<0.001
Anterior	18.0±17.7	98%	21.8±8.2	38%	0.280	0.001
Anteroseptum	17.2±8.9	52%	16.1±6.1	38%	0.567	0.09
Inferoseptum	15.3±13.0	85%	15.3±3.7	24%	0.994	<0.001
Inferior	20.5±14.7	70%	19.1±5.7	30%	0.691	<0.001
Inferolateral	22.7±18.7	82%	19.2±9.3	48%	0.346	0.003
Anterolateral	15.8±16.0	101%	18.5±7.2	39%	0.426	<0.001

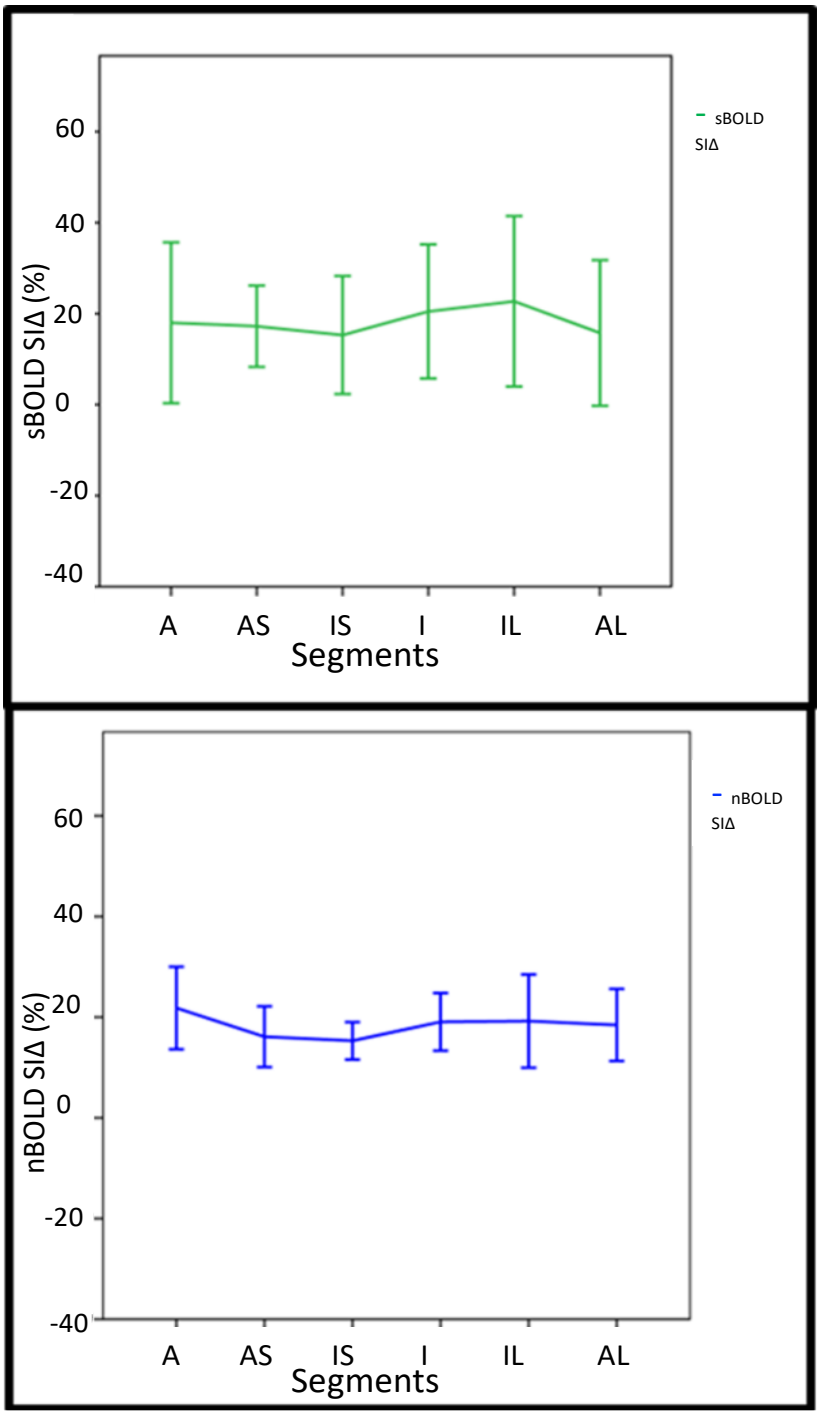

Figure 3. Comparison of segmental BOLD ΔSI for standard SSFP (sBOLD, green) and FLASH-normalised (nBOLD, blue) confirms a greater variance in segmental measurements of sBOLD in normal volunteers. (Error Bars represent standard deviation)

Origins of differences between sBOLD and nBOLD ΔSI in normal volunteers

Building linear mixed models for segmental BOLD responses showed that sBOLD ΔSI only showed a statistically significant dependence on stress heart rate (0.23%/bpm, equivalent to 17% BOLD ΔSI for the range of stress heart rates in these normal volunteers, p=0.03). In contrast, nBOLD ΔSI had no dependence on heart rate, rest or stress, but did have some segmental dependence (anterior ΔSI was 6.5% higher than inferoseptal, p=0.003). Only the heart rate dependence of sBOLD was reflected in the mixed model of the BOLD difference (sBOLD-nBOLD), which had a similar dependence on stress HR (0.24%/bpm, p=0.04) but no segmental dependence.

Slice and segmental reproducibility for normal volunteers

On a slice level, inter- and intra-observer ICC for nBOLD were excellent at 0.88 (95%CI 0.71-0.95) and 0.90 (95% CI 0.74-0.96), p<0.001. Similarly, sBOLD had a high inter-observer ICC and intra-observer ICC at 0.84 (95% CI 0.59-0.93) and 0.92 (95%CI 0.79-0.97), p<0.001 respectively. Bland altman plots revealed an excellent level of agreement for both inter- and intraobserver measurements for nBOLD (Intra: mean bias ± SD 0.35±2.08%; Inter: mean bias ± SD 0.15±1.84%) and sBOLD (Intra: mean bias ± SD 0.45±5.25%; Inter: mean bias ± SD -2.35±6.61%). However, sBOLD showed a greater standard deviation of difference when compared to nBOLD for both inter and intraobserver measurements (Figure 4).

On a segmental level, nBOLD had a higher inter- and intra-observer ICC compared to sBOLD with very minimal overlap of confidence intervals (**Table 3**).

Table 3. Interobserver and intraobserver intra-class correlation coefficient for segmental analysis for sBOLD and nBOLD in normal volunteers

sBOLD	ICC	95% CI	p-value
Interobserver	0.77	0.67-0.84	<0.0001
Intraobserver	0.85	0.76-0.90	<0.0001
nBOLD	ICC	95% CI	p-value
Interobserver	0.89	0.84-0.92	<0.0001
Intraobserver	0.92	0.89-0.95	<0.0001

CI confidence interval, ICC intraclass correlation

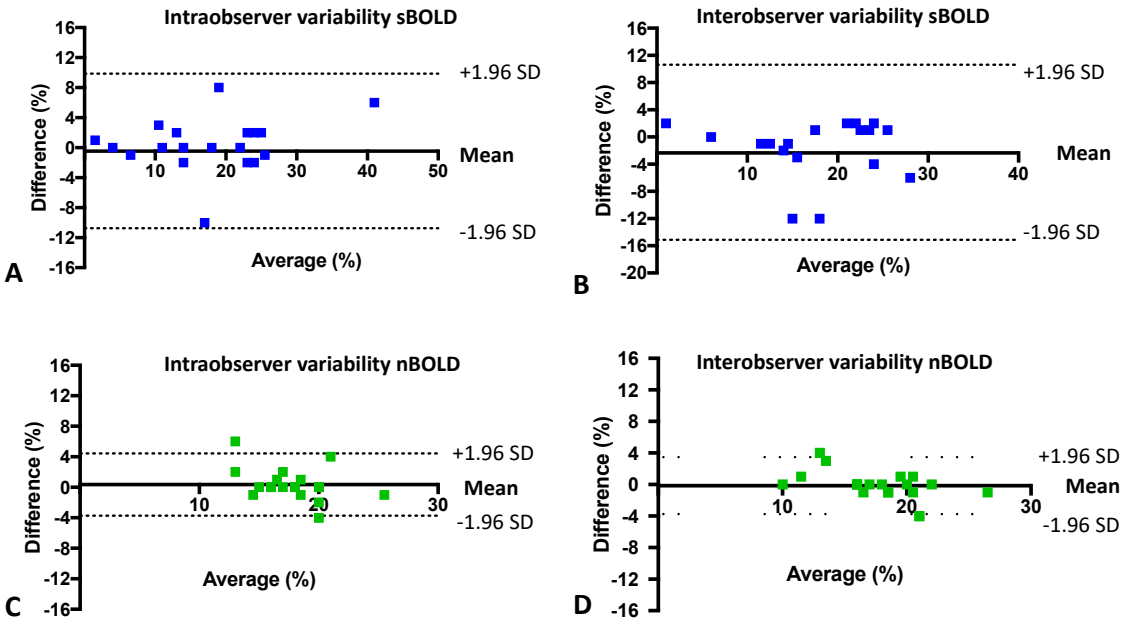

Figure 4. Bland Altman plots depicting the level of agreement for inter- and intra-observer measurements for sBOLD (A Intraobserver B Interobserver) and nBOLD (C Intraobserver D Interobserver).

Colour map

Illustrative examples of applying a colour map to images derived from the normal population are shown in **Figure 5**. When applied to the normalised images, the colour map enables clear visualization of the difference between rest and stress perfusion in this group of normal volunteers, even before calculating the change in BOLD SI (**Figure 5 A, B**).

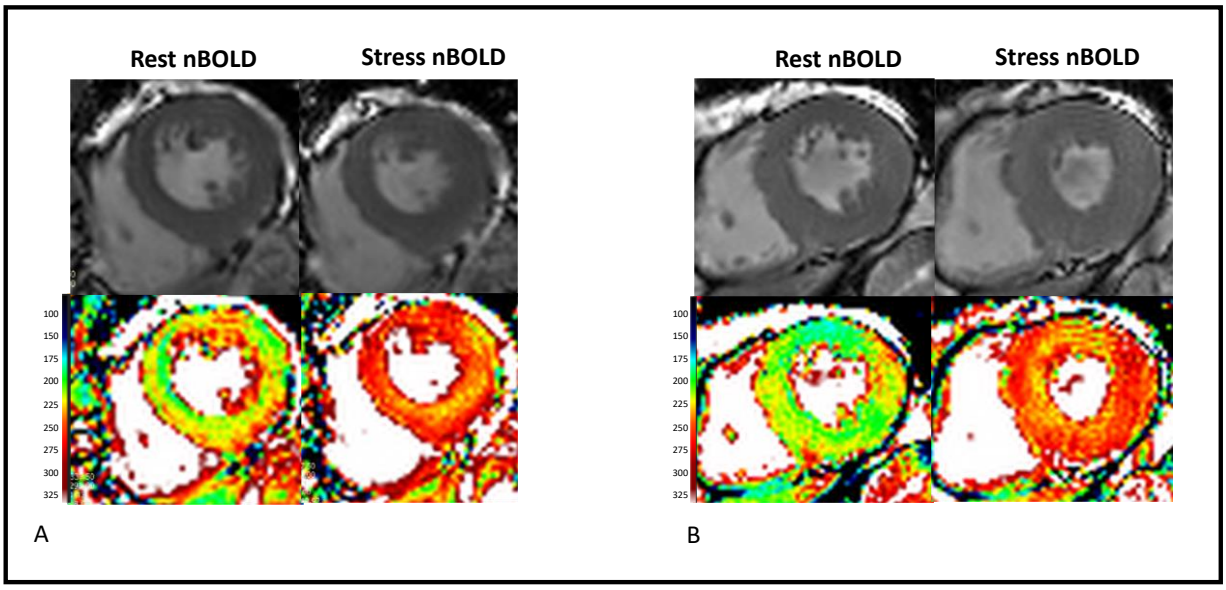

Figure 5. (A), (B) Two cases illustrating the difference in grey scale and colour nBOLD imaging from normal healthy subjects during rest (left) and stress (right) with stress BOLD response of 20% and 18% respectively.

Application of a colour map to the FLASH-normalised image without the need for additional HR correction also enabled the rapid identification of artefacts which are otherwise difficult to appreciate on the grey scale standard T2-prepared SSFP image. **Figure 6** demonstrates an example of susceptibility artefact (due to magnetic field in-homogeneity) or artefact near the heart-lung interface which can be more clearly visualised using the colour map than in the grey scale image.

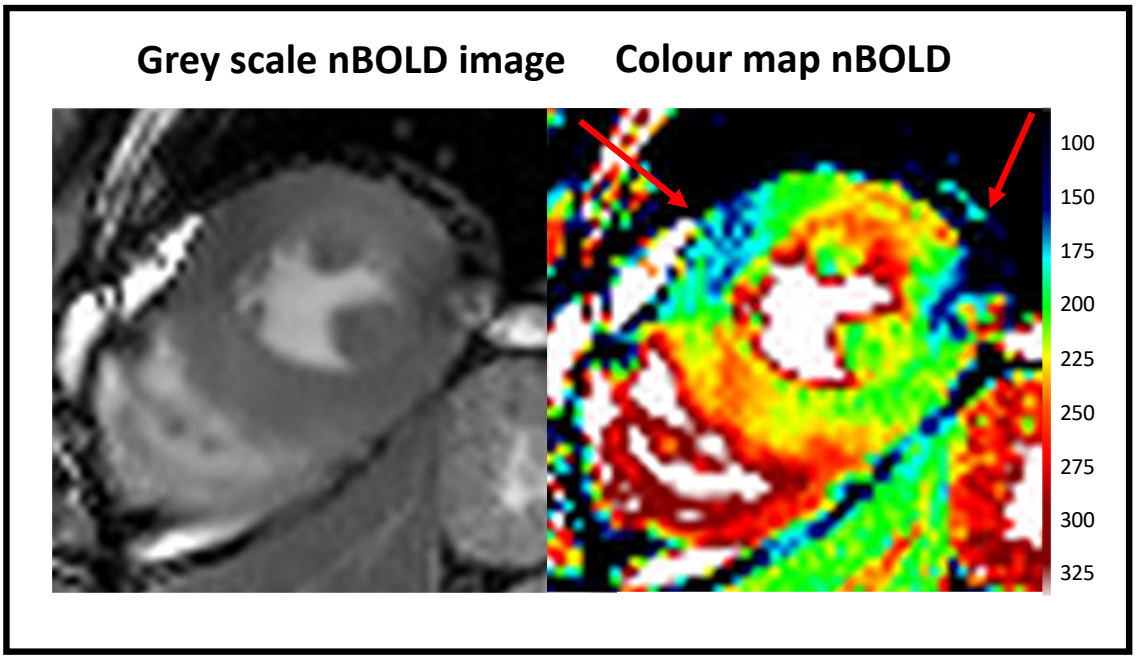

Figure 6. This case shows the easy identification of off-resonance artefacts (red arrow), which is more apparent on the colour map (right) as compared to the grey scale (left).

5.6 DISCUSSION

In this study, the normalisation of T2 prepared SSFP-BOLD images by an interleaved FLASH image considerably reduces both segmental and individual variability of the derived BOLD ΔSI without altering the size of BOLD effect measured. Additionally, using this novel method, it is now possible to visualise stress-induced oxygen sensitive signal using colour maps.

The normalisation process was originally developed to correct for surface coil sensitivity variations (99) but, in this context, also provides effective heart rate correction. Heart rate correction is required in the T2-weighted BOLD imaging method employed here, as in some T2*-weighted methods (145), because there is insufficient time during a breath hold for full T1 recovery between multiple T2 preparation pulses. As a result, the signal in the SSFP readouts is sensitive to the subject's heart rate as well as the T2 of the myocardium. Heart rate correction aims to remove this effect.

In this study, a relatively simple form of heart rate correction was chosen based on previous literature (145, 151), which is a straightforward exponential-based correction for the incomplete T1 relaxation of longitudinal magnetisation between T2 preparation modules. This was adjusted for using the sequence presented here by running a Bloch simulation to probe the effect of two R-R intervals between T2 preparation pulses and the inclusion of the low flip angle FLASH readout. However, the saturation from the T2 preparation and following SSFP readout is necessarily dependent on T2, which changes under adenosine stress (this being the origin of the BOLD signal). While we have previously shown that the same heart rate correction may be used in both rest

and stress, the correction is imperfect for normal volunteers under stress conditions, which leads to a statistically significant variation in sBOLD response with stress heart rate in the data presented here. Although it may be possible to calculate a more accurate HR correction factor for normal volunteers, based on an assumed reduction in deoxyhemoglobin, this would not necessarily be valid in patients with reduced myocardial flow reserve. Indeed, it could mask the very effect we are attempting to measure in myocardial BOLD CMR. Using the interleaved FLASH images to correct the SSFP signal intensity not only corrects for surface coil sensitivity variation, but also provides a sample of the longitudinal magnetisation which enables HR correction. This is demonstrated by the excellent across-subject coefficients of variation on the individual rest and stress normalised SSFP images, the lack of heart rate dependence of nBOLD, and its low standard deviation of 3% (equivalent to 18% CoV) over the normal volunteer population studied here.

Interestingly, a statistically significant difference in nBOLD ΔSI between the anterior and inferoseptal segments was revealed by the linear mixed model. This may be because the T2 preparation is designed to be robust to variations in B_0 and B_1, but the SSFP readout retains these sensitivities. It seems unlikely that a difference between anterior and inferoseptal segments arises from B_1 changes, which typically manifest as a monotonic decrease from septal to lateral segments (153). While B_0 inhomogeneity is usually most marked in the inferior segment, the anterior segment is also subject to larger B_0 field gradients than elsewhere in the myocardium (154). Therefore this difference may be related to subtle artefacts in the SSFP readout and a further study will be required to verify this.

Consistent with previous studies, we observed that both segmental and slice HR-corrected sBOLD ΔSI derived from standard T2-prepared SSFP-BOLD images have wide variations with significant overlap with previously reported disease ranges (149, 155). In contrast, the use of the FLASH-normalised T2-prepared SSFP images produced less segmental variation and tighter normal ranges. Importantly, we demonstrate that the magnitude of change did not differ between the two methods, with excellent inter- and intra-observer variability both methods at an individual level. At a segmental level, we observed that nBOLD had improved inter-observer and intra-observer agreement with significantly reduced variance compared to sBOLD. We believe that applying the FLASH normalisation method to T2-prepared SSFP BOLD is likely to augment the accuracy and effect size for this technique. Further work will be required to test the role of FLASH normalisation on T2 prepared SSFP-BOLD signal in larger disease cohorts.

As far as we are aware, there is only one published report using the same sequence to study BOLD effects in the myocardium (156). However, these authors used hypercapnia rather than adenosine stress to induce hyperemia in human subjects with a wide normal range (11.2%±10.6) and it is unclear whether they used the FLASH-normalised SSFP images or standard SSFP images in their analysis.

5.7 CLINICAL IMPLICATIONS

FLASH normalised T2 SSFP has a low CoV across subjects of 4% for the rest and stress signal intensities which is much smaller than the standard BOLD ΔSI CoV of 18%. This enables the application of an intuitive colour map to the normalised BOLD

image which permits a qualitative appreciation of changes in tissue oxygenation which was previously not possible using the standard method.

In the future, FLASH normalised T2 SSFP BOLD colour map could be applied directly on the scanner to enable qualitative assessment of BOLD at the time of imaging, prior to subsequent quantitative analysis. The application of colour map to the FLASH normalised image also permits the rapid identification of artefacts which can be difficult to assess on the grey scale image, giving scan operator an opportunity to improve acquisition by repeating the scan with appropriate adjustments to shim.

5.8 STUDY LIMITATION

One of the main limitations of this study is the lack of external validation for the proposed approach. We were unable to use exactly the same sequence previously validated using PET (151), however, the sBOLD response range in normal volunteers found here is consistent with the range reported in that work of 17±8.5% (standard error of the mean multiplied by the square root of the number of participants). Further work will be required to assess the strength of association between tissue oxygenation and nBOLD ΔSI.

While the application of colour maps to FLASH normalised images does not mitigate the occurrence of susceptibility or off-resonance artefacts in cardiac imaging, a rapid qualitative assessment enables appropriate shim adjustments to improve image quality. Rest and stress BOLD were undertaken on a single slice; the role of multi-slice nBOLD imaging needs further consideration. We also note that in this study, we have

not studied how changes in acquisition parameters may change the normalised image SI and therefore, the limits in the colour maps may depend on specific acquisition parameters.

Coronary angiography to exclude a flow limiting stenosis was not performed in our healthy controls, however, all participants had a low 10 year Framingham risk of coronary disease and normal myocardial perfusion reserve. The clinical value of rest and stress FLASH-normalised T2-prepared SSFP SI over and above the relative nBOLD response remains to be tested and is beyond the scope of this paper.

5.9 CONCLUSIONS

Here we demonstrate an important step at improving the assessment of oxygen sensitive signal in the myocardium with T2 prepared SSFP-BOLD. The application of FLASH-normalisation in T2-prepared SSFP BOLD produces highly reproducible signal intensities, with tight normal BOLD response ranges. The use of a colour map that can be applied directly to the FLASH-normalised images offers tremendous potential for direct clinical application and incorporation into clinical workflow.

CHAPTER 6: STRESS MYOCARDIAL OXYGENATION: DETERMINANTS AND ASSOCIATION WITH FIBROSIS

6.1 ABSTRACT

Background: In hypertrophic cardiomyopathy, myocardial ischaemia in the absence of significant coronary disease is believed to promote myocardial fibrosis.

Objectives: To examine the determinants of stress myocardial oxygenation using the novel fast low angle shot (FLASH) normalised T2-prepared SSFP BOLD in HCM and investigate the relationship between myocardial oxygenation and fibrosis.

Methods and results: 103 genotyped HCM patients and 32 healthy controls underwent adenosine stress blood oxygen level-dependent (BOLD) and perfusion imaging, myocardial energetics assessment and late gadolinium imaging (LGE). Stress myocardial oxygenation was reduced in HCM compared to controls (9.1±0.4% vs17.0±0.6%, $p<0.0001$). On univariate analysis, sarcomeric mutation status, myocardial perfusion reserve, energetics and hypertrophy were univariate predictors of stress oxygenation. On multivariable analysis, sarcomeric mutation status independently predicted the extent of stress oxygenation (β -0.14, $p<0.0001$). HCM patients in the lowest quartile of stress myocardial oxygenation displayed the highest burden of myocardial fibrosis. Blunted stress oxygenation (β 5.17, $p=0.02$), myocardial perfusion (β -8.29, $p<0.0001$) and left ventricular mass (β 0.07, $p<0.0001$) were associated with myocardial fibrosis on multivariable analysis.

Conclusion: In HCM, the presence of sarcomeric mutation is a strong determinant of stress-induced myocardial oxygenation. Severe impairment in myocardial oxygenation is associated with increased burden of myocardial fibrosis.

6.2 INTRODUCTION

Hypertrophic cardiomyopathy is a genetically determined disease (5), known for its risk of sudden cardiac death and heart failure (3, 6). Although the prophylactic insertion of implantable cardioverter defibrillators has considerably reduced the risk of sudden cardiac death (128, 157), recent studies suggest that the incidence of heart failure and arrhythmia remain high (73). A better understanding of factors that promote adverse remodelling and heart failure onset is required to develop therapeutic strategies that alter the natural history of this disease.

In this regard, microvascular dysfunction and myocardial fibrosis may serve as important mediators of adverse remodelling (56, 131). In one study by Olivotto *et al.,* the extent of microvascular dysfunction on positron emission tomography (PET) imaging was shown to predict the risk of left ventricular dysfunction and heart failure onset (131). In another, Chan *et al.* demonstrated that the extent of myocardial fibrosis was predictive of left ventricular dysfunction in HCM (53). Whether or not abnormalities in microvascular response promote adverse remodelling via ischaemic necrosis and eventually fibrosis is unclear (20, 58).

Blood oxygen level-dependent (BOLD) cardiovascular magnetic imaging (CMR) allows the in vivo assessment of myocardial ischaemia (140, 144), by exploiting the paramagnetic property of deoxygenated haemoglobin as intrinsic contrast during vasodilator stress (140). Stress BOLD CMR has been shown to accurately detect myocardial ischaemia in patients with flow limiting coronary stenoses (143). We have

previously shown that in patients with HCM, myocardial oxygenation on stress BOLD may be blunted (45, 92), and correlates with the extent of perfusion impairment. Despite this however, hypertrophy negative sarcomeric mutation carriers with normal perfusion display impaired myocardial oxygenation. This suggests that factors other than myocardial perfusion may be important in determining myoardial oxygenation in HCM.

We sought to investigate the factors that associate with impaired stress oxygenation in HCM including the role of myocardial metabolism/energetics and genotype. We further examined the relationship between stress oxygenation impairment and myocardial fibrosis.

6.3 METHODS

The study was approved by our institutional ethics committee (reference12/LO/1979) and informed written consent was obtained from each participant. The inclusion and exclusion criteria are listed in Chapter 2. A total of 103 genotyped HCM subjects were recruited from the University of Oxford Inherited Cardiac Conditions clinic, John Radcliffe Hospital, UK. Thirty-two healthy subjects served as controls.

All HCM patients underwent exercise stress testing for risk stratification, and those with angina or evidence of myocardial ischemia were investigated with a coronary angiogram. Patients with significant coronary disease were excluded. None of the subjects included had late gadolinium enhancement (LGE) on CMR to indicate previous myocardial infarction. Healthy volunteers had no cardiovascular risk factors

or symptoms, no family history of cardiomyopathy or sudden death, and had normal 12-lead electrocardiogram (ECG).

CMR scanning protocol

31-Phosphorus (^{31}P) MRS was performed on CMR (3T) to measure myocardial energetics as described in Chapters 2 and 4 (95). Phospho-creatine to adenosine triphosphate ratio (PCr/ATP) ratio was obtained from a mid-ventricular septal voxel was (132).

Cine CMR was planned and acquired from standard pilot images. Short-axis cine images covering the entire left ventricle were acquired using a retrospectively ECG-gated SSFP sequence. Cardiac-gated B0 shimming (Siemens WIP 452) and frequency adjustments were performed before BOLD imaging to generate images free from off-resonance artefacts. For BOLD-CMR, a single mid-slice (matched to ^{31}P slice) was acquired at systole using FLASH normalised BOLD; ie, ECG-gated T2-prepared segmented SSFP sequence with interleaved low flip angle FLASH (fast low angle shot) reference readouts on alternate heartbeats were acquired as described in Chapter 5 (99) (Siemens WIP 567, VB17). Adenosine was then infused at a dose of 140 mcg/kg/min and at peak vasodilator stress (at least 3-4 minutes) a slice-matched stress BOLD image was acquired. Blood pressure was recorded by a vital signs monitor machine at baseline and at 1-minute intervals during stress. First-pass perfusion imaging was undertaken on three slices- base, mid and apex using a T1-weighted gradient echo sequence with saturation recovery magnetisation preparation. A dose of

0.03 mmol/kg of Dotarem® (gadoterate meglumine, Guerbet, Roissy CdG, France) was injected at 6ml/sec during stress followed by a saline flush 12 ml at 6 ml/sec and the same dose for rest acquisition (95). For late gadolinium enhancement (LGE) CMR, a top-up bolus of 0.06 mmol/kg Dotarem® followed by a 15-ml saline flush was administered. This was followed by ECG- gated images acquired in long- and short-axis planes identical to those of the cine images by using a breath-hold T1-weighted phase-sensitive inversion recovery images as described in Chapter 2.

CMR analysis

Post-processing of ^{31}P-MRS data was performed using the OXSA toolbox. The spectrum from a mid-ventricular septal voxel was fitted using a custom implementation of AMARES (the advanced method for accurate, robust, and efficient spectral fitting) in the “OXSA” semi-automated spectroscopy post-processing pipeline (96) (Refer to Chapter 4 for details).

Left ventricular (LV) volumes, mass and ejection fraction were analysed as previously described (Refer to Chapter 2, General Methods) (69). Quantitative analysis of LGE was undertaken by setting a signal intensity threshold at five standard deviations (5-SD) above the mean intensity of a reference region of interest placed in a remote area of myocardium with no visual evidence of enhancement (110, 158).

For BOLD analysis, myocardial signal intensity (SI) was measured after manually tracing endocardial and epicardial contours using Circle Cardiovascular Imaging Inc.,

Calgary, Canada. Mean SI was calculated for resting and stress conditions by averaging signal measurements from images during rest and adenosine stress, respectively.

The SI change was calculated as (without heart rate correction):

$$\text{BOLD } \Delta\text{SI}\% = \frac{Stress\ SI\ - RestSI}{RestSI} \text{ x } 100$$

The assessment of BOLD and LGE measurements were undertaken by observers KC and SS respectively who were blinded to clinical outcomes.

For perfusion analysis, signal intensity curves were generated to measure myocardial perfusion reserve index (MPRI) (69). MPRI was averaged across all three slices – base, mid and apex to represent each subject (Refer to Chapters 2 and 4).

6.4 STATISTICAL ANALYSIS

Statistical analyses were undertaken using IBM SPSS Statistics 23.0 (IBM Corp., Armonk, NY, USA) and GraphPad Prism 7.0 (GraphPad Software, San Diego, California, USA). Normality of data was assessed by visually inspecting the plots. Values are expressed as mean±SD unless otherwise stated. Analyses of variance with post hoc Bonferroni comparisons were used to compare baseline characteristics and the hemodynamic response to stress. The $\chi 2$ and Fisher's exact tests were used to compare proportions. Linear mixed effects model was used to assess dependence of segment (repeated measures) with BOLD response in HCM patients. As there was no

significant association between segment and BOLD response (β =0-.13, p=0.38), a slice average of BOLD ΔSI was used to represent individual patients. A general linear model (GLM) analysis of variance was undertaken for genotype comparisons with age, gender and BMI as covariates (due to differences in baseline characteristics of genotype groups which are listed in the **Table 3**). Myocardial perfusion and oxygenation data from GLM models are presented as estimates of mean±standard error of the mean (SEM). Univariate and multivariable linear regression was used to assess predictors of stress-induced myocardial oxygenation or BOLD ΔSI (112). Patients were divided into quartiles based on decreasing myocardial oxygenation. Univariate and multivariable linear regression was used to determine predictors of myocardial fibrosis (112). The covariates included were variables known to be potential confounders or univariate predictors and were adjusted for in the model. All tests were two-tailed and p-values <0.05 were considered significant.

6.5 RESULTS

Study population

A total of 103 HCM patients and 32 age and gender-matched healthy controls were enrolled in this study. Sixteen patients underwent a coronary angiogram for symptoms of angina and/or positive exercise stress test. All sixteen had non-obstructive coronaries.

Subject characteristics are described in **Table 1**. The mean age of HCM patients was 50±17 years. Seventy six (74%) were male. There were 14 (14%) patients with left

ventricular outflow tract obstruction (LVOT gradient≥30mm Hg) at rest. Forty one (40%) received betablockers.

Rate pressure product increments during vasodilator stress were similar between HCM and controls. As expected, HCM patients had a higher left ventricular ejection fraction, left ventricular mass index, maximum wall thickness and LGE mass compared to controls (**Table 2**).

Table 1. Baseline characteristics of healthy controls and HCM patients

	Control (n=32)	HCM (n=103)	p-value (controls vs HCM)
Age (years)	50±17	47±15	0.46
Male, % (n)	69(22)	74(76)	0.65
Body mass index (kg/m$^{2)}$	25±3	26±5	0.10
Hypertension % (n)	-	14(14)	-
Atrial fibrillation, % (n)	-	14(14)	-
SCD risk			
Family history of SCD, % (n)	-	22(21)	-
Unexplained syncope, % (n)	-	6(6)	-
NSVT on Holter monitor, % (n)	-	25(25)	-
Abnormal exercise BP response, % (n)	-	8(8)	-
Maximum LV wall thickness ≥30 mm, % (n)	-	3(3)	-
LV outflow tract gradient ≥ 30mmHg, % (n)	-	14(14)	-
Mitral regurgitation(mild-moderate)		3(3)	
NYHA Class I,II,III,IV, % (n)	-	81,19,3,0 (79,18,3,0)	-
SCD risk factors (0/1/2/3 risk factors), %(n)	-	50, 38,10,0 (52,40,11,0)	-
ESC SCD risk (%)		2.3±1.2%	
Medications			
β-Blockers, % (n)	-	41(40)	-
Calcium channel blockers, % (n)	-	17(17)	-
Disopyramide, % (n)	-	8(8)	-
ACEI/ ARB, % (n)	-	6(6)	-
Diuretics, % (n)	-	8(8)	-
Aspirin, % (n)	-	40(39)	-
Warfarin or NOAC's, % (n)	-	12(12)	-

Data are mean±standard deviation. ACEI angiotensin converting enzyme inhibitor; ARB angiotensin receptor blocker; BP blood pressure; ESC risk European risk score; HCM hypertrophic cardiomyopathy; LVOT left ventricular outflow tract;NSVT Non sustained ventricular tachycardia; NYHA new York Heart Association; RPP Rate pressure product increase during stress); SCD sudden cardiac death.

Table 2. Cardiac magnetic resonance parameters for HCM and healthy controls

CMR findings	Control	HCM	P value
LVEF, %	67±7	71±7	0.02
LVEDV (ml)	159±42	158±30	0.87
LVEDV index (ml/m^2)	85±19	82±13	0.31
LVESV (ml)	54±24	47±17	0.06
Stroke volume (ml)	105±21	111±20	0.14
LV Mass (g)	104±27	138±52	<0.0001
LV Mass index (g/m2)	56±12	71±23	<0.0001
Presence of LGE %(n)	-	63(61)	
LGE mass (g)	-	5.3g(IQR1.5- 12.3g)	
RPP	67±44	60±38	0.33
MPRI	2.03±0.32	1.5±0.37	<0.0001
PCr/ATP	2.02±0.31	1.8±0.30	0.04

Data are mean±standard deviation. CMR cardiac magnetic resonance imaging; LGE late gadolinium enhancement (5-SD); LV Left ventricular; EDV end-diastolic volume; ESV end-systolic volume; EF ejection fraction; LA left atrial; HCM hypertrophic cardiomyopathy; RPP Rate pressure product, MPRI myocardial perfusion reserve index; PCr/ATP ratio Phosphocreatine to adenosine tri-phosphate ratio.

Mutation analysis

Of the 103 HCM patients, 65 had a sarcomeric mutation, 33 were genotype-negative (G-HCM) patients, five had a variant of uncertain significance in a sarcomeric gene (VUS). Of those with a sarcomeric mutation, 37 had a mutation in myosin binding protein C-3 (*MYBPC3*), 27 in myosin heavy chain (*MYH7*), one in myosin light chain. 16 were hypertrophy-negative (sarcomeric myofilament mutation) carriers (Sarc+P-). Baseline characteristics for the genetic groups (sarcomeric vs genotype negative HCM) are listed in **Table 3** and **Table 4** lists the sarcomeric genes involved in Sarc+P- subjects.

Table 3. Baseline characteristics and CMR indices for genotype groups.

	Control (n=32)	G-HCM(n=33)	Sarc+HCM (n=49)	Sarc-P- (n=16)
Age (years)	50±17	51±12	50±14	32±13*§‡
Male, % (n)	69(25)	94(32)*§†	64(45)	44(4)
Body mass index (kg/m$^{2)}$	25±3	28±3*§	26±5	24±5
Hypertension % (n)	-	21(7)	11(8)	11(1)
Atrial fibrillation, % (n)	-	15(5)	14(10)	0(0)
RPP increase	67±44	46±19	66±41	77±48
SCD risk				
Family history of SCD, % (n)	-	9(3)‡	30(15)	19(3)
Unexplained syncope, % (n)	-	6(2)	4(2)	6(1)
NSVT on Holter monitor, % (n)	-	33(11)	18(9)	13(2)
Abnormal exercise BP response, % (n)	-	15(5)	6(3)	0(0)
Maximum LV wall thickness ≥30 mm, % (n)	-	3(1)	0(0)	0(0)
LV outflow tract gradient ≥ 30mmHg, % (n)	-	27(9)	8(4)	0(0)
NYHA Class I,II,III,IV, % (n)	-	67,30,3,0 (22,10,1,0)†	84,12,4,0 (41,6,2,0)	100,0,0,0 (16,0,0,0)
SCD risk factors (0/1/2/3 or more risk factors), %(n)	-	49,36,15,0 (16,12,5,0)	51,39,8,2 (25,19,4,1)	63,38,0,0 (10,6,0,0)
Medications				
β-Blockers, % (n)	-	58(19) †	35(17)	19(3)
Calcium channel blockers, % (n)	-	18(6)	16(8)	0(0)
ACEI/ ARB, % (n)	-	9(3)	6(3)	0(0)
Aspirin, % (n)	-	36(12)	51(25) §†	0(0)
Warfarin or NOAC's, % (n)	-	24(8) †‡	6(3)	0(0)
CMR findings				
LVEF, %	67±7	74±8*†	70±7*†	68±6
LVEDV (ml)	159±42	160±31	157±32	158±23
LVEDV index (ml/m2)	85±19	79±12*†	82±13	86±10
LVESV (ml)	54±24	43±18	48±18	50±11
Stroke volume (ml)	105±21	117±22*†	108±19	108±19
LV Mass (g)	104±27	173±60*†	128±38§†	97±21
LV Mass index (g/m2)	56±12	86±28*†	66±17§†	52±8
Max LVWT(mm)	11±1	21±4*†	20±4*†	11±1
Presence of LGE, % (n)	-	73(24) †	71(35)†	6(1)

Data are mean±standard deviation. ACEI angiotensin converting enzyme inhibitor; ARB angiotensin receptor blocker; BP blood pressure; EF ejection fraction; ESV end-systolic volume; ESC European Society of Cardiology; LV left ventricular; EDV end-diastolic volume; LA left atrial; LGE late gadolinium enhancement; LVOT left ventricular outflow tract; HCM hypertrophic cardiomyopathy; NSVT Non sustained ventricular tachycardia; NYHA new York Heart Association; SCD sudden cardiac death (compared with *control, † Sarc+P-, ‡Sarc+HCM, G-HCM § <0.05)

Table 4. Sarcomeric genes involved in Sarc+P- patients.

Genotype (n = 16)	
MYH7, %(n)	37(6)
MYBPC3, %(n)	63(10)
MYH7, Myosin heavy chain, MYBPC3, myosin-binding protein C	

Stress-induced myocardial oxygenation in hypertrophic cardiomyopathy

Illustrative examples of BOLD images with corresponding MPRI measurements are shown in **Figure 1**. BOLD colour maps produced by FLASH interleaved SSFP BOLD demonstrate an increase in oxygen-sensitive signal from rest (green) to stress (red) in healthy controls (**Figure 1 B** left). There is noticeably less transition in oxygen-sensitive signal from rest to stress in HCM hearts (**Figure 1 B** right). This was seen even in sarcomeric mutation carriers without hypertrophy (**Figure 1** LVH-). Confirming previous findings from a smaller HCM cohort (69), myocardial oxygenation (BOLD ΔSI) during vasodilator stress was significantly impaired in all HCM patients (9.1$\pm$0.4%; $p<0.0001$) compared to healthy controls (17.0$\pm$0.6%) (**Figure 1 C**).

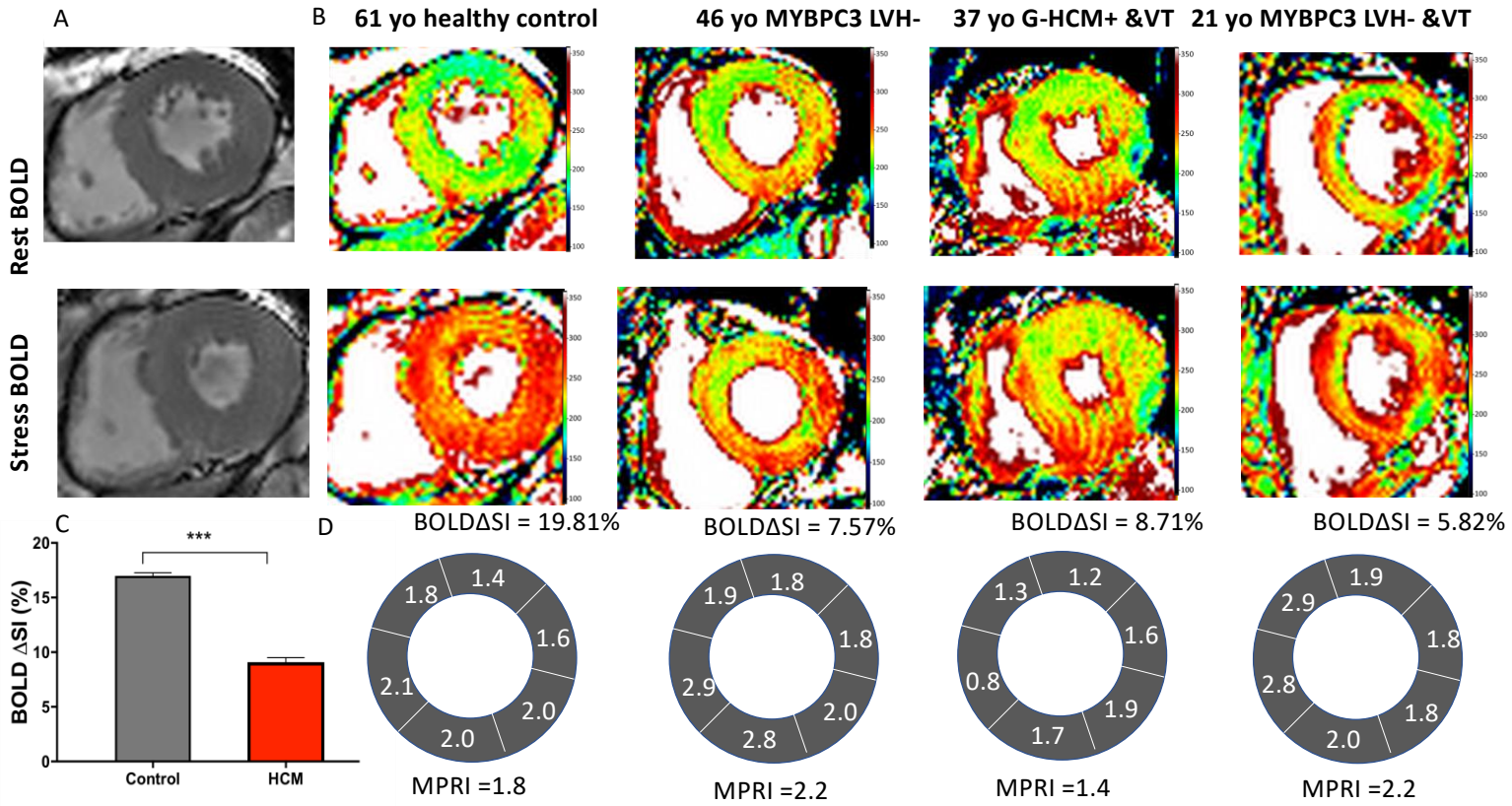

Figure 1. (A) Illustrative examples of rest and stress BOLD images from a 61 year old healthy individual (grey scale normalised image) (B) Examples of colour maps from the same healthy subject, pre-hypertrophic mutation carriers and HCM patients (C) Mean BOLD SIΔ was significantly higher in healthy controls versus HCM patients (D) Corresponding myocardial perfusion reserve index for each case shows a dissociation in MPRI and BOLD for pre-hypertrophic mutation carriers. (Error Bar represents mean±standard error of mean; ***p<0.0001; BOLD Blood Oxygen Level-Dependent Imaging, MPRI myocardial perfusion reserve index, LVH left ventricular hypertrophy, G-HCM genotype negative HCM, VT ventricular tachycardia**).**

Predictors of stress myocardial oxygenation in HCM

Here, we examined the determinants of stress myocardial oxygenation in HCM.The presence of a sarcomeric mutation (β -2.06, p=0.02), MPRI (β 3.16, p<0.0001), myocardial energetics (β 3.01, p=0.02) and maximum wall thickness (β -0.19, p<0.0001) were univariate predictors of stress myocardial oxygenation (**Table 5**). Resting LVOT gradient (>30mmHg; n=15) did not associate with stress oxygenation. On multivariable analysis, only sarcomeric mutation remained an independent predictor of BOLD response (β -1.96 p=0.02) (**Table 5**).

Table 5: Univariate and multivariable predictors of stress-induced myocardial oxygenation in hypertrophic cardiomyopathy.

UVA	β	95% CI	p-value	MVA	β	95% CI	p-value
Age	-0.04	-0.09-0.02	0.18				
Sex	0.10	-1.75-1.95	0.91				
Sarcomere+	-2.06	-3.76- -0.37	0.02	Sarcomere+	-1.95	-3.64--0.26	0.02
MPRI	3.16	1.08-5.23	<0.001	MPRI	1.46	-1.03-3.95	0.25
Max LVWT	-0.19	-0.33- -0.04	<0.001	Max LVWT	-0.14	-0.31-0.03	0.11
Haematocrit	-12.53	-35.48-10.43	0.28				
LVMass	-0.01	-0.03-0.01	0.24				
LVEF	0.09	-0.02-0.20	0.11				
LVOT obstruction	0.64	-1.73-3.01	0.59				
Beta blocker or CaCB	-0.50	-2.16-1.16	0.55				
RPPincrease	0.009	-0.01-0.03	0.40				
Myocardial energetics (PCr/ATP ratio)	3.01	0.44-5.59	0.02	PCr/ATP	1.69	-0.91-4.29	0.20

LV left ventricular; LVWT left ventricular wall thickness, EF ejection fraction; LGE late gadolinium enhancement; CI confidence interval; *Sarcomere+: presence of sarcomeric mutation (1/0); MPRI Myocardial perfusion reserve index; LVOT obstruction left ventricular tract obstruction >30mm Hg; Blood oxygen level-dependent imaging BOLD.

Genotype - oxygenation, myocardial perfusion reserve and energetics

Sarcomeric HCM (8.3±0.5%) showed more severe impairment in stress oxygenation response compared to genotype negative HCM (10.5±0.6%, p=0.001) and healthy controls (17.0±0.6%, p<0.0001), (**Figure 2 A**). Consistent with findings previously (69), pre-hypertrophic sarcomeric mutation carriers also had blunted oxygenation (10.4±0.9%) relative to controls (**Figure 2 A**). Both genotype negative patients (1.53±0.06) and sarcomeric mutation carriers (1.45±0.05) had similar reduction in MPRI (p=1), which were significantly lower than controls (2.03±0.06, p<0.0001 for both comparisons) (**Figure 2 B**). As before (69), myocardial perfusion reserve in phenotype negative sarcomeric mutation carriers (1.89±0.09 vs 2.03±0.06 p=0.58) was preserved (69). Myocardial energetics was most impaired in sarcomeric HCM when compared with controls (HCM 1.79±0.04 vs controls 2.02±0.03, p=0.01) but not between genotype negative HCM (1.95±0.06) or phenotype negative mutation carriers (2.02±0.04) and controls (2.02±0.03).

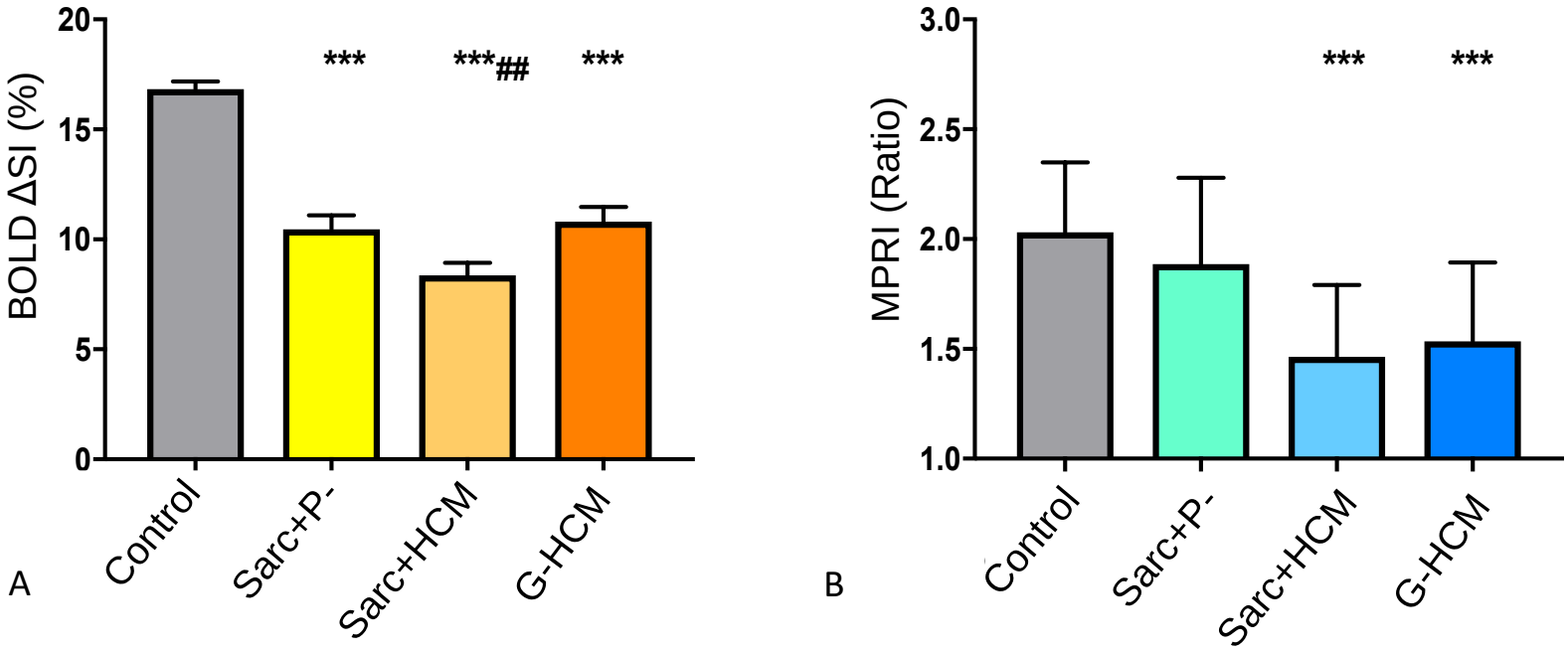

Figure 2. (A) Sarcomeric HCM patients had more severe impairment in myocardial oxygenation or BOLD ΔSI (%) compared to healthy controls and genotype negative HCM (G-HCM) (B) Sarcomeric HCM (Sarc+HCM) and genotype negative HCM (G-HCM) had equally impaired myocardial perfusion reserve index (MPRI) compared to healthy controls. (Error bars represent SEM, ***p<0.0001 comparison with healthy controls, ## p<0.01 comparison between G-HCM and or Sarc+P-;Sarc Sarcomeric mutation carrier).

Association of stress-induced myocardial de-oxygenation with myocardial fibrosis

Myocardial fibrosis as assessed on LGE imaging was found in 63% (61) of HCM patients with median LGE mass 5.3g (IQR 1.5-12.3g). Fibrosis was most extensive in those with severe stress oxygenation impairment (median LGE mass 12.32g, IQR 6.59g - 51.70g) (lowest quartile of myocardial oxygenation) compared to other quartiles, with no significant difference seen in median fibrosis burden between other quartiles (**Figure 3**). Severely impaired stress oxygenation (lowest quartiles; BOLD $\Delta SI<6.5\%$) was strongly associated with myocardial fibrosis on both univariate and multivariable (β 5.17, $p=0.02$) analysis. As expected, MPRI (β -8.29, $p<0.0001$) and left ventricular mass (β 0.07, $p<0.0001$) also associated with myocardial fibrosis (**Table 6**)

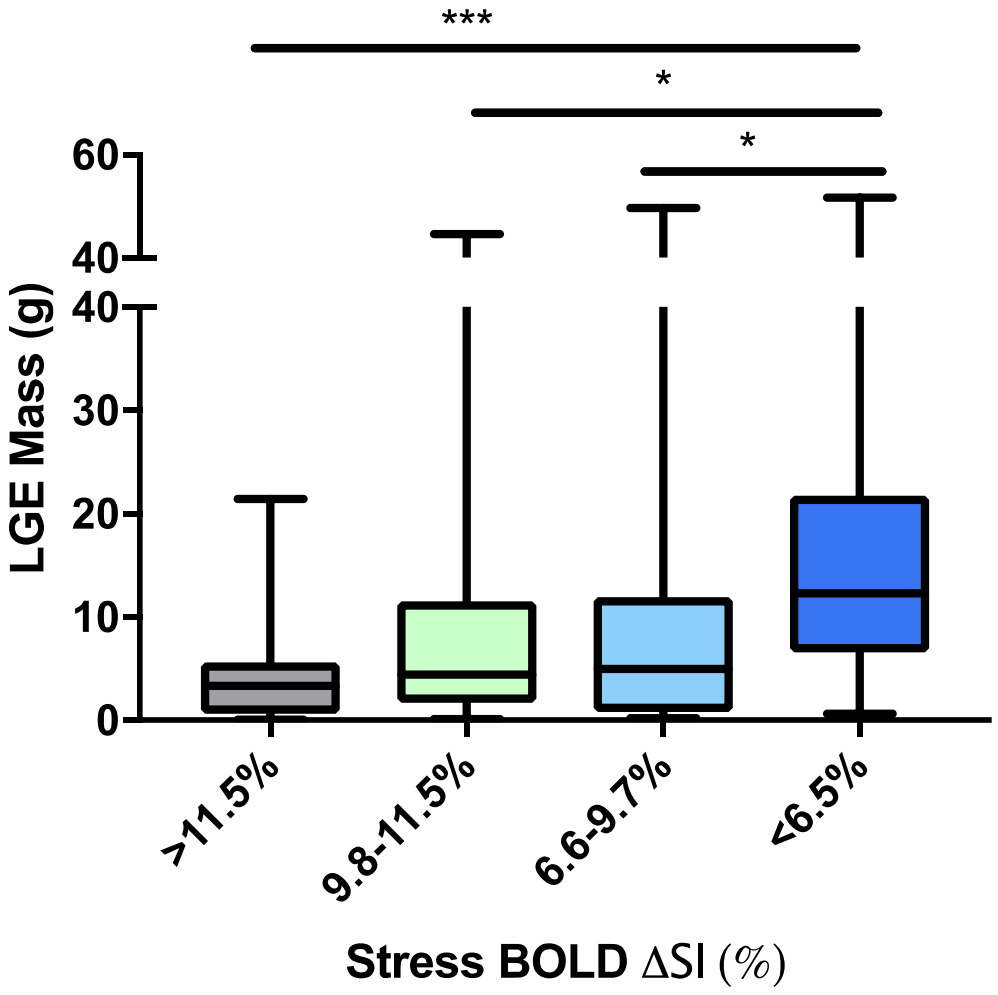

Figure 3. Late gadolinium enhanced mass was highest in those with the lowest quartile of myocardial oxygenation with no significant difference in LGE between other groups (Error bars median with minimum and maximum; ***p<0.0001 comparison of highest and quartile of stress oxygenation, *p<0.05 comparison of intermediate quartile and lowest quartile).

Table 6. Univariate and multivariable predictors of myocardial fibrosis in HCM

UVA	***β***	95% CI	p-value	MVA	***β***	95% CI	p-value
Age	-0.17	-0.29-0.31	0.02	Age	0.05	-0.08-0.18	0.45
Sex	1.94	-2.94-6.85	0.43				
Sarcomere+(0 or 1)	-0.87	-5.49-3.76	0.71				
MPRI	-13.49	-18.61- -8.37	<0.0001	MPRI	-8.29	-13.58--3.01	<0.0001
Max LVWT	1.07	0.74-1.41	<0.0001	*****			
LVMass	0.10	0.06-0.13	<0.0001	LVMass	0.07	0.03-0.10	<0.0001
LVEF	-0.22	-0.51-0.06	0.13				
LVOT obstruction	0.77	-5.35-6.89	0.80				
Beta blocker or CaCB	3.59	-0.68-7.86	0.10				
ACEI/ARB	5.59	-3.57-14.74	.23				
Myocardial energetics	-3.53	-10.95-3.89	0.35				
BOLD ΔSI (%)	-0.75	-1.25--0.25	0.004				
BOLD ΔSI <6.5%	8.53	3.85-13.20	<0.0001	BOLD ΔSI <6.5%	5.17	0.82-9.51	0.02

ACEI Angiotensin converting enzyme; ARB Angiotensin receptor blocker; Blood oxygen level-dependent imaging BOLD; CaCB Calcium channel blockers; CI confidence interval; LGE late gadolinium enhancement; LV left ventricular; LVEF left ventricular ejection fraction; LVOT obstruction left ventricular tract obstruction >30mm Hg; LVWT left ventricular wall thickness; MPRI Myocardial perfusion reserve index; *Sarcomere+: presence of sarcomeric mutation; ***** As left ventricular wall thickness and mass represent the similar aspect of phenotypic severity, we have used LV mass alone in the multivariable analysis.

6.6 DISCUSSION

In this chapter, the predictors of stress-induced myocardial oxygenation were examined in a large cohort of genotyped HCM patients. We show for the first time that the presence of sarcomeric mutations is a strong independent determinant of stress oxygenation. Additionally, we show that impaired oxygenation associates with myocardial fibrosis, with the burden of fibrosis in HCM being greatest in those with the most severe impairment in stress oxygenation.

Hypertrophy, perfusion, metabolism and genotype are associated with stress oxygenation

The direct assessment of myocardial ischaemia non-invasively has been a formidable challenge for physicians for many years. The development and validation of cardiac BOLD as a robust oxygen sensitive method marked the beginning of a new era of ischaemia detection non-invasively; where intrinsic MR contrast, generated by changes in deoxygenated blood during pharmacological stress, could be harnessed (145, 149, 151, 159, 160). Indeed, the application of stress BOLD CMR to cardiovascular diseases has provided numerous insights into the pathophysiology of diseases, in particular the relative role of perfusion and metabolism in determining oxygenation (149, 151, 159, 160).

In a previous small proof of principle study, myocardial oxygenation during stress was assessed in HCM (69) and found to be blunted. Stress oxygenation correlated with the extent of hypertrophy and perfusion (69). However, oxygenation remained impaired even in pre-hypertrophic sarcomeric mutation carriers with preserved perfusion

(Sarc+P-). These findings were in agreement with another study of Sarc+P- patients, where myocardial oxygen efficiency was found to be significantly reduced (161). To understand the basis of this dissociation between perfusion and oxygenation in HCM, we examined the role of myocardial metabolism and genotype, in addition to other clinical parameters.

In support of our previous observations (69), we found a significant association between phenotypic markers of severity, such as the extent of hypertrophy, myocardial perfusion reserve and stress oxygenation on univariate analysis. Additionally, we show for the first time that both genotype and myocardial energetics or metabolism, were associated with myocardial oxygenation on univariate analysis. These findings provide further support to the notion that energy inefficient processes which escalate oxygen requirements likely contribute to blunted stress oxygenation. Of interest, we did not see any relationship between LVOT obstruction and stress oxygenation. Indeed, Olivotto *et al*. (70), in a study of 61 HCM patients also found a lack of association between LVOT obstruction and dipyridamole induced myocardial blood flow assessed on PET imaging. Nevertheless, as the number of patients with resting obstruction in both studies are small, more adequately powered studies to clarify this relationship between stress oxygenation and LVOT obstruction may be required.

Sarcomeric mutation and myocardial oxygenation

Hypertrophic cardiomyopathy is typically a monogenic disease, with up to 60% of cases found to be due to mutations in sarcomeric myofilament genes (162, 163). With the increasing use of predictive gene testing, studies have emerged indicating that sarcomeric myofilament HCM have a more adverse phenotype with a greater burden of clinical events than non-sarcomeric HCM (70, 73, 164).

In this study, sarcomeric HCM displayed more severe impairment in oxygenation compared to genotype negative HCM and healthy controls. Of interest, this differed from the extent of perfusion impairment, which was similar, between genotype subgroups. In line with a previous study, sarcomeric HCM additionally displayed reduced myocardial energetics, indicating evidence of significant energetic depletion (38). Of interest, in a recent study, Witjas-Paalberends *et al.* has also suggested that tension energy costs of contraction may be higher in sarcomeric than genotype negative HCM (71). Therefore, it is concievable that myocardial efficiency in sacromeric HCM, may be diminished due to a combination of both increased metabolic demand and impaired perfusion (71). Given that blunted stress oxygenation precedes the onset of hypertrophy, it is tempting to speculate that genotype differences in oxygenation play a role in the natural history of disease and could explain a higher burden of clinical events in sarcomeric HCM patients (73, 164, 165). Indeed, in a longitudinal CMR study of 72 patients, sarcomeric HCM was found to have more progression in myocardial fibrosis than genotype negative HCM (94)

Myocardial fibrosis is more extensive in HCM with the greatest impairment in oxygenation

In HCM, microvascular abnormalities have been extensively described in histological studies (16, 30, 166). Manifesting as an inadequate rise in myocardial blood flow during vasodilator stress (56, 57), microvascular dysfunction predisposes to myocardial ischemia. The evidence for myocardial ischemia is compelling, as studies have shown both a rise in coronary sinus lactate and or ischemic ECG changes on pacing, exercise and vasodilator stress testing in HCM (167-169). Several mechanisms have been proposed including compression of septal vessels due to abnormalities in relaxation, increased oxygen demand secondary to outflow obstruction, myocardial bridge, inadequate capillary density and small intramyocardial coronary arteries. Although we have detected evidence of impaired oxygenation in HCM using BOLD CMR (69), the extent to which myocardial ischemia promotes myocardial fibrosis remains unknown (56).

In the current study, we show for the first time that the burden of myocardial fibrosis was most severe in HCM patients with the lowest quartile of myocardial oxygenation. There are two possible explanations for this. The first is that impaired oxygenation could be the result of capillary rarefaction and hypoperfusion, seen commonly in regions of myocardial fibrosis (20). In a study by Ismail *et al.*, myocardium with fibrosis tended to have greater impairment in myocardial blood flow on CMR than non fibrotic regions (58). However, this would not explain the presence of blunted oxygenation in phenotype negative mutations carriers without fibrosis. The second is that severely

impaired oxygenation promotes replacement fibrosis through a process of ischaemic necrosis (55). This is supported by a ‘dose-response’ relationship between myocardial oxygenation and fibrosis, where severe deoxygenation (lowest quartile) was clearly associated with more extensive fibrosis compared to other quartiles (**Figure 3**). Nevertheless, given the cross-sectional nature of this study, the pathophysiological role of blunted stress oxygenation in promoting fibrosis cannot be definitively ascertained. Further longitudinal studies examining the effects of impaired oxygenation on fibrosis progression and cardiac remodelling may therefore be insightful (16, 90, 170).

6.7 CLINICAL IMPLICATIONS

For the management of HCM, a desired therapeutic target would be one that is amenable to early intervention prior to onset of symptoms of heart failure (138). The association of oxygenation with myocardial fibrosis raises the prospect that treating factors that predispose to ischemia, such as reduced perfusion and energetic impairment, may potentially modify the natural history of this disease (74, 130). Therefore, the role of vasoactive and metabolic therapies on myocardial oxygenation and fibrosis in HCM merit further evaluation in future studies.

6.8 STUDY LIMITATIONS

This is a single-centre study examining the role of pathogenic mutations in HCM on myocardial oxygenation. We undertook BOLD CMR on a single slice and the role of multi-slice BOLD imaging needs further consideration. In the genotyped cohort, there were five patients with sarcomeric gene mutations, classified as variant of uncertain significance and were excluded in genotype comparisons. While we did not systematically undertake a coronary angiogram in all, exercise testing was undertaken in all HCM patients and those with angina or a positive stress test were further investigated with a coronary angiogram.

6.9 CONCLUSIONS

In HCM, sarcomeric mutation status independently predicts the extent of stress oxygenation. HCM patients with the most severe impairment in stress oxygenation have the greatest burden of myocardial fibrosis. This study serves to illustrate the potential role of stress oxygenation assessment in identifying those at risk of fibrosis progression and adverse cardiac remodelling.

CHAPTER 7: GENERAL CONCLUSIONS AND FUTURE DIRECTIONS

Myocardial fibrosis is a pathological hallmark in HCM and the past two decades have seen a growing recognition of its prognostic significance. The extent of late gadolinium enhancement (LGE) is shown to predict both cardiovascular mortality and adverse cardiac remodelling in HCM (21, 48, 118).

In this thesis, I have shown that myocardial fibrosis as assessed on LGE CMR can progress over a relatively short period in some adult patients with established HCM. Serial CMR with LGE imaging separated by only a few years can detect meaningful changes in fibrotic burden in HCM. Substantial LGE progression (ΔLGE≥ 4.75g) increases the risk of clinical events by five-fold even after adjusting for baseline LGE mass. The extent of LGE mass at any given time point is predictive of LGE progression in the future, a finding which is consistent across the literature (37, 105). In this work, a longer scan interval allowed for left ventricular remodelling to manifest, which was not apparent on previous studies (37, 105), providing further insights into the role of fibrosis progression in the natural history and clinical outcomes of this disease.

The complex relationship between left ventricular hypertrophy and replacement fibrosis was also highlighted here, as left ventricular thinning was found to occur due to a growing burden of fibrosis. Given that LGE is associated with adverse outcomes, the

assessment of left ventricular wall thickness without knowledge of LGE burden may potentially underestimate risks perceived based on contemporary guidelines.

In Chapters 3 and 6 of the thesis, the role of genotype was examined. Sarcomeric HCM were at greatest risk of impaired oxygenation and fibrosis progression over genotype negative HCM. These findings resonate with the work of others (70, 164), where genotype differences amongst HCM patients have been described in fibrosis extent and microvascular burden, highlighting the need for larger, more adequately powered studies to assess the pathological role of genotype.

In Chapter 4, the relationships between microvascular dysfunction and metabolism and LGE progression were discussed. Both microvascular dysfunction and impaired energetics were shown to associate with a greater burden of fibrosis progression. While this does not prove a causal role, the association raises the prospect that pharmacotherapy aimed at improving myocardial perfusion and metabolism could potentially reduce the risk of adverse remodelling and development of fibrosis in HCM.

As both impaired perfusion and increased metabolic demands contribute to myocardial ischaemia, the main focus of Chapters 5 and 6 was to accurately assess stress-induced myocardial oxygenation in HCM and assess its relationship with myocardial fibrosis.

In Chapter 5, a precise and visually informative method for the detection of myocardial stress-induced oxygenation was described. FLASH interleaved T2 prepared SSFP

considerably improves both between-subject and within-subject variability of standard BOLD measurements in healthy controls, with superior segmental inter- and intra-observer reproducibility than the standard method. The use of a colour map further allowed the visualization of oxygen sensitive signal, with clear potential for clinical applications. Although I was unable to provide biological validation for this method, FLASH-normalised T2 prepared SSFP did not differ from the standard method (69) in its mean BOLD effect. Furthermore, previous groups have demonstrated that standard T2 prepared SSFP BOLD correlates well with coronary sinus oxygen saturation. Nevertheless, further efforts to provide biological validation for the signal detected with FLASH-normalised BOLD will be required.

In the final chapter, the relationship between blunted stress-induced oxygenation, (assessed on FLASH normalised BOLD CMR) and myocardial fibrosis was examined along with the determinants of stress oxygenation in HCM. Myocardial fibrosis was most extensive in those patients with the lowest quartile of stress oxygenation, providing support to the notion that myocardial ischaemia may promote fibrosis in HCM. Sarcomeric mutation status was also found to independently predict the extent of stress oxygenation in HCM.

In summary, the non-invasive assessment of myocardial perfusion, metabolism, oxygenation and fibrosis has afforded numerous insights into pathophysiological mechanisms underlying fibrosis and its evolution in HCM.

Based on the work outlined in this thesis, I propose that myocardial fibrosis in HCM is triggered by processes that increase myocyte stress which directly or indirectly activate profibrotic pathways. One such stress is myocardial ischaemia which occurs due to an imbalance in oxygen delivery and metabolic/oxygen demands. While adverse microvascular remodelling may contribute to impaired oxygen delivery, increased metabolic demands may be the result of energy costly sarcomeric mutations which increase calcium sensitivity, alter cross bridge kinetics and increase myosin ATPase activity. The altered calcium homeostasis and energetic depletion may additionally result in mitochondrial dysfunction and an increasing burden of oxidative stress, eventually triggering both inflammatory and profibrotic pathways. This is also reflected by the pattern of myocardial fibrosis seen in HCM which is often both reparative and reactive in response to ischaemic and non-ischaemic stressors. Therefore, targetting pathways that improve myocardial metabolism and perfusion may help prevent progression of fibrosis and reduce the risk of clinical deterioration in HCM patients.

REFERENCES

1. Semsarian C, Ingles J, Maron MS, Maron BJ. New perspectives on the prevalence of hypertrophic cardiomyopathy. J Am Coll Cardiol. 2015;65(12):1249-54.
2. Maron BJ, Ommen SR, Semsarian C, Spirito P, Olivotto I, Maron MS. Hypertrophic cardiomyopathy: present and future, with translation into contemporary cardiovascular medicine. J Am Coll Cardiol. 2014;64(1):83-99.
3. American College of Cardiology Foundation/American Heart Association Task Force on Practice G, American Association for Thoracic S, American Society of E, American Society of Nuclear C, Heart Failure Society of A, Heart Rhythm S, et al. 2011 ACCF/AHA guideline for the diagnosis and treatment of hypertrophic cardiomyopathy: executive summary: a report of the American College of Cardiology Foundation/American Heart Association Task Force on Practice Guidelines. J Thorac Cardiovasc Surg. 2011;142(6):1303-38.
4. Richard P, Charron P, Carrier L, Ledeuil C, Cheav T, Pichereau C, et al. Hypertrophic cardiomyopathy: distribution of disease genes, spectrum of mutations, and implications for a molecular diagnosis strategy. Circulation. 2003;107(17):2227-32.
5. Maron BJ, Maron MS, Semsarian C. Genetics of hypertrophic cardiomyopathy after 20 years: clinical perspectives. J Am Coll Cardiol. 2012;60(8):705-15.
6. Authors/Task Force m, Elliott PM, Anastasakis A, Borger MA, Borggrefe M, Cecchi F, et al. 2014 ESC Guidelines on diagnosis and management of hypertrophic cardiomyopathy: the Task Force for the Diagnosis and Management of Hypertrophic Cardiomyopathy of the European Society of Cardiology (ESC). Eur Heart J. 2014;35(39):2733-79.
7. Maron BJ, Udelson JE, Bonow RO, Nishimura RA, Ackerman MJ, Estes NA, 3rd, et al. Eligibility and Disqualification Recommendations for Competitive Athletes With Cardiovascular Abnormalities: Task Force 3: Hypertrophic Cardiomyopathy, Arrhythmogenic Right Ventricular Cardiomyopathy and Other Cardiomyopathies, and Myocarditis: A Scientific Statement From the American Heart Association and American College of Cardiology. Circulation. 2015;132(22):e273-80.
8. Frenneaux MP. Assessing the risk of sudden cardiac death in a patient with hypertrophic cardiomyopathy. Heart. 2004;90(5):570-5.
9. Siontis KC, Geske JB, Ong K, Nishimura RA, Ommen SR, Gersh BJ. Atrial fibrillation in hypertrophic cardiomyopathy: prevalence, clinical correlations, and mortality in a large high-risk population. J Am Heart Assoc. 2014;3(3):e001002.
10. Olivotto I, DiDonna P, Baldi M, Sgalambro A, Maron BJ, Cecchi F. [Atrial fibrillation in hypertrophic cardiomyopathy: determinants, clinical course and management]. Zhonghua Xin Xue Guan Bing Za Zhi. 2009;37(4):303-7.
11. Maron BJ, Olivotto I, Bellone P, Conte MR, Cecchi F, Flygenring BP, et al. Clinical profile of stroke in 900 patients with hypertrophic cardiomyopathy. J Am Coll Cardiol. 2002;39(2):301-7.
12. Guttmann OP. Atrial fibrillation and thromboembolism in hypertrophic cardiomyopathy - An underestimated risk. Int J Cardiol. 2018;273:187-8.

13. Biagini E, Coccolo F, Ferlito M, Perugini E, Rocchi G, Bacchi-Reggiani L, et al. Dilated-hypokinetic evolution of hypertrophic cardiomyopathy: prevalence, incidence, risk factors, and prognostic implications in pediatric and adult patients. J Am Coll Cardiol. 2005;46(8):1543-50.
14. Harris KM, Spirito P, Maron MS, Zenovich AG, Formisano F, Lesser JR, et al. Prevalence, clinical profile, and significance of left ventricular remodeling in the end-stage phase of hypertrophic cardiomyopathy. Circulation. 2006;114(3):216-25.
15. Teare D. Asymmetrical hypertrophy of the heart in young adults. Br Heart J. 1958;20(1):1-8.
16. Varnava AM, Elliott PM, Sharma S, McKenna WJ, Davies MJ. Hypertrophic cardiomyopathy: the interrelation of disarray, fibrosis, and small vessel disease. Heart. 2000;84(5):476-82.
17. Varnava AM, Elliott PM, Mahon N, Davies MJ, McKenna WJ. Relation between myocyte disarray and outcome in hypertrophic cardiomyopathy. Am J Cardiol. 2001;88(3):275-9.
18. Davies MJ. The current status of myocardial disarray in hypertrophic cardiomyopathy. Br Heart J. 1984;51(4):361-3.
19. St John Sutton MG, Lie JT, Anderson KR, O'Brien PC, Frye RL. Histopathological specificity of hypertrophic obstructive cardiomyopathy. Myocardial fibre disarray and myocardial fibrosis. Br Heart J. 1980;44(4):433-43.
20. Hughes SE. The pathology of hypertrophic cardiomyopathy. Histopathology. 2004;44(5):412-27.
21. Bruder O, Wagner A, Jensen CJ, Schneider S, Ong P, Kispert EM, et al. Myocardial scar visualized by cardiovascular magnetic resonance imaging predicts major adverse events in patients with hypertrophic cardiomyopathy. J Am Coll Cardiol. 2010;56(11):875-87.
22. Jiang M, Wang Z, Su X, Gong X, Pu J, Wu L, et al. The Significance of Interstitial Fibrosis on Left Ventricular Function in Hypertensive versus Hypertrophic Cardiomyopathy. Sci Rep. 2018;8(1):9995.
23. Ellims AH, Iles LM, Ling LH, Hare JL, Kaye DM, Taylor AJ. Diffuse myocardial fibrosis in hypertrophic cardiomyopathy can be identified by cardiovascular magnetic resonance, and is associated with left ventricular diastolic dysfunction. J Cardiovasc Magn Reson. 2012;14:76.
24. Kitamura M, Shimizu M, Ino H, Okeie K, Yamaguchi M, Funjno N, et al. Collagen remodeling and cardiac dysfunction in patients with hypertrophic cardiomyopathy: the significance of type III and VI collagens. Clin Cardiol. 2001;24(4):325-9.
25. Factor SM, Butany J, Sole MJ, Wigle ED, Williams WC, Rojkind M. Pathologic fibrosis and matrix connective tissue in the subaortic myocardium of patients with hypertrophic cardiomyopathy. J Am Coll Cardiol. 1991;17(6):1343-51.
26. Weber KT, Brilla CG. Factors associated with reactive and reparative fibrosis of the myocardium. Basic Res Cardiol. 1992;87 Suppl 1:291-301.
27. Kai H, Kuwahara F, Tokuda K, Imaizumi T. Diastolic dysfunction in hypertensive hearts: roles of perivascular inflammation and reactive myocardial fibrosis. Hypertens Res. 2005;28(6):483-90.
28. van den Borne SW, Diez J, Blankesteijn WM, Verjans J, Hofstra L, Narula J. Myocardial remodeling after infarction: the role of myofibroblasts. Nat Rev Cardiol. 2010;7(1):30-7.

29. Shinde AV, Frangogiannis NG. Fibroblasts in myocardial infarction: a role in inflammation and repair. J Mol Cell Cardiol. 2014;70:74-82.
30. Galati G, Leone O, Pasquale F, Olivotto I, Biagini E, Grigioni F, et al. Histological and Histometric Characterization of Myocardial Fibrosis in End-Stage Hypertrophic Cardiomyopathy: A Clinical-Pathological Study of 30 Explanted Hearts. Circ Heart Fail. 2016;9(9).
31. Maron MS, Appelbaum E, Harrigan CJ, Buros J, Gibson CM, Hanna C, et al. Clinical profile and significance of delayed enhancement in hypertrophic cardiomyopathy. Circ Heart Fail. 2008;1(3):184-91.
32. Geer JC, Crago CA, Little WC, Gardner LL, Bishop SP. Subendocardial ischemic myocardial lesions associated with severe coronary atherosclerosis. Am J Pathol. 1980;98(3):663-80.
33. Levine HD. Myocardial fibrosis in constrictive pericarditis. Electrocardiographic and pathologic observations. Circulation. 1973;48(6):1268-81.
34. Friedrich MG, Sechtem U, Schulz-Menger J, Holmvang G, Alakija P, Cooper LT, et al. Cardiovascular magnetic resonance in myocarditis: A JACC White Paper. J Am Coll Cardiol. 2009;53(17):1475-87.
35. Oda S, Kawano Y, Okuno Y, Utsunomiya D, Nakaura T, Tsujita K, et al. Base-to-apex gradient pattern of cardiac impairment identified on myocardial T1 mapping in cardiac amyloidosis. Radiol Case Rep. 2019;14(1):72-4.
36. Lee GY, Kim HK, Choi JO, Chang SA, Oh JK, Jeon ES, et al. Visual Assessment of Relative Apical Sparing Pattern Is More Useful Than Quantitative Assessment for Diagnosing Cardiac Amyloidosis in Borderline or Mildly Increased Left Ventricular Wall Thickness. Circ J. 2015;79(7):1575-84.
37. Todiere G, Aquaro GD, Piaggi P, Formisano F, Barison A, Masci PG, et al. Progression of myocardial fibrosis assessed with cardiac magnetic resonance in hypertrophic cardiomyopathy. J Am Coll Cardiol. 2012;60(10):922-9.
38. Crilley JG, Boehm EA, Blair E, Rajagopalan B, Blamire AM, Styles P, et al. Hypertrophic cardiomyopathy due to sarcomeric gene mutations is characterized by impaired energy metabolism irrespective of the degree of hypertrophy. J Am Coll Cardiol. 2003;41(10):1776-82.
39. Debold EP, Schmitt JP, Patlak JB, Beck SE, Moore JR, Seidman JG, et al. Hypertrophic and dilated cardiomyopathy mutations differentially affect the molecular force generation of mouse alpha-cardiac myosin in the laser trap assay. Am J Physiol Heart Circ Physiol. 2007;293(1):H284-91.
40. Lombardi R, Rodriguez G, Chen SN, Ripplinger CM, Li W, Chen J, et al. Resolution of established cardiac hypertrophy and fibrosis and prevention of systolic dysfunction in a transgenic rabbit model of human cardiomyopathy through thiol-sensitive mechanisms. Circulation. 2009;119(10):1398-407.
41. Shirani J, Pick R, Roberts WC, Maron BJ. Morphology and significance of the left ventricular collagen network in young patients with hypertrophic cardiomyopathy and sudden cardiac death. J Am Coll Cardiol. 2000;35(1):36-44.
42. Camici PG, Crea F. Coronary microvascular dysfunction. N Engl J Med. 2007;356(8):830-40.

43. Geisterfer-Lowrance AA, Christe M, Conner DA, Ingwall JS, Schoen FJ, Seidman CE, et al. A mouse model of familial hypertrophic cardiomyopathy. Science. 1996;272(5262):731-4.
44. Kim JB, Porreca GJ, Song L, Greenway SC, Gorham JM, Church GM, et al. Polony multiplex analysis of gene expression (PMAGE) in mouse hypertrophic cardiomyopathy. Science. 2007;316(5830):1481-4.
45. Ho CY, Lopez B, Coelho-Filho OR, Lakdawala NK, Cirino AL, Jarolim P, et al. Myocardial fibrosis as an early manifestation of hypertrophic cardiomyopathy. N Engl J Med. 2010;363(6):552-63.
46. Teekakirikul P, Eminaga S, Toka O, Alcalai R, Wang L, Wakimoto H, et al. Cardiac fibrosis in mice with hypertrophic cardiomyopathy is mediated by non-myocyte proliferation and requires Tgf-beta. J Clin Invest. 2010;120(10):3520-9.
47. Chan RH, Maron BJ, Olivotto I, Assenza GE, Haas TS, Lesser JR, et al. Significance of Late Gadolinium Enhancement at Right Ventricular Attachment to Ventricular Septum in Patients With Hypertrophic Cardiomyopathy. Am J Cardiol. 2015;116(3):436-41.
48. O'Hanlon R, Grasso A, Roughton M, Moon JC, Clark S, Wage R, et al. Prognostic significance of myocardial fibrosis in hypertrophic cardiomyopathy. J Am Coll Cardiol. 2010;56(11):867-74.
49. Moon JC, Reed E, Sheppard MN, Elkington AG, Ho SY, Burke M, et al. The histologic basis of late gadolinium enhancement cardiovascular magnetic resonance in hypertrophic cardiomyopathy. J Am Coll Cardiol. 2004;43(12):2260-4.
50. Kim RJ, Chen EL, Lima JA, Judd RM. Myocardial Gd-DTPA kinetics determine MRI contrast enhancement and reflect the extent and severity of myocardial injury after acute reperfused infarction. Circulation. 1996;94(12):3318-26.
51. Flacke SJ, Fischer SE, Lorenz CH. Measurement of the gadopentetate dimeglumine partition coefficient in human myocardium in vivo: normal distribution and elevation in acute and chronic infarction. Radiology. 2001;218(3):703-10.
52. Moravsky G, Ofek E, Rakowski H, Butany J, Williams L, Ralph-Edwards A, et al. Myocardial fibrosis in hypertrophic cardiomyopathy: accurate reflection of histopathological findings by CMR. JACC Cardiovasc Imaging. 2013;6(5):587-96.
53. Chan RH, Maron BJ, Olivotto I, Pencina MJ, Assenza GE, Haas T, et al. Prognostic value of quantitative contrast-enhanced cardiovascular magnetic resonance for the evaluation of sudden death risk in patients with hypertrophic cardiomyopathy. Circulation. 2014;130(6):484-95.
54. Maron BJ, Wolfson JK, Epstein SE, Roberts WC. Intramural ("small vessel") coronary artery disease in hypertrophic cardiomyopathy. J Am Coll Cardiol. 1986;8(3):545-57.
55. Basso C, Thiene G, Corrado D, Buja G, Melacini P, Nava A. Hypertrophic cardiomyopathy and sudden death in the young: pathologic evidence of myocardial ischemia. Hum Pathol. 2000;31(8):988-98.
56. Cecchi F, Olivotto I, Gistri R, Lorenzoni R, Chiriatti G, Camici PG. Coronary microvascular dysfunction and prognosis in hypertrophic cardiomyopathy. N Engl J Med. 2003;349(11):1027-35.
57. Petersen SE, Jerosch-Herold M, Hudsmith LE, Robson MD, Francis JM, Doll HA, et al. Evidence for microvascular dysfunction in hypertrophic cardiomyopathy: new insights from multiparametric magnetic resonance imaging. Circulation. 2007;115(18):2418-25.

58. Ismail TF, Hsu LY, Greve AM, Goncalves C, Jabbour A, Gulati A, et al. Coronary microvascular ischemia in hypertrophic cardiomyopathy - a pixel-wise quantitative cardiovascular magnetic resonance perfusion study. J Cardiovasc Magn Reson. 2014;16:49.
59. Basso C, Thiene G, Mackey-Bojack S, Frigo AC, Corrado D, Maron BJ. Myocardial bridging, a frequent component of the hypertrophic cardiomyopathy phenotype, lacks systematic association with sudden cardiac death. European heart journal. 2009;30(13):1627-34.
60. Timmer SA, Germans T, Gotte MJ, Russel IK, Dijkmans PA, Lubberink M, et al. Determinants of myocardial energetics and efficiency in symptomatic hypertrophic cardiomyopathy. European journal of nuclear medicine and molecular imaging. 2010;37(4):779-88.
61. Watkins H, Rosenzweig A, Hwang DS, Levi T, McKenna W, Seidman CE, et al. Characteristics and prognostic implications of myosin missense mutations in familial hypertrophic cardiomyopathy. The New England journal of medicine. 1992;326(17):1108-14.
62. Geisterfer-Lowrance AA, Kass S, Tanigawa G, Vosberg HP, McKenna W, Seidman CE, et al. A molecular basis for familial hypertrophic cardiomyopathy: a beta cardiac myosin heavy chain gene missense mutation. Cell. 1990;62(5):999-1006.
63. Seidman CE, Seidman JG. Identifying sarcomere gene mutations in hypertrophic cardiomyopathy: a personal history. Circ Res. 2011;108(6):743-50.
64. Maron BJ. Hypertrophic cardiomyopathy: a systematic review. JAMA. 2002;287(10):1308-20.
65. Dandona S, Roberts R. Identification of myofilament mutations: its role in the diagnosis and management of hypertrophic cardiomyopathy. Mayo Clin Proc. 2008;83(6):626-7.
66. Jarcho JA, McKenna W, Pare JA, Solomon SD, Holcombe RF, Dickie S, et al. Mapping a gene for familial hypertrophic cardiomyopathy to chromosome 14q1. The New England journal of medicine. 1989;321(20):1372-8.
67. Ho CY. Genetics and clinical destiny: improving care in hypertrophic cardiomyopathy. Circulation. 2010;122(23):2430-40; discussion 40.
68. Sabater-Molina M, Perez-Sanchez I, Hernandez Del Rincon JP, Gimeno JR. Genetics of hypertrophic cardiomyopathy: A review of current state. Clin Genet. 2018;93(1):3-14.
69. Karamitsos TD, Dass S, Suttie J, Sever E, Birks J, Holloway CJ, et al. Blunted myocardial oxygenation response during vasodilator stress in patients with hypertrophic cardiomyopathy. J Am Coll Cardiol. 2013;61(11):1169-76.
70. Olivotto I, Girolami F, Sciagra R, Ackerman MJ, Sotgia B, Bos JM, et al. Microvascular function is selectively impaired in patients with hypertrophic cardiomyopathy and sarcomere myofilament gene mutations. J Am Coll Cardiol. 2011;58(8):839-48.
71. Witjas-Paalberends ER, Guclu A, Germans T, Knaapen P, Harms HJ, Vermeer AM, et al. Gene-specific increase in the energetic cost of contraction in hypertrophic cardiomyopathy caused by thick filament mutations. Cardiovasc Res. 2014;103(2):248-57.
72. Ellims AH, Iles LM, Ling LH, Chong B, Macciocca I, Slavin GS, et al. A comprehensive evaluation of myocardial fibrosis in hypertrophic cardiomyopathy with cardiac magnetic resonance imaging: linking genotype with fibrotic phenotype. Eur Heart J Cardiovasc Imaging. 2014;15(10):1108-16.

73. Ho CY, Day SM, Ashley EA, Michels M, Pereira AC, Jacoby D, et al. Genotype and Lifetime Burden of Disease in Hypertrophic Cardiomyopathy: Insights from the Sarcomeric Human Cardiomyopathy Registry (SHaRe). Circulation. 2018;138(14):1387-98.
74. Ashrafian H, McKenna WJ, Watkins H. Disease pathways and novel therapeutic targets in hypertrophic cardiomyopathy. Circulation research. 2011;109(1):86-96.
75. Watkins H, Ashrafian H, Redwood C. Inherited cardiomyopathies. N Engl J Med. 2011;364(17):1643-56.
76. Redwood CS, Moolman-Smook JC, Watkins H. Properties of mutant contractile proteins that cause hypertrophic cardiomyopathy. Cardiovasc Res. 1999;44(1):20-36.
77. Lowey S. Functional consequences of mutations in the myosin heavy chain at sites implicated in familial hypertrophic cardiomyopathy. Trends Cardiovasc Med. 2002;12(8):348-54.
78. Bing W, Redwood CS, Purcell IF, Esposito G, Watkins H, Marston SB. Effects of two hypertrophic cardiomyopathy mutations in alpha-tropomyosin, Asp175Asn and Glu180Gly, on Ca2+ regulation of thin filament motility. Biochem Biophys Res Commun. 1997;236(3):760-4.
79. Robinson P, Mirza M, Knott A, Abdulrazzak H, Willott R, Marston S, et al. Alterations in thin filament regulation induced by a human cardiac troponin T mutant that causes dilated cardiomyopathy are distinct from those induced by troponin T mutants that cause hypertrophic cardiomyopathy. J Biol Chem. 2002;277(43):40710-6.
80. Burton D, Abdulrazzak H, Knott A, Elliott K, Redwood C, Watkins H, et al. Two mutations in troponin I that cause hypertrophic cardiomyopathy have contrasting effects on cardiac muscle contractility. Biochem J. 2002;362(Pt 2):443-51.
81. Merante F, Tein I, Benson L, Robinson BH. Maternally inherited hypertrophic cardiomyopathy due to a novel T-to-C transition at nucleotide 9997 in the mitochondrial tRNA(glycine) gene. Am J Hum Genet. 1994;55(3):437-46.
82. Lodi R, Cooper JM, Bradley JL, Manners D, Styles P, Taylor DJ, et al. Deficit of in vivo mitochondrial ATP production in patients with Friedreich ataxia. Proc Natl Acad Sci U S A. 1999;96(20):11492-5.
83. Aoyama T, Souri M, Ushikubo S, Kamijo T, Yamaguchi S, Kelley RI, et al. Purification of human very-long-chain acyl-coenzyme A dehydrogenase and characterization of its deficiency in seven patients. J Clin Invest. 1995;95(6):2465-73.
84. Kaplan JH. Ion movements through the sodium pump. Annu Rev Physiol. 1985;47:535-44.
85. Robinson P, Liu X, Sparrow A, Patel S, Zhang YH, Casadei B, et al. Hypertrophic cardiomyopathy mutations increase myofilament Ca(2+) buffering, alter intracellular Ca(2+) handling, and stimulate Ca(2+)-dependent signaling. J Biol Chem. 2018;293(27):10487-99.
86. Konno T, Chen D, Wang L, Wakimoto H, Teekakirikul P, Nayor M, et al. Heterogeneous myocyte enhancer factor-2 (Mef2) activation in myocytes predicts focal scarring in hypertrophic cardiomyopathy. Proc Natl Acad Sci U S A. 2010;107(42):18097-102.
87. Richter K, Kietzmann T. Reactive oxygen species and fibrosis: further evidence of a significant liaison. Cell Tissue Res. 2016;365(3):591-605.

88. Lamke GT, Allen RD, Edwards WD, Tazelaar HD, Danielson GK. Surgical pathology of subaortic septal myectomy associated with hypertrophic cardiomyopathy. A study of 204 cases (1996-2000). Cardiovasc Pathol. 2003;12(3):149-58.
89. Baandrup U, Florio RA, Rehahn M, Richardson PJ, Olsen EG. Critical analysis of endomyocardial biopsies from patients suspected of having cardiomyopathy. II: Comparison of histology and clinical/haemodynamic information. Br Heart J. 1981;45(5):487-93.
90. Zen K, Irie H, Doue T, Takamiya M, Yamano T, Sawada T, et al. Analysis of circulating apoptosis mediators and proinflammatory cytokines in patients with idiopathic hypertrophic cardiomyopathy: comparison between nonobstructive and dilated-phase hypertrophic cardiomyopathy. Int Heart J. 2005;46(2):231-44.
91. Andrabi SA, Umanah GK, Chang C, Stevens DA, Karuppagounder SS, Gagne JP, et al. Poly(ADP-ribose) polymerase-dependent energy depletion occurs through inhibition of glycolysis. Proc Natl Acad Sci U S A. 2014;111(28):10209-14.
92. Feng FY, de Bono JS, Rubin MA, Knudsen KE. Chromatin to Clinic: The Molecular Rationale for PARP1 Inhibitor Function. Mol Cell. 2015;58(6):925-34.
93. Bhute VJ, Palecek SP. Metabolic responses induced by DNA damage and poly (ADP-ribose) polymerase (PARP) inhibition in MCF-7 cells. Metabolomics. 2015;11(6):1779-91.
94. Raman B, Ariga R, Spartera M, Sivalokanathan S, Chan K, Dass S, et al. Progression of myocardial fibrosis in hypertrophic cardiomyopathy: mechanisms and clinical implications. Eur Heart J Cardiovasc Imaging. 2018.
95. Dass S, Cochlin LE, Suttie JJ, Holloway CJ, Rider OJ, Carden L, et al. Exacerbation of cardiac energetic impairment during exercise in hypertrophic cardiomyopathy: a potential mechanism for diastolic dysfunction. Eur Heart J. 2015;36(24):1547-54.
96. Purvis LAB, Clarke WT, Biasiolli L, Valkovic L, Robson MD, Rodgers CT. OXSA: An open-source magnetic resonance spectroscopy analysis toolbox in MATLAB. PLoS One. 2017;12(9):e0185356.
97. Schulz-Menger J, Bluemke DA, Bremerich J, Flamm SD, Fogel MA, Friedrich MG, et al. Standardized image interpretation and post processing in cardiovascular magnetic resonance: Society for Cardiovascular Magnetic Resonance (SCMR) board of trustees task force on standardized post processing. J Cardiovasc Magn Reson. 2013;15:35.
98. Nagel E, Klein C, Paetsch I, Hettwer S, Schnackenburg B, Wegscheider K, et al. Magnetic resonance perfusion measurements for the noninvasive detection of coronary artery disease. Circulation. 2003;108(4):432-7.
99. Kellman P, Aletras AH, Mancini C, McVeigh ER, Arai AE. T2-prepared SSFP improves diagnostic confidence in edema imaging in acute myocardial infarction compared to turbo spin echo. Magn Reson Med. 2007;57(5):891-7.
100. Elliott PM, Poloniecki J, Dickie S, Sharma S, Monserrat L, Varnava A, et al. Sudden death in hypertrophic cardiomyopathy: identification of high risk patients. J Am Coll Cardiol. 2000;36(7):2212-8.
101. Acc/Aha/Esc. [ACC/AHA/ESC 2006 guidelines for management of patients with ventricular arrhythmias and the prevention of sudden death]. Kardiologiia. 2011;51(7):65-96.
102. Mavrogeni S, Petrou E, Kolovou G, Theodorakis G, Iliodromitis E. Prediction of ventricular arrhythmias using cardiovascular magnetic resonance. Eur Heart J Cardiovasc Imaging. 2013;14(6):518-25.

103. O'Hanlon R, Grasso A, Roughton M, Moon JC, Clark S, Wage R, et al. Prognostic significance of myocardial fibrosis in hypertrophic cardiomyopathy. J Am Coll Cardiol.56(11):867-74.
104. Axelsson Raja A, Farhad H, Valente AM, Couce JP, Jefferies JL, Bundgaard H, et al. Prevalence and Progression of Late Gadolinium Enhancement in Children and Adolescents with Hypertrophic Cardiomyopathy. Circulation. 2018.
105. Choi HM, Kim KH, Lee JM, Yoon YE, Lee SP, Park EA, et al. Myocardial fibrosis progression on cardiac magnetic resonance in hypertrophic cardiomyopathy. Heart. 2015;101(11):870-6.
106. Ersoy H, Rybicki FJ. Biochemical safety profiles of gadolinium-based extracellular contrast agents and nephrogenic systemic fibrosis. J Magn Reson Imaging. 2007;26(5):1190-7.
107. Thomsen HS, Morcos SK, Esur. ESUR guidelines on contrast media. Abdom Imaging. 2006;31(2):131-40.
108. Grobner T. Gadolinium--a specific trigger for the development of nephrogenic fibrosing dermopathy and nephrogenic systemic fibrosis? Nephrol Dial Transplant. 2006;21(4):1104-8.
109. Li R, Yang ZG, Xu HY, Shi K, Liu X, Diao KY, et al. Myocardial Deformation in Cardiac Amyloid Light-chain Amyloidosis: Assessed with 3T Cardiovascular Magnetic Resonance Feature Tracking. Sci Rep. 2017;7(1):3794.
110. Mikami Y, Kolman L, Joncas SX, Stirrat J, Scholl D, Rajchl M, et al. Accuracy and reproducibility of semi-automated late gadolinium enhancement quantification techniques in patients with hypertrophic cardiomyopathy. J Cardiovasc Magn Reson. 2014;16:85.
111. Nicholls M. The 2014 ESC Guidelines on the Diagnosis and Management of Hypertrophic Cardiomyopathy have been published. European heart journal. 2014;35(41):2849-50.
112. Steyerberg EW, Eijkemans MJ, Harrell FE, Jr., Habbema JD. Prognostic modeling with logistic regression analysis: in search of a sensible strategy in small data sets. Med Decis Making. 2001;21(1):45-56.
113. Noureldin RA, Liu S, Nacif MS, Judge DP, Halushka MK, Abraham TP, et al. The diagnosis of hypertrophic cardiomyopathy by cardiovascular magnetic resonance. J Cardiovasc Magn Reson. 2012;14:17.
114. Weng Z, Yao J, Chan RH, He J, Yang X, Zhou Y, et al. Prognostic Value of LGE-CMR in HCM: A Meta-Analysis. JACC Cardiovascular imaging. 2016;9(12):1392-402.
115. Global Burden of Disease Health Financing Collaborator N. Future and potential spending on health 2015-40: development assistance for health, and government, prepaid private, and out-of-pocket health spending in 184 countries. Lancet. 2017;389(10083):2005-30.
116. O'Mahony C, Jichi F, Monserrat L, Ortiz-Genga M, Anastasakis A, Rapezzi C, et al. Inverted U-Shaped Relation Between the Risk of Sudden Cardiac Death and Maximal Left Ventricular Wall Thickness in Hypertrophic Cardiomyopathy. Circ Arrhythm Electrophysiol. 2016;9(6).

117. Spirito P, Autore C, Rapezzi C, Bernabo P, Badagliacca R, Maron MS, et al. Syncope and risk of sudden death in hypertrophic cardiomyopathy. Circulation. 2009;119(13):1703-10.
118. Chan RH, Maron BJ, Olivotto I, Pencina MJ, Assenza GE, Haas T, et al. Prognostic value of quantitative contrast-enhanced cardiovascular magnetic resonance for the evaluation of sudden death risk in patients with hypertrophic cardiomyopathy. Circulation. 2014;130(6):484-95.
119. Marian AJ, Yu QT, Workman R, Greve G, Roberts R. Angiotensin-Converting Enzyme Polymorphism in Hypertrophic Cardiomyopathy and Sudden Cardiac Death. Lancet. 1993;342(8879):1085-6.
120. Marian AJ. Modifier genes for hypertrophic cardiomyopathy. Curr Opin Cardiol. 2002;17(3):242-52.
121. Spindler M, Saupe KW, Christe ME, Sweeney HL, Seidman CE, Seidman JG, et al. Diastolic dysfunction and altered energetics in the alphaMHC403/+ mouse model of familial hypertrophic cardiomyopathy. J Clin Invest. 1998;101(8):1775-83.
122. Ashrafian H, Redwood C, Blair E, Watkins H. Hypertrophic cardiomyopathy: a paradigm for myocardial energy depletion. Trends Genet. 2003;19(5):263-8.
123. Gersh BJ, Maron BJ, Bonow RO, Dearani JA, Fifer MA, Link MS, et al. 2011 ACCF/AHA Guideline for the Diagnosis and Treatment of Hypertrophic Cardiomyopathy: a report of the American College of Cardiology Foundation/American Heart Association Task Force on Practice Guidelines. Developed in collaboration with the American Association for Thoracic Surgery, American Society of Echocardiography, American Society of Nuclear Cardiology, Heart Failure Society of America, Heart Rhythm Society, Society for Cardiovascular Angiography and Interventions, and Society of Thoracic Surgeons. J Am Coll Cardiol. 2011;58(25):e212-60.
124. Elliott PM, Anastasakis A, Borger MA, Borggrefe M, Cecchi F, Charron P, et al. 2014 ESC Guidelines on diagnosis and management of hypertrophic cardiomyopathy. European heart journal. 2014;35(39):2733-79.
125. Konno T, Hayashi K, Fujino N, Nagata Y, Hodatsu A, Masuta E, et al. High sensitivity of late gadolinium enhancement for predicting microscopic myocardial scarring in biopsied specimens in hypertrophic cardiomyopathy. PLoS One. 2014;9(7):e101465.
126. Kramer CM, Appelbaum E, Desai MY, Desvigne-Nickens P, DiMarco JP, Friedrich MG, et al. Hypertrophic Cardiomyopathy Registry: The rationale and design of an international, observational study of hypertrophic cardiomyopathy. American heart journal. 2015;170(2):223-30.
127. Maron MS, Rowin EJ, Olivotto I, Casey SA, Arretini A, Tomberli B, et al. Contemporary Natural History and Management of Nonobstructive Hypertrophic Cardiomyopathy. J Am Coll Cardiol. 2016;67(12):1399-409.
128. Maron BJ, Maron MS. Contemporary strategies for risk stratification and prevention of sudden death with the implantable defibrillator in hypertrophic cardiomyopathy. Heart Rhythm. 2016;13(5):1155-65.
129. Maron BJ. Clinical Course and Management of Hypertrophic Cardiomyopathy. The New England journal of medicine. 2018;379(20):1977.

130. Abozguia K, Elliott P, McKenna W, Phan TT, Nallur-Shivu G, Ahmed I, et al. Metabolic modulator perhexiline corrects energy deficiency and improves exercise capacity in symptomatic hypertrophic cardiomyopathy. Circulation. 2010;122(16):1562-9.
131. Olivotto I, Cecchi F, Gistri R, Lorenzoni R, Chiriatti G, Girolami F, et al. Relevance of coronary microvascular flow impairment to long-term remodeling and systolic dysfunction in hypertrophic cardiomyopathy. J Am Coll Cardiol. 2006;47(5):1043-8.
132. Tyler DJ, Robson MD, Henkelman RM, Young IR, Bydder GM. Magnetic resonance imaging with ultrashort TE (UTE) PULSE sequences: technical considerations. J Magn Reson Imaging. 2007;25(2):279-89.
133. Liu A, Wijesurendra RS, Liu JM, Forfar JC, Channon KM, Jerosch-Herold M, et al. Diagnosis of Microvascular Angina Using Cardiac Magnetic Resonance. J Am Coll Cardiol. 2018;71(9):969-79.
134. Bakir M, Wei J, Nelson MD, Mehta PK, Haftbaradaran A, Jones E, et al. Cardiac magnetic resonance imaging for myocardial perfusion and diastolic function-reference control values for women. Cardiovasc Diagn Ther. 2016;6(1):78-86.
135. Raphael CE, Cooper R, Parker KH, Collinson J, Vassiliou V, Pennell DJ, et al. Mechanisms of Myocardial Ischemia in Hypertrophic Cardiomyopathy: Insights From Wave Intensity Analysis and Magnetic Resonance. J Am Coll Cardiol. 2016;68(15):1651-60.
136. Takemura G, Takatsu Y, Fujiwara H. Luminal narrowing of coronary capillaries in human hypertrophic hearts: an ultrastructural morphometrical study using endomyocardial biopsy specimens. Heart. 1998;79(1):78-85.
137. Kuusisto J, Karja V, Sipola P, Kholova I, Peuhkurinen K, Jaaskelainen P, et al. Low-grade inflammation and the phenotypic expression of myocardial fibrosis in hypertrophic cardiomyopathy. Heart. 2012;98(13):1007-13.
138. Vakrou S, Abraham MR. Hypertrophic cardiomyopathy: a heart in need of an energy bar? Front Physiol. 2014;5:309.
139. Teekakirikul P, Padera RF, Seidman JG, Seidman CE. Hypertrophic cardiomyopathy: translating cellular cross talk into therapeutics. J Cell Biol. 2012;199(3):417-21.
140. Ogawa S, Lee TM, Kay AR, Tank DW. Brain magnetic resonance imaging with contrast dependent on blood oxygenation. Proc Natl Acad Sci U S A. 1990;87(24):9868-72.
141. Atalay MK, Forder JR, Chacko VP, Kawamoto S, Zerhouni EA. Oxygenation in the rabbit myocardium: assessment with susceptibility-dependent MR imaging. Radiology. 1993;189(3):759-64.
142. Wendland MF, Saeed M, Lauerma K, de Crespigny A, Moseley ME, Higgins CB. Endogenous susceptibility contrast in myocardium during apnea measured using gradient recalled echo planar imaging. Magn Reson Med. 1993;29(2):273-6.
143. Walcher T, Manzke R, Hombach V, Rottbauer W, Wohrle J, Bernhardt P. Myocardial perfusion reserve assessed by T2-prepared steady-state free precession blood oxygen level-dependent magnetic resonance imaging in comparison to fractional flow reserve. Circ Cardiovasc Imaging. 2012;5(5):580-6.
144. Vohringer M, Flewitt JA, Green JD, Dharmakumar R, Wang J, Jr., Tyberg JV, et al. Oxygenation-sensitive CMR for assessing vasodilator-induced changes of myocardial oxygenation. J Cardiovasc Magn Reson. 2010;12:20.

145. Friedrich MG, Niendorf T, Schulz-Menger J, Gross CM, Dietz R. Blood oxygen level-dependent magnetic resonance imaging in patients with stress-induced angina. Circulation. 2003;108(18):2219-23.
146. Wacker CM, Bock M, Hartlep AW, Bauer WR, van Kaick G, Pfleger S, et al. BOLD-MRI in ten patients with coronary artery disease: evidence for imaging of capillary recruitment in myocardium supplied by the stenotic artery. MAGMA. 1999;8(1):48-54.
147. Fieno DS, Shea SM, Li Y, Harris KR, Finn JP, Li D. Myocardial perfusion imaging based on the blood oxygen level-dependent effect using T2-prepared steady-state free-precession magnetic resonance imaging. Circulation. 2004;110(10):1284-90.
148. Fischer K, Guensch DP, Friedrich MG. Response of myocardial oxygenation to breathing manoeuvres and adenosine infusion. Eur Heart J Cardiovasc Imaging. 2015;16(4):395-401.
149. Arnold JR, Karamitsos TD, Bhamra-Ariza P, Francis JM, Searle N, Robson MD, et al. Myocardial oxygenation in coronary artery disease: insights from blood oxygen level-dependent magnetic resonance imaging at 3 tesla. J Am Coll Cardiol. 2012;59(22):1954-64.
150. Dass S, Holloway CJ, Cochlin LE, Rider OJ, Mahmod M, Robson M, et al. No Evidence of Myocardial Oxygen Deprivation in Nonischemic Heart Failure. Circ Heart Fail. 2015;8(6):1088-93.
151. Karamitsos TD, Leccisotti L, Arnold JR, Recio-Mayoral A, Bhamra-Ariza P, Howells RK, et al. Relationship between regional myocardial oxygenation and perfusion in patients with coronary artery disease: insights from cardiovascular magnetic resonance and positron emission tomography. Circ Cardiovasc Imaging. 2010;3(1):32-40.
152. Karamitsos TD, Hudsmith LE, Selvanayagam JB, Neubauer S, Francis JM. Operator induced variability in left ventricular measurements with cardiovascular magnetic resonance is improved after training. J Cardiovasc Magn Reson. 2007;9(5):777-83.
153. Sung K, Nayak KS. Design and use of tailored hard-pulse trains for uniformed saturation of myocardium at 3 Tesla. Magn Reson Med. 2008;60.
154. Noeske R, Seifert F, Rhein KH, Rinneberg H. Human cardiac imaging at 3 T using phased array coils. Magn Reson Med. 2000;44(6):978-82.
155. Parnham S, Gleadle JM, Bangalore S, Grover S, Perry R, Woodman RJ, et al. Impaired Myocardial Oxygenation Response to Stress in Patients With Chronic Kidney Disease. J Am Heart Assoc. 2015;4(8):e002249.
156. Yang HJ, Yumul R, Tang R, Cokic I, Klein M, Kali A, et al. Assessment of myocardial reactivity to controlled hypercapnia with free-breathing T2-prepared cardiac blood oxygen level-dependent MR imaging. Radiology. 2014;272(2):397-406.
157. Maron BJ, Spirito P, Shen WK, Haas TS, Formisano F, Link MS, et al. Implantable cardioverter-defibrillators and prevention of sudden cardiac death in hypertrophic cardiomyopathy. JAMA. 2007;298(4):405-12.
158. Adabag AS, Maron BJ, Appelbaum E, Harrigan CJ, Buros JL, Gibson CM, et al. Occurrence and frequency of arrhythmias in hypertrophic cardiomyopathy in relation to delayed enhancement on cardiovascular magnetic resonance. J Am Coll Cardiol. 2008;51(14):1369-74.

159. Levelt E, Rodgers CT, Clarke WT, Mahmod M, Ariga R, Francis JM, et al. Cardiac energetics, oxygenation, and perfusion during increased workload in patients with type 2 diabetes mellitus. Eur Heart J. 2016;37(46):3461-9.
160. Mahmod M, Francis JM, Pal N, Lewis A, Dass S, De Silva R, et al. Myocardial perfusion and oxygenation are impaired during stress in severe aortic stenosis and correlate with impaired energetics and subclinical left ventricular dysfunction. J Cardiovasc Magn Reson. 2014;16:29.
161. Timmer SA, Germans T, Brouwer WP, Lubberink M, van der Velden J, Wilde AA, et al. Carriers of the hypertrophic cardiomyopathy MYBPC3 mutation are characterized by reduced myocardial efficiency in the absence of hypertrophy and microvascular dysfunction. Eur J Heart Fail. 2011;13(12):1283-9.
162. Marian AJ, Roberts R. Molecular Genetic Basis of Hypertrophic Cardiomyopathy. Journal of Cardiovascular Electrophysiology. 1998;9(1):88-99.
163. Van Driest SL, Ommen SR, Tajik AJ, Gersh BJ, Ackerman MJ. Yield of genetic testing in hypertrophic cardiomyopathy. Mayo Clin Proc. 2005;80(6):739-44.
164. Olivotto I, Girolami F, Ackerman MJ, Nistri S, Bos JM, Zachara E, et al. Myofilament protein gene mutation screening and outcome of patients with hypertrophic cardiomyopathy. Mayo Clin Proc. 2008;83(6):630-8.
165. Coppini R, Ho CY, Ashley E, Day S, Ferrantini C, Girolami F, et al. Clinical phenotype and outcome of hypertrophic cardiomyopathy associated with thin-filament gene mutations. J Am Coll Cardiol. 2014;64(24):2589-600.
166. Schwartzkopff B, Mundhenke M, Strauer BE. Alterations of the architecture of subendocardial arterioles in patients with hypertrophic cardiomyopathy and impaired coronary vasodilator reserve: a possible cause for myocardial ischemia. J Am Coll Cardiol. 1998;31(5):1089-96.
167. Miyai N, Kawasaki T, Taniguchi T, Kamitani T, Kawasaki S, Sugihara H. [Exercise-induced ST-segment depression and myocardial ischemia in patients with hypertrophic cardiomyopathy: myocardial scintigraphic study]. J Cardiol. 2005;46(4):141-7.
168. Matsuo S, Nakamura Y, Takahashi M, Mitsunami K, Kinoshita M. Myocardial metabolic abnormalities in hypertrophic cardiomyopathy assessed by iodine-123-labeled beta-methyl-branched fatty acid myocardial scintigraphy and its relation to exercise-induced ischemia. Jpn Circ J. 1998;62(3):167-72.
169. Cannon RO, 3rd, Rosing DR, Maron BJ, Leon MB, Bonow RO, Watson RM, et al. Myocardial ischemia in patients with hypertrophic cardiomyopathy: contribution of inadequate vasodilator reserve and elevated left ventricular filling pressures. Circulation. 1985;71(2):234-43.
170. Fang L, Ellims AH, Beale AL, Taylor AJ, Murphy A, Dart AM. Systemic inflammation is associated with myocardial fibrosis, diastolic dysfunction, and cardiac hypertrophy in patients with hypertrophic cardiomyopathy. Am J Transl Res. 2017;9(11):5063-73.

APPENDIX 1: EXTENT OF INVOLVEMENT IN THE WORK

The majority of patients for this work were recruited by me. After applying for ethical approval to undertake CMR scans, I invited patients to participate in this study. For the work described in this thesis, I received training in CMR acquisition and post procession analysis. I also updated my skills in advanced life support to undertake stress perfusion scans. For the fibrosis progression work (Chapter 3 and Chapter 4), some of the earlier scans (2010-2012) were performed by Dr Sairia Dass and by Dr Rina Ariga between (2012-2015). All scans from 2015 - 2018 were undertaken by myself. For the recruitment of HCM patients, I participated in the Inherited Cardiac Conditions clinic regularly and worked closely with the research nurses to recruit patients. All healthy volunteers were invited to participate in this study via posters in hospital and clinic waiting rooms. Patient information leaflets and personalised invitations were sent by me via post or email to eligible patients and interested healthy participants. This was then followed up with a phone call to check their eligibility and safety to undergo the scans. When patients agreed, I would organise the CMR scan slot and arrange transport for every patient, while coordinating activities with the team of radiographers and research nurses on site. For those patients undergoing stress perfusion imaging, a phone call was made prior to their visit to ensure that the patient was caffeine free for at least 24 hours prior to the scan. As per the departmental standard operating procedures (SOP), an additional person trained in providing advanced life support had to be present for the scan and this was arranged prior to patient visits. On the day of the participant visit, every participant was assigned a random identification number for anonymisation of data. The CMR scanner was prepared with the set of coils for appropriate imaging prior to every visit. Preparation of adenosine infusion, where necessary, and gadolinium contrast infusion pumps were also undertaken by me, with dose and expiry dates cross checked by the radiographers or another second person. Eligibility of participants was reassessed and a brief medical history including family history, alcohol and smoking history was documented. I undertook a comprehensive transthoracic echocardiogram for all participants prior to the MRI. Participants also had a 12 lead electrocardiogram as part of departmental SOP for adenosine stress perfusion scans. Following this, I would cannulate participants on both arms to allow the injection of gadolinium-based contrast in one arm while adenosine infusion would run in the other. Routine blood tests were taken prior to the CMR scan and sent off to a pathology lab. I would then undertake the CMR scan independently, receiving support from another person only during the stress part of the scan. All haemodynamic parameters such as blood pressure and heart rate at rest were carefully recorded during the adenosine part of the protocol. At the end of every visit, participants were given an opportunity to claim back expenses for the study visit including travel and refreshments. In the case of incidental findings from CMR or blood tests, the case was discussed with one of my supervisors and then the appropriate clinical team. A letter would be promptly sent to the general practitioner informing him/her of the findings. For those patients who agreed to have a repeat CMR, I contacted them again for eligibility and safety to undertake the scan. All procedures for the first scan visit were then repeated where indicated. All HCM participants were followed up in the Inherited

Cardiac Conditions clinic and all medical records and investigations were reviewed by myself. In the case of clinical events, a second person/ supervisor was requested to cross check the validity of events. Image analysis of key endpoints for each chapter was undertaken by operators that were blinded to the clinical background and risk profile as detailed in the methods section. I was involved with the analysis of left ventricular indices for Chapters 4 and 5 and all echocardiograms. I undertook the data entry of all baseline characteristics, assessment of risk profiles and clinical outcomes. For data interpretation and analysis, I consulted a senior statistician from the University of Oxford, Dr Eric Ohuma, for statistical advice and input

APPENDIX 2: FIGURE

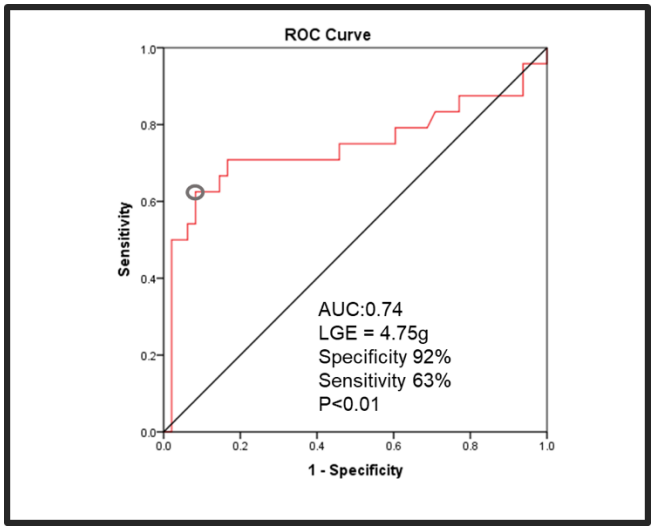

Figure 1. Diagnostic performance of ΔLGE≥4.75g for predicting clinical events.

Receiver Operator Curve (ROC) depicts that late gadolinium enhancement (LGE) increment threshold of 4.75 g (Youden index) has good specificity of 93% and reasonable sensitivity of 63% for detecting a composite clinical endpoint of heart failure hospitalisation, progression of NYHA class and new onset ventricular tachycardia.

APPENDIX 3: PAPERS AND ABSTRACTS

Raman B, Ariga R, Chan K, Sivalokanathan S, Selvanayagam J, Karamitsos T, Hess A, Tunnicliffe EM, Mahmod M, Neubauer S, Watkins H. Myocardial de-oxygenation during stress in hypertrophic cardiomyopathy: Determinants and association with ventricular arrhythmia. (Manuscript in preparation)

Raman B, Chan K, Ariga R, Hundermartz M, Karamitsos T, Mahmod M, Neubauer S, Hess A, Tunnicliffe EM. Increased precision of Blood Oxygen Level-dependent signal using interleaved FLASH normalisation of T2 prepared SSFP acquisition. JCMR. 2018 (submitted)

Ariga R, Tunnicliffe EM, Manohar SJ, Mahmod M, **Raman B**, Piechnik SK, Francis JM, Robson MD, Neubauer S, Watkins H. Diffusion tensor cardiac magnetic resonance imaging to measure disarray in vivo in hypertrophic cardiomyopathy. JACC. 2018 (accepted).

Clarke W, Peterzan M, Rayner J, Sayeed R, Petrou M, KrasopoulosG, Lake H, **Raman B**, Watson W, Cox P, Hundertmark M, AppsA, Lygate C, NeubauerS, Rider O and Rodgers CT.Localized rest and stress human cardiac creatine kinase reaction kinetics at 3 tesla. NMR Biomed. 2018 (under revision)

Raman B, Ariga R, Spartera M, Sivalokanathan S, Chan K, Dass S, Petersen SE, Daniels MJ, Francis J, Smillie R, Lewandowski A, Ohuma E, Rodgers C, Kramer C, Mahmod M, Watkins H, and Neubauer S. Progression of myocardial fibrosis in hypertrophic cardiomyopathy: mechanisms and clinical implications. Eur Heart J Cardiovasc Imaging. 2018 doi.org/10.1093/ehjci/jey135

Raman B, Wen D, Chan K, Watkins H, Neubauer S, Mahmod M Discrepancy Between Pathological Progression and Clinical Stability in a Young Patient with Hypertrophic Cardiomyopathy. Circulation: Cardiovascular Imaging. 2018;11:e008154

Mahmod M, Pal N, Rayner J; Holloway C; **Raman B**; Dass S; Levelt E et al. The interplay between metabolic alterations, diastolic strain rate and exercise capacity in mild heart failure with preserved ejection fraction. Journal of Cardiovascular Magnetic Resonance. 2018 (accepted Nov 2018).

Ladislav Valkovic, Ph D, Clarke WT, Schmid, **Raman B,** Ellis J, Watkins H, Robson M, Neubauer S, Rodgers CT. Measuring inorganic phosphate and intracellular pH in the healthy and diseased human heart by in vivo 7T 31P-MRS. Journal of Cardiovascular Magnetic Resonance. 2018 (under revision)

Lewandowski AJ, **Raman B**, Banerjee R, Milanesi M. Novel Insights into Complex Cardiovascular Pathologies Using 4d Flow Analysis by Cardiovascular Magnetic Resonance Imaging. Curr Pharm Des. 2017 Mar 17. PMID: 28317480.

CONFERENCE ABSTRACTS

Raman B, Ariga R, Spartera M, Sivalokanathan S, Chan K, Dass S, Petersen SE, Daniels MJ, Francis J, Smillie R, Lewandowski A, Ohuma E, Rodgers C, Kramer C, Mahmod M, Neubauer S and Watkins H. Novel insights into mechanisms and clinical implications of myocardial fibrosis progression in hypertrophic cardiomyopathy. British Cardiac Society of Magnetic Resonance Awards Abstract. V104: Suppl(5); Oral presentation, Annual Inherited Cardiac Conditions, London, 2018

Ariga R, Tunnicliffe E, Manohar S, Mahmod M, **Raman B**, Piechnik SK, Francis JM, Robson MD, Watkins H, Neubauer S. Diffusion tensor magnetic resonance imaging of myocardial disarray in hypertrophic cardiomyopathy. Oral Presentation, BCS, Edinburgh. 2018

Raman B, Clarke W, Ariga R, Mahmod M, Hundertmark M, Han J, Watkins H, Rodgers C, Rider O, Neubauer S. Novel insights into disease mechanism from in-vivo assessment of creatine kinase kinetics in hypertrophic cardiomyopathy. Oral Presentation, SCMR, Barcelona 2018

Raman B, Lewandowski A, Leal J, Francis J, Mahmod M, Dirk V, Untenberger M, Frahm J, Neubauer S, Robson MD, Hess AT. The one minute short-axis stack: cardiac assessment with ultra-fast real time imaging compared to cine at 1.5 T. Poster, SCMR, Washington DC 2017.

Raman B, Ariga R, Mahmod M, Piechnik S, Liu A, Borlotti A , Jerosch-Herold M , Francis J , Dall'Armellina E, Sivalokanathan S , Robson M, Watkins H, Ferreira V, Neubauer S. Adenosine stress T1-mapping offers a novel gadolinium-free approach for perfusion assessment in hypertrophic cardiomyopathy. Oral Presentation, Early Career Award Finalist, SCMR, Barcelona 2018.

Raman B, Ariga R, Mahmod M, Piechnik S, Liu A, Borlotti A , Jerosch-Herold M , Francis J , Dall'Armellina E, Sivalokanathan S , Robson M, Watkins H, Ferreira V, Neubauer S. Adenosine stress T1-Mapping: A novel contrast free method to assess myocardial perfusion and inducible ischaemia in Hypertrophic Cardiomyopathy. Poster presentation, Manchester, 2017.

Raman B, Ariga R, Mahmod M, Piechnik S, Liu A, Borlotti A , Jerosch-Herold M , Francis J , Dall'Armellina E, Sivalokanathan S , Robson M, Watkins H, Ferreira V, Neubauer S. Adenosine stress CMR T1 mapping detects impaired perfusion and inducible myocardial ischaemia without gadolinium contrast or ionizing radiation in hypertrophic cardiomyopathy. European Society of Cardiology, Barcelona, 2017.